MATHEMATICAL MODELLING AND COMPUTATIONAL SIMULATION OF *IN VITRO* TISSUE CULTURE PROCESSES

A Thesis Submitted to the College of

Graduate Studies and Research

In Partial Fulfillment of the Requirements

For the Degree of Doctor of Philosophy

In the Department of Mechanical Engineering

University of Saskatchewan

Saskatoon, Saskatchewan

By

MD SHAKHAWATH HOSSAIN

Permission to Use

In presenting this thesis in partial fulfilment of the requirements for a Postgraduate degree from the University of Saskatchewan, I agree that the Libraries of this University may make it freely available for inspection. I further agree that permission for copying of this thesis in any manner, in whole or in part, for scholarly purposes may be granted by Dr. Donald J. Bergstrom and Dr. X.B. Chen who supervised my thesis work or, in their absence, by the Head of the Department or the Dean of the College in which my thesis work was done. It is understood that any copying or publication or use of this thesis or parts thereof for financial gain shall not be allowed without my written permission. It is also understood that due recognition shall be given to me and to the University of Saskatchewan in any scholarly use which may be made of any material in my thesis.

Requests for permission to copy or to make other use of material in this thesis in whole or part should be addressed to:

Head of the Department of Mechanical Engineering

University of Saskatchewan

Saskatoon, Saskatchewan, Canada

S7N 5A9

Abstract

To develop or engineer artificial tissues in tissue engineering, a detailed knowledge of the *in vitro* culture process including cell and tissue growth inside porous scaffolds, nutrient transport, and the shear stress acting on the cells is of great advantage. It has been shown that obtaining such information by means of experimental techniques is exceedingly difficult and in some ways impossible. Mathematical modelling and computational simulation based on computational fluid dynamics (CFD) has emerged recently to be a promising tool to characterize the culture process. However, due to the complicated structure of porous scaffolds, modelling and simulation of the *in vitro* cell culture process has been shown to be a challenging task. Furthermore, due to the cell growth during the culture process, the geometry of the scaffold structure is not constant, but changes with time, which makes the task even more challenging. To overcome these challenges, the research presented in this thesis is aimed at developing a CFD-based mathematical model and multi-time scale computational framework for culturing cell-scaffold constructs placed in perfusion bioreactors.

To predict the three-dimensional (3D) cell growth in a porous tissue scaffold placed inside a perfusion bioreactor, a model is developed based on the continuity and momentum equations, a convection-diffusion equation and a suitable cell growth equation, which characterize the fluid flow, nutrient transport and cell growth, respectively. To solve these equations in a coupled fashion, an in-house FORTRAN code is developed based on the multiple relaxation time lattice Boltzmann method (MRT LBM), where the D3Q19 MRT LBM and D3Q7 MRT LBM models have been used for the fluid flow and mass transfer simulation, respectively. In the model cell growth equation, the transport of nutrients, i.e. oxygen and glucose, as well as the shear stress induced on the cells are considered for predicting the cell growth rate. In the developed model and computational framework, the influence of the dynamic strand surface on the local flow and nutrient concentration has been addressed by using a two-way coupling between the cell growth and local flow field and nutrient concentration, where a control-volume method within the LBM framework is applied. The simulation results provide quantification of the biomechanical environment, i.e. fluid velocity, shear stress and nutrient concentration inside the bioreactor.

The final simulation applied the cell growth model to the culture of a three-zone tissue scaffold where the scaffold strands were initially seeded with cells. The prediction for the 3D cell growth rate indicates that the increase in the cell volume fraction is much higher in the front region of the scaffold due to the higher nutrient supply. The higher cell growth in the front zone reduces the permeability of the porous scaffold and significantly reduces the nutrient supply to the middle and rear regions of the scaffold, which in turn limit the cell growth in those regions. However, implementation of a bi-directional perfusion approach, which reverses the flow direction for second half of the culture period, is shown to significantly improve the nutrient transport inside the scaffold and increase the cell growth in the rear zone of the scaffold. The results in this study also demonstrate that the developed mathematical model and computational framework are capable of realistically simulating the 3D cell growth over extended culture periods. As such, they represent a promising tool for enhancing the growth of tissues in perfusion bioreactors.

Key words: Tissue engineering; modelling and simulation; lattice Boltzmann method; cell growth modelling; nutrient transport

Acknowledgments

First and foremost, I would like to acknowledge and warmly thank my PhD supervisors, Professor Donald J. Bergstrom and Professor X.B. Chen for their support, patience, encouragement and advice throughout the completion of this thesis. Also I wish to thank Mrs. Bergstrom and Mrs. Chen for their kind invitations to their houses, and great hospitality.

I sincerely thank members of my advisory committee: Dr. J.D. Bugg, Dr. J.D. Johnston and Dr. G.A. Ferguson for their valuable comments which helped me to improve the quality of my research work. I appreciate the help and support I receive from the faculty and staff at the Department of Mechanical Engineering. I would like to extend a special thanks to Mr. David Deutscher and Mr. Rick Retzlaff for their valuable assistance during the lab demonstration experience, and also in helping with the Computational Fluid Dynamics (CFD) lab facilities. I would like to express my gratitude to the CFD and Tissue Engineering Research Group members. I gratefully acknowledge the funding support of the Natural Sciences and Engineering Research Council (NSERC) of Canada.

I also would like to take this opportunity to thank my parents Md Shamsuddin Ahmed and Jahanara Begum, my younger brother Jubair Hossain, my family members and friends in Dhaka, Mankato, and Saskatoon for encouraging me and believing in me in every single step.

Lastly, I would like to thank my wife, Fahmidazaman Irin, whose love and encouragement provided me the inspiration to complete this work.

Table of Contents

List of Figures

List of Tables

Chapter 1

Introduction

1.1 Motivation

Tissue engineering is a multi-disciplinary research field which combines the principles of life sciences, engineering, biotechnology, biochemistry and chemistry to develop artificial tissues which can replace damaged or injured tissues (Langer and Vacanti 1993; Blitterswijk 2008). In the past two decades, artificially developed or engineered tissues have shown great promise compared to the traditional approaches of using autografts and allografts to repair damaged tissue (Voronov *et al.* 2010). Autografts are those obtained from the patient's own tissue which are used for surgical reconstruction of the damaged tissues; allografts are those collected from other persons and then incorporated into the patient's body. These traditional approaches are limited by the availability of autografts and allografts as well as the complicated procedure due to the need of surgery for both tissue collecting and implanting. To avoid these limitations, the approach of *in vitro* tissue engineering provides a promising option by regenerating the viable artificial tissues in an *in vitro e*nvironment (such as petri-dishes and bioreactors), which are then implanted into the patient.

In current tissue engineering, the cells are typically seeded into three-dimensional (3D) scaffolds that are placed inside the bioreactor for tissue regeneration prior to implanting (Korossis *et al.* 2005). The development of a specific type of tissue requires a specific type of cell to be seeded into the scaffold, e.g. chondrocyte cells are required for the regeneration of cartilage tissues (Sacco *et al.* 2011). The 3D porous tissue scaffolds are generally made from biodegradable biomaterials, e.g. polymers, by various methods including 3D printing and solid free form fabrication techniques (Adachi *et al.* 2006). Due to advances in these techniques, nowadays it is possible to fabricate tissue scaffolds with the desired geometry and micro-structure, i.e. a specific pore size, shape, and connectivity. The geometry and micro-structure of the porous scaffold are important for facilitating the supply of nutrients to the scaffold which in turn affects the growth, migration, and proliferation of cells on the scaffold (Singh and

Hutmacher 2009). For example it was reported that the chondrocyte cell viability decreases if the supply of glucose falls below the critical value of 0.3 mM (Zhou *et al.* 2008).

The cell-seeded scaffolds are typically cultured in petri-dishes with static culture media. Recently, the dynamic culture process using bioreactors has shown significant improvement over the static culture process (Singh and Hutmacher 2009). Bioreactors can play an important role during the culture process by providing a controlled biomechanical environment, i.e. flow rate, pH value, flow induced shear stress level, etc. for the development of viable tissues. The dynamic flow conditions inside the bioreactors enhance the nutrient transport by introducing convective transport in addition to the diffusive transport (Singh and Hutmacher 2009). However, for low Reynolds number flow inside the bioreactor the diffusive mass transport still plays a significant role. The biophysical stimuli, i.e. the shear stress induced on the cells due to the fluid flow inside the bioreactor, can also enhance the cell differentiation and proliferation if it is in an appropriate range (Porter *et al.* 2005; Hossain *et al.* 2012). However, a higher level of shear stress can remove cells from the scaffold and even cause cell injury and death (Chung *et al.* 2007).

A number of bioreactors with different working principles can be found in the literature for the culture process. Some commonly-used bioreactors include the spinner flask, rotating wall vessel, and perfusion bioreactors (Singh and Hutmacher 2009). The spinner flask bioreactor uses a magnetic stir bar to stir the culture media to improve the supply of nutrients to the cell-seeded scaffold placed in the bioreactor (Plunkett and O'Brian 2011). In a rotating wall-vessel bioreactor, the scaffold is suspended in the culture media in a bioreactor vessel that rotates at a given angular speed. The centrifugal force produced by the rotating vessel keeps the scaffold suspended in the media (Plunkett and O'Brian 2011). The movement and circulation of the culture media improves the nutrient transport inside the bioreactor and porous scaffold, thus promoting the cell and tissue growth. In a perfusion bioreactor, the fluid is directed to flow through the bioreactor and porous scaffold, hence improving the supply of nutrients inside the porous constructs (Chung *et al.* 2007). The flow of the culture media through the porous scaffold can also remove the waste products generated during the culture process (Blitterswijk 2008). For example, during the culture process cells produce a significant amount of lactate due to the presence of glycolysis. A rising level of lactate can decrease the pH level and hamper cell

growth. A pH value lower than 6.8 in the culture media might be harmful for cell viability (Zhou *et al.* 2008), hence removal of the waste products from the scaffold constructs can improve the culture environment. Among various types of bioreactor, the perfusion bioreactor is found to be a simple and effective approach for obtaining a controlled biomechanical environment for the cell growth. Therefore, the perfusion bioreactor is considered the most promising compared to other bioreactors and the static cell culture process. This is especially true when using the bi-directional flow perfusion bioreactor (Gardel *et al.* 2013, Mayer *et al.* 2014).

To fully achieve the advantages of the dynamic culture process, effective control of the biomechanical environment inside the bioreactor is essential. In the past, the culture process was often designed and controlled based on the operator's empirical knowledge and experience (Singh and Hutmacher 2009). However, empirical methods have significant limitations to improve the biomechanical environment for the cell culture; instead a comprehensive knowledge of the overall culture process is required. For example insight into the fluid flow inside the bioreactor is critical for quantifying the nutrient supply as well as the magnitude of the shear stress acting on the cells. Characterization of the cell and tissue growth rates is essential for predicting the required culture period for the development of the tissue constructs prior to their implantation into patients. Improved knowledge and understanding of the underlying physics of the culture process will ultimately enhance the quality of the developed tissue constructs and the supporting tissue growth models (Hossain *et al.* 2012). However, a detailed analysis of the overall culture process by using state-of-the-art experimental techniques is exceedingly difficult and in some ways impossible. For example, characterizing the local fluid flow and cell growth inside a porous scaffold structure would be impossible using conventional visualization and flow measurement techniques, since the scaffolds are often made with opaque biomaterials. Furthermore, since the overall culture process typically varies from 30 to 150 culture days (Li *et al.* 2014), performing experiments over such a long period might not be feasible.

Mathematical modelling and computational simulation of the dynamic *in vitro* tissue growth process using computational fluid dynamics (CFD) can play a significant role in analysing the tissue growth process within a porous tissue scaffold placed inside a bioreactor (Singh and Hutmacher 2009). For example, a number of studies have used CFD to investigate the magnitude of the shear stress values, supply of nutrients, cell growth rate and cell volume

fraction (CVF) distribution within a tissue scaffold, and also developed mathematical models for tissue regeneration in a perfusion bioreactor (Porter *et al.*, 2005; Chung *et al.*, 2007; Voronov *et al.*, 2010; Sacco *et al.*, 2011; Nava *et al.* 2013). A more detailed discussion of recent developments and achievements in the application of CFD to investigate the fluid flow, nutrient transport and cell growth inside the porous scaffold is presented in Chapter 2.

1.2 Research issues

For effective cell culture inside a perfusion bioreactor, selection of the input culture parameters i.e. inlet flow rates, nutrient concentration etc. is important. As mentioned in the previous section, increasing the flow rate inside the bioreactor will increase the convective nutrient transport. However, due to the higher flow rate the subsequent shear stress level will also increase. Therefore, knowledge of the magnitude of the shear stress level is critical for the culture process and a suitable flow rate needs to be selected which will induce favourable shear stress levels on the cells.

To maintain a favourable shear stress level on the cells, the flow rate inside a bioreactor is very low: typically the Reynolds number based on the scaffold strand diameter is less than 1. For this low Reynolds number regime, both the diffusive and convective transport of the nutrients is important. A clear understanding and quantification of the nutrient transport process for this flow regime will be useful for improving the overall culture process.

CFD can be very useful for obtaining detailed information of the shear stress and nutrient transport during the culture process. A resolved-scale simulation can provide the local values of the shear stress and nutrient concentration inside the tissue scaffold. Use of a resolved-scale simulation is essential for studying the influence of the micro-architecture and geometry of a complex porous scaffold. However, to perform a resolved-scale simulation of the fluid flow and nutrient transport through a porous tissue structure, a large number of computational nodes are required to fully resolve the scaffold geometry, which in turn increases the computational time and effort. To address this issue, the selection of a suitable computational method and algorithm is very important.

The complexity of the simulation procedure increases dramatically since the geometry of the scaffold structure is not constant during the culture process. The cells seeded on the scaffold strands will grow and proliferate. The growth of the cells typically depends on the supply of nutrients and biophysical stimuli. Therefore, a cell growth equation which considers the local values of the nutrient concentration, as well as the shear stress induced on the cells, should be included in the overall tissue growth model, and the cell growth equation needs to be coupled with the fluid flow and mass transfer equations. The cell growth inside the scaffold changes the micro-architecture of the scaffold during the culture process. The changes in the micro-architecture of the scaffold subsequently influence the local fluid flow and nutrient concentration. Hence, the movement and change in the cell-fluid interface needs to be considered; the scaffold strand surface is essentially a dynamic surface. The influence of the dynamic strand surface on the local environment should be addressed, and a two-way coupling between the cell growth and local flow field should be included in the model development.

Typically, the cell and tissue growth rate is slow so that the change in the cell-fluid interface due to the growth does not greatly influence the external fluid flow and nutrient distribution during the initial culture period. However, for longer culture periods, the increase in overall cell and tissue growth will influence the flow pattern and subsequent nutrient transport inside the bioreactor and scaffold. Hence, to develop a realistic cell and tissue growth model, a computational framework which includes the interaction between the cell and local biomechanical environment is important. A major issue for methods which include the influence of cell growth on the fluid flow and nutrient transport is that the time scales for the fluid flow, mass transfer and cell growth processes are all different. Specifically, the cell growth rate occurs at a much slower rate compared to the fluid flow and mass transfer process. To address this issue, a multi-time scale simulation approach is required.

1.3 Objectives

In the overall context of developing models and a computational framework for culturing cell-scaffold constructs placed in perfusion bioreactors, the specific objectives of this thesis work are as follows:

1. To develop a 3D tissue growth model. The model will include the continuity and momentum equations, a convection-diffusion equation and a suitable cell growth equation for characterizing the fluid flow, nutrient transport and cell growth within a porous tissue scaffold placed inside a perfusion bioreactor. The cell growth equation will consider the influence of the local nutrient supply and the flow-induced shear stress acting on the cells.
2. To develop a computational framework to solve the mathematical model using the multiple relaxation time lattice Boltzmann method (MRT LBM). The computational framework will be used to perform a resolved-scale simulation to study :
    a) The fluid velocity, shear stress, nutrient distribution and the chondrocyte cell growth rate on the surface of the circular scaffold strands inside a perfusion bioreactor to investigate the influence of the distance between the strands and to understand the general flow pattern and nutrient transport over the strands;
    b) The generation and transport of waste products through the simplified tissue scaffold with a single unit pore and to understand the influence of waste generation on the cell growth rate;
    c) The dynamic two-way coupling between the chondrocyte growth and the local flow field and nutrient distribution for a scaffold-free cell culture.
3. To simulate the chondrocyte growth inside a 3D porous tissue scaffold cultured in a bi-directional flow perfusion bioreactor.

To accomplish the aforementioned objectives, an in-house FORTRAN code based on the MRT LBM has been developed. For large-scale complex flow problems, the MRT LBM has become an attractive methodology due to its simple computational procedure, and the local nature of the calculation (Premnath *et al.* 2009). Development of the in-house code required a detailed and comprehensive knowledge of the modelling approach and numerical methods. The

in-house code provided the opportunity to have complete control of the models, boundary conditions and numerical methods which is not feasible for most commercial software. In this thesis, the in-house code provided the opportunity to address the following key issues in the computational framework:

i. A cell growth equation which considers the local nutrient supply as well as the shear stress level induced on the cells, and
ii. The dynamic two-way coupling between the cell growth and local flow field and nutrient concentration using a multi-time scale simulation approach.

1.4 Scope of the thesis

In this thesis work, the cells are considered to be rigid and impermeable to the fluid. No-slip boundary conditions are applied at the surface of the cell phase. Due to the substantial amount of work required to accomplish the objectives in Section 1.3, the transport of nutrients due to diffusion through the cell phase is not considered. The movement and deformation of the cells due to the external biomechanical forces, i.e. shear stress, is also not within the scope of this study.

For longer culture periods, extra-cellular matrix (ECM) production and degradation will also occur in addition to the cell growth. However, to include the ECM production or degradation into the model, a better understanding of the physical process of the ECM formation is required. Knowledge of the properties of the developed ECM and the interaction between the ECM production and/or degradation and the cell growth is also required. Due to the lack of a mature model in the literature which addresses these issues, the ECM formation was not included in the present study.

The scaffolds used for the *in vitro* tissue culture process are often made of biocompatible and biodegradable biomaterials. For longer culture periods, the biodegradation of the scaffolds can influence the overall structure of the developed tissues. To include the scaffold degradability into the model it would be necessary to study and investigate the scaffold material properties, select the appropriate degradation model and include the model into the computational

framework. Since this would require a substantial amount of additional time, the scaffold degradation was not considered in the present study.

1.5 Thesis organization

This manuscript-based dissertation consists of seven chapters. Chapter 1 introduces the overall motivation behind the thesis, research issues to be addressed and specific objectives. Each of Chapters 2, 3, 4, 5 and 6 consists of a manuscript that has been published, accepted for publication, or submitted for publication. All of these manuscripts are co-authored by Md Shakhawath Hossain, Prof. Bergstrom, and Prof. Chen. The research work documented in the manuscripts was performed by Md Shakhawath Hossain under the supervision of Prof. Bergstrom and Prof. Chen. Each manuscript was first drafted by Md Shakhawath Hossain and then edited with the help of Prof. Bergstrom and Prof. Chen. The references for this thesis are presented in a single list at the end of the conclusion chapter (Chapter 7).

Chapter 2 provides a comprehensive background of the mathematical models and numerical methods as well as a literature review. Chapters 3, 4, 5 and 6 provide the additional references related to the incremental work performed in each chapter to achieve the specific objectives as outlined previously.

Chapter 3 addresses objectives 1 and 2a). This chapter describes the development of the mathematical model and computational codes to obtain the resolved-scale simulation results of the fluid velocity, shear stress and nutrient concentration using the MRT LBM. The chondrocyte cell growth rate was calculated on the surface of the circular scaffold strand using the surface nutrient concentration and shear stress values. The influence of the distance between the scaffold strands on the cell growth rate was also investigated in this chapter. Based on the models developed in Chapter 3, Chapter 4 addresses objective 2b) and presents a study of the fluid flow, transport of nutrients and waste products, and the cell growth rate at the strand surface for a simplified tissue scaffold in a single unit pore.

To address objective 2c), Chapter 5 incorporates the dynamic two-way coupling between the chondrocyte cell growth and the local flow field and nutrient distribution into the mathematical model and computational algorithm. This chapter also studied the influence of the

chondrocyte cell growth on the local nutrient concentration and shear stress field for a scaffold-free culture process inside a perfusion bioreactor.

Chapter 6 addresses objective 3 and presents the final goal of this research, i.e. a mathematical model and computational framework to investigate the 3D cell growth in a porous scaffold placed inside a perfusion bioreactor which includes the two-way coupling between the cell growth and local flow field and glucose concentration. The simulation was performed for 30 culture days for porous scaffold which includes three pores in the streamwise direction. The 3D cell growth inside the individual pores was studied and compared against each other for a bi-directional fluid flow and nutrient supply process.

Chapter 7 summarizes the conclusions from the present study and also discusses opportunities for the future research on this topic.

Chapter 2

Investigation of the *in vitro* Culture Process for Skeletal-Tissue-Engineered Constructs using Computational Fluid Dynamics and Experimental Methods

Md. Shakhawath Hossain, X.B. Chen, D.J. Bergstrom

(A similar version of this chapter has been published in: ASME J. Biomech. Eng., 2012, vol. 134, pp. 121003 (1-12))

Abstract

The *in vitro* culture process via bioreactors is critical to create tissue engineered constructs (TECs) to repair or replace the damaged tissues/organs in various engineered applications. In the past, the TEC culture process was typically treated as a black box and performed on the basis of trial and error. Recently, computational fluid dynamics (CFD) has demonstrated its potential to analyze the fluid flow inside and around the TECs, therefore being able to provide insight into the culture process, such as information on the velocity field and shear stress distribution that can significantly affect such cellular activities as cell viability and proliferation during the culture process. This paper briefly reviews the CFD and experimental methods used to investigate the *in vitro* culture process of skeletal-type TECs in bioreactors, where the wear and mechanical deformation of the TEC can be ignored. Specifically, this paper presents CFD modeling approaches for the analysis of the velocity and shear stress fields, mass transfer, and cell growth during the culture process, and also describes various particle image velocimetry (PIV) based experimental methods to measure the velocity and shear stress in the *in vitro* culture process. Some key issues and challenges are also identified and discussed along with recommendations for future research.

2.1 Introduction

Tissue engineering is an interdisciplinary field that utilizes the principles of engineering, biology and biochemistry for the development of biological substances that can replace damaged or missing tissues or organs (Blitterswijk 2008; Meyer *et al.* 2009). Made from biomaterials, tissue engineered constructs (TECs) or tissue scaffolds act as both structural supports for cells, once seeded on the TECs, and vehicles for sustained-release of therapeutic agents *in vitro* and *in vivo*.

In vitro cultures of TECs are mainly performed in bioreactors with controlled environmental conditions (*e.g.*, pH, temperature, pressure) and nutrient/product concentrations (Blitterswijk 2008). The flow of culture media through porous TECs in bioreactors greatly enhances the nutrient transport and removal of wastes, thus promoting cell growth and new tissue generation in the TECs. As such, flow-based bioreactors can improve the quality of engineered tissues compared to diffusion-based static culture systems. During the culture process, cell attachment, migration, proliferation, differentiation, and extracellular matrix (ECM) production take place, eventually forming structural and functional replacement of the target organ or tissue (Blitterswijk 2008). *In vivo* culture of TECs involves placement directly into a living organism to replace injured tissues. For example, TECs can be implanted directly into the body as cell free structures to aid in bone regeneration; in such cases, cells that are recruited from the neighboring tissues to heal the defect site invade TEC pores, forming the TEC geometry as a tissue (Milan *et al.* 2010). Cell colonization and differentiation strongly depends on the biochemical processes as well as the mechanical and hydrodynamic environment (Milan *et al.* 2010).

The interaction between TECs and cellular fluids is very important for the successful development of new tissue capable of replacing the functions of damaged or missing tissue. Inside flow-based bioreactors, the movement of the culture medium induces fluid stresses, in particular shear stresses, on the cells attached to the surface and inside of the TECs. Within a certain range, flow-induced shear stress has a positive impact on modulating cell physiology and developing the engineered tissues. The flow-induced shear stress causes cell membrane stretching and may increase cell proliferation. On the other hand, excessive shear stress can cause cell damage (Porter *et al.* 2005). The movement of the culture medium also affects cell

migration into the interior of the TECs. Previous studies (Xie *et al.* 2006; Li *et al.* 2009; Yeatts *et al.* 2011) also suggest that the mass transfer and shear stress levels can be optimized for enhanced cell-cell signaling mechanisms and thus cell growth. Thus, careful attention should be paid to the interaction between tissue and cellular fluids both *in vivo* and *in vitro* (Singh *et al.* 2009). In the literature reviewed in this paper, information regarding the effect of a normal stress on TECs is lacking. This may imply the effect of the normal stress on both cells and TECs may be less important compared to that of the shear stress, especially for skeletal-type TECs where deformation is not considered.

Typically, the cell culture of TECs in bioreactors is performed based on the trial and error method. To be able to predict the tissue growth, cell differentiation, proliferation and migration, the velocity field in bioreactors as well as the transport of the culture media through the porous TECs should be better understood. Analysis of the flow and transport of the culture medium within the porous TECs is difficult due to the complexity of the tissue properties and the flow of the culture medium through the porous, yet tiny, TECs. Experimental analysis of such complex flow and transport problems may be possible, but would be expensive and time consuming. CFD can be used to eliminate the reliance on trial and error methods in the culture process. It can be used to simulate the hydrodynamic environment inside the bioreactor, as well as the porous TECs, and thus can help to improve the design of both bioreactors and the *in vitro* TEC culture process. The *in vitro* CFD simulation will also be useful for better understanding the perfusion process upon the implantation of scaffolds *in vivo* (Meyer *et al.* 2009). However, in all cases the models developed and the results obtained using CFD must be validated by experiments. Therefore, the coupling of computational simulations and experimental methods is essentially needed to form a synergy for cell culture studies.

This paper aims to review the recent developments and achievements in the application of CFD to investigate the fluid flow and nutrient transport through the TECs *in vitro* and their experimental validation. Section 2 provides a brief description of CFD and the governing equations for CFD modeling. Section 3 reviews recent studies which have been conducted on the culture process. Most of these studies were conducted for bone and cartilage or more generally skeletal-tissue engineering applications. However the modeling approaches described in section 2 are also applicable to soft tissue engineering applications, with some modifications

such as including mechanical deformation of the TECs which can be ignored for the skeletal tissues. Section 4 presents various experimental techniques to obtain information on the culture process. Some suggested future research directions are discussed in Section 5.

2.2 Computational fluid dynamics (CFD)

2.2.1 Brief introduction

CFD has become a very powerful and versatile tool for the analysis of complex flows in engineering and recently for the analysis of biological systems, such as the flow through and around TECs both *in vivo* and *in vitro* (Meyer *et al.* 2009). For example, CFD was employed in the development of ventricular assist devices (VADs) or design of mechanical pumps to replace the function of one or more chambers of the failing heart (Fraser *et al.* 2011). Without actually constructing the physical devices or prototypes, CFD allows exploration of the functional performance of different designs under a wide range of operating conditions. It is noted the TECs used in tissue engineering are typically porous and thus the physics of flow is different from many other biological flows. CFD is able to predict the flow characteristics of fluids flowing through porous media. CFD has so far successfully predicted fluid flow and heat transfer through porous high conductivity graphite foam (Betchen *et al.* 2010), transport phenomena of liquid water through the electrodes of fuel cells (Djilali 2007), and fuel flow through the porous Rigimesh material used for liquid rocket engines (Sozer *et al.* 2007). Therefore, applying CFD to predict fluid flow characteristics through porous TECs is clearly feasible.

The complexities encountered in these flows arise from such aspects as the underlying physics, the complex geometries and micro-architectures of the TECs, material properties of the TECs, e.g. when biodegradable materials are used, flow patterns inside the bioreactors, and the biological properties of tissues. In most cases, biological tissues have complex geometries and furthermore, these geometries change during the culture process as cell differentiation and ECM production take place. As a result, the local mass transfer and shear stress field vary during the culture process (Yeatts *et al.* 2011). In the simulation of Voronov *et al.* (2010), it is shown that even small manufacturing defects of TECs can have an impact on the shear stress distribution. Specifically, a uniform shear stress distribution was obtained for the TECs with no defects;

whereas for the TECs with defects the flow rate was higher in the area where the solid material is less and near the defect sites a higher local surface shear stress was induced. Hence, advanced and accurate computational modeling and simulation is required to determine the mass transfer, velocity and shear stress fields inside the TECs while culturing *in vitro*.

Various CFD commercial software packages have been developed for fluid flow simulation, and their use is helping to clarify flow phenomena in TEC cultures both *in vivo* and *in vitro*. FIDAP, ANSYS, and COMSOL are examples of CFD software packages that have been used in complex fluid flow simulations. These software packages use different numerical methods to solve and analyze fluid flow problems. Developing specific in-house codes based on numerical techniques is also an option for analyzing flow problems. A numerical solution begins with a mathematical model of the flow. The mathematical model consists of the governing equations describing the flow, which typically involves a set of partial differential equations with appropriate boundary and initial conditions. Next, a discretization method is used to approximate the differential equations by a system of algebraic equations. The algebraic equations are solved at discrete locations on a numerical grid in space and time. The algebraic equations involved in evaluating the flow variables at the grid points are also called the discrete equations. The number and distribution of grid points in the solution domain is an important consideration for the accuracy of the solution. As the number of grid points increases, the solution to the discrete equations is expected to better approximate the solution of the corresponding differential equations (Patankar 1980). The structured generation of grid points is well suited for fluid flow with a simple geometry, but for a sufficiently complex geometry unstructured mesh generation has distinct advantages. Adaptive mesh generation can also be employed to efficiently solve the problem with complex geometry. The accuracy of the result can also be increased by using a higher-order discretization scheme, but this may increase the computational time and the computer code may also become more complicated. The most commonly used discretization methods are finite difference (FD), finite element (FE), and finite volume (FV) methods. Other methods, such as boundary element methods and cellular automata, are also used in CFD for some cases (Ferziger *et al.* 2002).

Effective grid generation is important for resolving the boundaries of a porous TEC. A large number of grid points may be required to capture the complex geometry of a TEC. Complexity in the simulation also arises as the geometry and the porosity of the TECs change during the culture process due to cell proliferation, differentiation and migration. The cell population dynamics should be coupled with the flow and mass transfer equations in the model, since the cell proliferation, differentiation and migration depends largely on the nutrient transport. In some cases biodegradable materials are used for the construction of the TECs. For these cases the rate of degradation needs to be included in the model, as the degradation of material changes the interior surface and geometry of the TECs. The production of ECM during the cell culture process is another important issue that needs to be considered. The ECM provides the structural framework for the tissue, so that the impact of flow on its production and the permeability of porous structure also need to be taken into account.

2.2.2 Modeling fluid flow and nutrient transport through porous TECs

Fluid flow and the associated mass transfer through porous media is a fundamental multi-phase fluid mechanics problem, where one of the phases is solid and stationary. In tissue engineering, the TECs cultured both *in vivo* and *in vitro* are porous structures. A one-dimensional empirical model for flow in porous media introduced by Darcy (1856) aimed at empirically correlating pore level flow effects to the bulk fluid motion. In Darcy's model, the average fluid velocity depends on the permeability and the pressure gradient. Brinkman (1949) modified the Darcy equation to include the viscosity term. Note that the Darcy equation can only be used to obtain the bulk fluid information.

A related formulation of the problem is based on the volume averaging method, which is a well-established modeling technique in fluid mechanics. This method has been successfully used in different engineering applications to obtain information about fluid flow through porous media. In this method, a representative elementary volume (REV) is analyzed rather than the whole porous structure with its complex boundary conditions. The REV contains both solid and fluid phases as shown in Fig. 2.1. The averaging procedure can be applied to the governing equations. A local volume averaged equation is derived by using pore-scale information of the REV, which is valid everywhere inside the structure. By solving the volume-averaged equation

only the averaged flow information for the whole structure can be obtained rather than the local flow information.

To obtain more detailed flow and mass transfer information, the interaction of fluid and solid phases in each individual pore must be accounted for. Typically, TECs have complex geometries and determining the interaction of the fluid and solid phases in each individual pore would require a resolved scale simulation. In the resolved scale simulation a large number of nodes are used to fully resolve the geometry of the porous structure which in turn makes for a large scale calculation.

Transport Equations

Resolved scale method

To obtain the resolved scale simulation the governing equations which describe the single-phase incompressible flow through a solid porous medium need to be solved. The flow governing equations are the continuity and momentum equations, which represent conservation of mass and momentum, respectively:

$$\nabla \cdot \vec{v}_\beta = 0 \tag{2.1}$$

$$\frac{\partial}{\partial t}\left(\rho_\beta \vec{v}_\beta\right) + \nabla \cdot \left(\rho_\beta \vec{v}_\beta \vec{v}_\beta\right) = -\nabla p_\beta + \rho_\beta \vec{g} + \mu_\beta \nabla^2 \vec{v}_\beta \tag{2.2}$$

where p_β is the pressure and $\vec{v}_\beta$ is the velocity of the fluid phase. These equations assume that the dynamic viscosity μ_β and the density ρ_β are constant. The fluid is identified as the β-phase and the solid as the σ-phase as indicated in Fig. 2.1. Solving the governing equations numerically yields the velocity and pressure fields.

From the velocity information, the viscous stress τ, can be obtained by using the appropriate constitutive relation, e.g. for an incompressible Newtonian fluid,

$$\tau_{ij} = \mu_\beta \left(\frac{\partial u_i}{\partial x_j} + \frac{\partial u_j}{\partial x_i} \right) \tag{2.3}$$

Volume averaging method

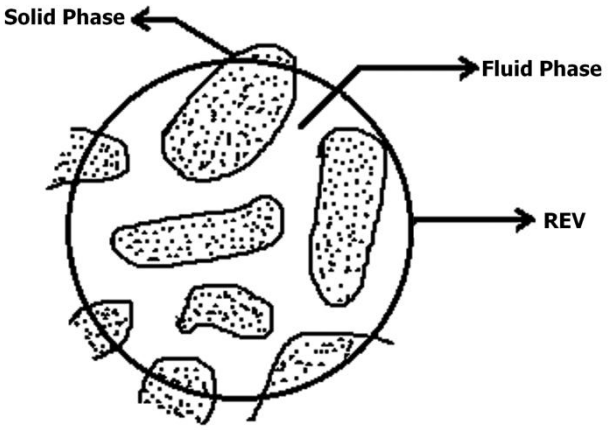

Figure 2.1: A representative elementary volume of the porous medium which consists of both the solid (σ) and fluid (β) phase

By applying the volume averaging method to the governing equations, a volume averaged continuity equation can be obtained (Whitaker 1986),

$$\nabla \cdot \left\langle \vec{v}_\beta \right\rangle = 0 \tag{2.4}$$

as well as a volume-averaged momentum equation (Whitaker 1986),

$$\rho_\beta \frac{\partial \left\langle \vec{v}_\beta \right\rangle^\beta}{\partial t} + \rho_\beta \left\langle \vec{v}_\beta \right\rangle^\beta \cdot \nabla \left\langle \vec{v}_\beta \right\rangle^\beta = -\nabla \left\langle p_\beta \right\rangle^\beta + \rho_\beta \vec{g} + \mu_\beta \nabla^2 \left\langle \vec{v}_\beta \right\rangle^\beta + \mu_\beta K^{-1} \left\langle \vec{v}_\beta \right\rangle + \frac{C_E}{\sqrt{K}} \rho_\beta \left| \left\langle \vec{v}_\beta \right\rangle \right| \left\langle \vec{v}_\beta \right\rangle \tag{2.5}$$

where K is the permeability and C_E is the Ergun coefficient. The last two terms account for the contributions from the spatial deviations of pressure and velocity (Whitaker 1986) and distinguish the volume-averaged equation from of the momentum equation. It is evident from the averaging procedure that these two terms depend on the local velocity field for a specific porous geometry. These parameters can be estimated using existing empirical correlations or obtained from experiments (Sozer *et al.* 2007; Whitaker 1986; Chung *et al.* 2007). By solving the volume averaged momentum equation the volume-averaged velocity and pressure fields within the porous structure can be obtained.

Mass Transfer Equations

Resolved scale method

The governing equation for single-phase mass transfer through a porous media is the convection-diffusion equation (Whitaker 1986),

$$\frac{\partial c_A}{\partial t} + \nabla \cdot \left(c_A \vec{v}_\beta \right) = D_\beta \nabla^2 c_A \tag{2.6}$$

where c_A is the concentration of the scalar component A and D_β is the diffusion coefficient.

Volume averaging method

By applying the volume averaging method to equation (2.6), the volume averaged mass transfer equation can be obtained (Whitaker 1986; Boccaccio *et al.* 2011),

$$\left(\varepsilon + a_V K_{\text{eq}} \right) \frac{\partial \langle c_A \rangle}{\partial t} + \nabla \left(\varepsilon \langle \vec{v}_\beta \rangle^\beta \langle c_A \rangle^\beta \right) = \nabla \cdot \left(D^*_{\text{eff}} \nabla \langle c_A \rangle^\beta \right) \tag{2.7}$$

where ε is the volume fraction, and K_{eq} is a function of the bulk concentration c_A. The symbol D^*_{eff} denotes the effective dispersion tensor which is defined by the following equation,

$$D^*_{\text{eff}} = \varepsilon D_\beta I + D_\beta \frac{1}{V_\beta} \int_{A_{\beta\sigma}} \vec{n}_{\beta\sigma} \vec{b} \, dA - \left\langle \tilde{\vec{v}}_\beta \vec{b} \right\rangle \tag{2.8}$$

The integral in the above equation represents a quantity that influences the effective diffusion coefficient of the porous media, while the final term represents transport due to the "spatial fluctuation" of the velocity field on the pore scale and is associated with hydrodynamic dispersion (Golfier *et al.* 2009). The volume-averaged convective-diffusive equation can be coupled with the volume-averaged momentum equation to predict the volume-averaged nutrient transfer throughout the TECs. Table 2.1 summarizes the two approaches, i.e. the resolved scaled method and volume averaging

Table 2.1: Summary of resolved scale method and volume averaging method

	Resolved scale method	***Volume averaging method***
Flow equations	Continuity and momentum equations with appropriate initial and boundary conditions	Volume-averaged continuity and momentum equation with appropriate initial and boundary conditions
Mass transfer equation	Convection diffusion equation with appropriate initial and boundary conditions	Volume-averaged convection diffusion equation with appropriate initial and boundary conditions
Advantages	The geometry of the porous structure is fully resolved and the local information is obtained.	The complex geometry of the structure does not need to be solved, so that the calculation is smaller compared to the resolved scale method.
Disadvantages	A large number of nodes are required to resolve the complex geometry of the structure, so that the calculation becomes large.	Only the average information for the whole structure is obtained.

2.2.3 Modeling of Cell Growth and Distribution

To simulate the growth of the cells within regenerating tissues the following diffusion equation has been used in various studies (Boccaccio *et al.* 2011):

$$\frac{\partial c}{\partial t} = D\nabla^2 c \tag{2.9}$$

In this equation c is the concentration of cells in a given volume, and D is the diffusion coefficient. However, in this equation the diffusion coefficient is independent of the tissue differentiation process, so in the model the cell mitosis (cell differentiation) and cell apoptosis (cell death) should be included (Lacroix *et al.* 2002). Therefore, the cell growth and distribution equation takes the form (Boccaccio *et al.* 2011):

$$\frac{\partial c}{\partial t} = D\nabla^2 c + cs\left(C_c\right) - kc \tag{2.10}$$

The first term of the right hand side of equation (2.10) describes cell migration modeled as diffusion, the second term describes cell differentiation, where C_c is the chemical or nutrient concentration and s is a function describing the differentiation rate per cell. The third term describes cell death or destruction, where the constant k describes the cell death rate (Boccaccio *et al.* 2011). So, the concentration of cells in a given volume (or the cell volume fraction) depends on the chemical or nutrient concentration, cell differentiation and death rate.

2.2.4 Modeling of three-dimensional (3-D) tissue growth

To predict three-dimensional (3-D) tissue growth a cell growth model and the corresponding change in porosity or permeability must be included in the flow and the nutrient transport equations. The velocity field from the flow equation can be used to solve the mass transfer equation and determine the nutrient concentration. As noted above, the cell growth model uses an equation that is a function of the nutrient concentration, cell differentiation and death rate. The nutrient concentration obtained from the mass transfer equation can be substituted into the cell growth equation to solve for the cell density. The cell density can be used to update the

permeability and porosity of the porous TECs. Then, the entire system can be marched forward in time to predict the tissue growth. A schematic of the 3-D tissue growth model is described in Fig. 2.2.

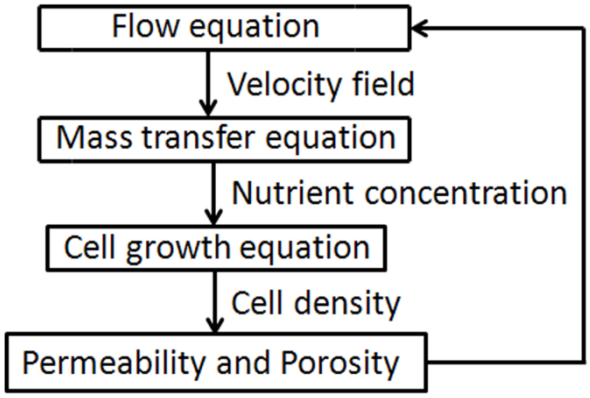

Figure 2.2: The algorithm which describes a tissue growth model.

This modeling approach has been adopted in a number of studies, i.e. Chung *et al.* (2007) and Shakeel (2011). In Chung *et al.* (2007) the cell population dynamics simulation shows an initial stage of exponential growth which later slows down when the fraction of occupied nodes becomes significant. One major disadvantage of these studies is the cell growth equation used was only a function of nutrient concentration. Chung *et al.* (2007) used a constant cell differentiation and apoptosis rate in the cell growth equation, and shear stress induced cell differentiation and death was ignored. It is well established that cell metabolism is affected by fluid shear stress levels, within limits, and tends to stimulate the release of specific enzymes and growth factors that enhance cellular proliferation (Singh *et al.* 2005). For example, chondrocytes proliferate better under the influence of non-severe shear stresses and hydrodynamic loads, which are a function of the flow velocity and structure of the TECs, as compared to chondrocytes cultured statically (Singh *et al.* 2005). In this study the influence of the shear stress and hydrodynamic load on the chondrocyte proliferation has been considered, however deformation of the TECs due to the shear stress and hydrodynamic load is ignored.

Sacco *et al.* (2011) and Raimondi *et al.* (2011) developed a multiphysics/multiscale computational model for the biomass growth simulation in a TEC cultured in an interstitial perfusion bioreactor. In their study, the term “biomass” represented the entire volume of

biological matter resulting from cell proliferation and ECM synthesis, and the influence of the shear stress on the biomass growth was investigated. The simulation results obtained from this model are in good agreement with those reported by Chung *et al.* (2007).

2.2.5 Mechanoregulation Theory

The mechanical environment of the culture process influences the tissue differentiation. Therefore, different mechanoregulation theories which consider the influence of fluid velocity, hydrostatic pressure, shear stress and strain, have been established to predict the tissue differentiation. For example, in the field of bone tissue engineering, Pauwels (1960) developed a mechanoregulation theory for tissue differentiation based on mechanical stimuli i.e. hydrostatic pressure and shear strain. Claes *et al.* (1999) proposed a theory which relates the local tissue formation in a fracture gap to the local stress and strain. A mechanoregulation theory based on octahedral shear strain and fluid velocity has been developed by Isakssona *et al.* (2006) to predict distraction osteogenesis and bone healing. Distraction osteogenesis is the procedure whereby large volumes of new bone can be generated by the controlled displacement of a bone fragment (Isakssona *et al.* 2006). Bone healing is a biomechanical phenomenon where the bone structure can be regenerated even after a multi-fragment fracture (Prendergast *et al.* 2002). More recently Khayyeri *et al.* (2009) also developed a mechanoregulation theory for mesenchymal stem cell differentiation based on a combination of fluid flow and shear strain obtained using finite element analysis. The computational simulation of the model was compared with experimental results of an *in vivo* bone chamber experiment (Tagil *et al.* 1999) and indicated qualitative agreement with histological data. In Khayyeri *et al.*'s study, the model of biophysical stimulus (S) for cell differentiation was given by:

$$S = \frac{\gamma}{a} + \frac{v}{b} \tag{2.11}$$

where γ is the shear strain rate, v is the fluid velocity, and a = 0.0375 and b = 3 μm/s. Cell differentiation occurs for favorable S values while for unfavorable S values, apoptosis occurs. The cell differentiated into fibroblasts, chondrocytes and osteoblasts, depending on the magnitude of S, for example, $S < 1$ results in osteoblasts, $1 < S < 3$ results in chondrocytes and S

< 3 results in fibroblasts. In this study the mechanical stimulus was created by applying pressure on the top surface of the chamber, and a lattice approach with stochastic cell migration, proliferation and selected differentiation was adopted to simulate the cell activity. The modeling approach of Khayyeri *et al.* (2009) was able to predict the tissue differentiation in some of the experimental specimens, but was unable to predict the full variability of responses for all the experimental specimens. To date, mechanoregulation theories have been used to predict the *in vivo* bone healing and distraction osteogenesis.

It is well established that the growth and differentiation of many cell types is regulated by external signaling; flow induced shear stresses as well as the oxygen and other nutrients supplied to the cells are important external sources (Bottaro *et al.* 2002). The cells can sense the extracellular signals; when the signal reaches the nucleus, it triggers the specific expression/repression of particular genes (Korossis *et al.* 2005). Thus, the extra-cellular signals promote or restrain cell and overall tissue growth. Several studies are also found in the literature which investigate the influence of the shear stress on the responses of different stem cells cultured *in vitro* (McCoy *et al.* 2012; Hidalgo-Bastida *et al.* 2012). These studies illustrate the feasibility of developing quantitative models for cell and tissue growth, which include the influence of shear stress and external mechanical environment. For the *in vitro* culture process the influence of mass transfer is also important and needs to be incorporated in the cell differentiation or growth equation. Although mechanoregulation theories are not widely applicable to predict the cell growth *in vitro* culture process, it is an example of a model formulation which tries to include the effect of velocity and flow induced strain on cell differentiation.

2.3 *In Vitro* Investigation of Tissue Engineered Constructs by CFD

In a bioreactor, several parameters can be used to control the fluid flow and mass transfer, thus providing a means to improve the *in vitro* culture of TECs (Singh *et al.* 2005). From the discussions in previous sections, it is clear that obtaining the fluid velocity and shear stress fields inside the porous TECs during the culture process is really important for predicting the overall tissue growth and to determine optimal operating conditions for tissue culturing. A number of experimental and computational studies have tried to measure or predict flow information inside

the bioreactor during the culture process. The shear stress induced on cells cultured in 3-D TECs varies for different bioreactors. Even within the same type of bioreactor, the shear stresses vary due to dissimilar bioreactor and construct geometries. A better understanding of the flow phenomena inside the different types of bioreactors would help to determine the shear stresses acting on cells attached on the surface or being convected inside of the TECs. CFD can provide this critical information. CFD can also efficiently assess design modifications and determine the variation in the wall shear stresses acting on the constructs, when their geometry and location inside the bioreactor is varied (Bilgen *et al.* 2007; Gutierrez *et al.* 2007).

Different types of direct perfusion bioreactors and non-perfusion bioreactors have been developed for *in vitro* tissue cultures (Singh *et al.* 2009), and these can be generally classified into spinner-flask, rotating-wall, wavy-walled, and dynamic compression type vessels. In spinner-flask bioreactors, mass transfer occurs via convection, and fluid flow at the surface of the tissue construct is turbulent (Lanza *et al.* 2000). This type of bioreactor has shown itself able to increase cell differentiation while culturing cartilage TECs (Vunjak-Novakovic *et al.* 2004). Although the turbulent eddies enhance mass transfer into the scaffolds, the turbulent flow can also create excessive shear stress levels in the vessel (Singh *et al.* 2006). In rotating-wall vessel bioreactors, flow at the surface of the TECs is laminar (Lanza *et al.* 2000). Cartilage TECs cultured in this type of bioreactor contain fewer cells but more glycosaminoglycan (GAG) and collagen than those cultured in spinner-flasks which increases the ECM production (Lanza *et al.* 2000). Gutierrez and Crumpler (2007) used a CFD model to simulate the shear stress on TECs with different structures, which were cultured in rotating-wall bioreactors under Couette flow conditions, and found that the wall shear stress could be significantly affected by the TEC structure. Both spinner-flask and rotating-wall vessel bioreactors produce mixing at the surface of the scaffolds that enhances the growth of the TECs compared to traditional culturing systems, such as petri dishes or solid-body rotation. However, the GAG or collagen growth is only improved at the surface of the TECs since these types of bioreactors are not capable of transporting the nutrients into the interior of the porous TECs.

Bilgen and Barabino (2007) employed a CFD model for unsteady turbulent flow to characterize the hydrodynamic environment in a wavy-walled bioreactor. A $k-\varepsilon$ turbulence model was created for the CFD simulation with the results showing that the velocity and shear

stress distribution varied with the axial and radial locations of the TECs. The simulation also indicated that this type of bioreactor reduces the shear stress applied to the TECs compared to the spinner flask bioreactor. To reduce the shear stress acting on the cells inside the TECs and also to improve the mass transfer inside the porous constructs during the culture process, different direct perfusion bioreactors have also been developed and in some studies direct perfusion bioreactors have been found advantageous over non-perfusion bioreactors (Chung *et al.* 2007).

Turning consideration to perfusion bioreactors, in these systems the flow is typically laminar, so the shear stress is much less than for the spinner flask and wavy-wall type bioreactors. Perfusion bioreactors typically enhance the mass transfer because they allow the medium to be transported through the interconnected pores of the constructs (Chung *et al.* 2007; Bancroft *et al.* 2003). The mass transfer is dominated by convection due to recirculation (Lanza *et al.* 2000). TECs within the perfusion bioreactors sometimes also suffer from cell "wash-out" (Singh *et al.* 2006). In this case, due to the hydrodynamic forces generated by the flow, cells near the TEC faces which are exposed directly to the flow tend to move, often resulting in tissue growth being restricted to the middle and rear regions of the TEC. McCoy *et al.* (2012) developed a model for cell detachment on the TECs within perfusion bioreactors supported by experimental validation; their experimental results show the cell detachment is affected by the shear stress imposed on the cells, depending on the flow rate, the pore size and the material properties of the TECs. As such, control over these parameters would provide cells with an environment which favors their attachment and growth (McCoy *et al.* 2012; Bilgen *et al.* 2007).

Porter *et al.* (2005) used a CFD code based on the lattice Boltzmann method (LBM) within the scaffold to simulate flow of the cell culture media through the complex 3-D structure for a perfusion type bioreactor. The geometry of the TEC was reconstructed by micro-computed tomography (MicroCT). MicroCT is capable of providing a 3-D image of the microarchitecture of interest. From the microCT images the TEC geometry can be reconstructed and then used with the appropriate geometry and boundary conditions for CFD analysis. By using microCT images, more realistic and accurate solutions are possible since the geometry and architecture of the TEC used in the simulation is more accurately defined. Porter *et al.* (2005) used the resulting 3-D velocity field to calculate the local internal shear stress distribution as shown in Fig. 2.3. The LBM numerical method was used to simulate the TEC, and 2.5 million 3-D elements were

solved, including 1.2 million fluid elements and 1.3 million solid elements. The study predicted that an average surface shear stress of 0.05 mPa resulted in the highest cell viability and proliferation for a perfusion flow rate of 0.1 mL/min (2005), although the authors did not mention exactly how this conclusion was reached. Important insight has been obtained in studies like Porter *et al.* (2005), but still more accurate and efficient numerical simulation methods are required in this area. For example, in this study the code was validated by comparison to the flow between parallel plates. The uncertainty of the LBM solution was within 5% for the surface shear stress when compared with the analytical solution, which might be considered relatively high for such a simple flow. The flow within the porous TEC is much more complex due to the complicated pore geometry.

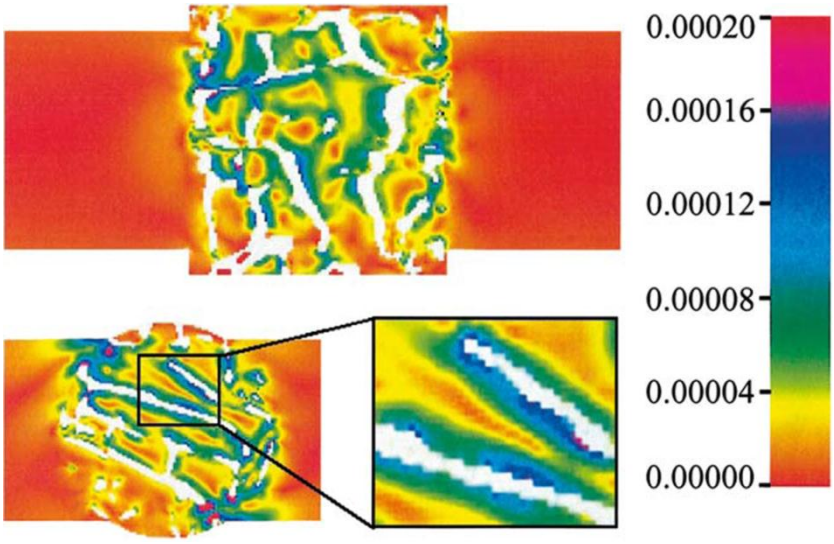

Figure 2.3: Map of local shear stresses (Pa) in media transversely perfused through a 3D trabecular bone TEC from side and top view (Porter *et al.* 2005).

Cioffi *et al.* (2006) reconstructed a TEC geometry from microCT images of a biodegradable polyestherurethane foam TEC and used the FLUENT software package for the flow simulation. The average, median, and mode shear stress values calculated at the construct walls were 3.48, 2.90, and 2.45 mPa, respectively, at a flow rate of 0.5 cm^3/min, perfused through a 15 mm diameter scaffold at an inlet fluid velocity of 53 μm/s. This average shear stress value is higher than that obtained by Porter *et al.* (2005) for a lower pore diameter and higher flow rate. Cioffi *et al.*'s median shear stress (2.90 mPa) value is similar to the median shear

stress (2.98 mPa) obtained by Raimondi *et al.* (2004) for a simplified construct micro architecture of the same (polyestherurethane foam) TEC used for the flow analysis. Also, in the study of Raimondi *et al.* (2004) the flow rate (0.5 cm^3/min) was the same as in Cioffi *et al.*'s work, but the inlet velocity (44 μm/s) was slightly different. This similarity in the results led Cioffi *et al.* (2006) to conclude that in direct perfusion bioreactors the actual micro geometry of the foam TEC with interconnected pores does not significantly affect the median shear stress acting on the inner TEC walls at low Reynolds numbers.

Chung *et al.* (2007) showed that a perfusion bioreactor enhances cell growth and the cell distribution is more uniform throughout the constructs than in static cultures and other types of bioreactors mostly due to a more even distribution of nutrients. In this study, the authors adopted the tissue growth model as described in section 2.3. By using the volume-averaged momentum and mass transfer equation, the macroscopic shear stress and nutrient concentration distribution were obtained, as shown in Fig. 2.4. The viscous shear stress (Fig. 2.4) has a maximum value of 0.18 mPa at the TEC periphery closest to the chamber wall (along $x = 0$). The simulations also indicate that the average shear stress values were 0.12 and 0.5 mPa for overall permeability values of 1.35×10^{-2} and 5.51×10^{-4} cm^2, respectively, at a perfusion rate of 20 μm/s. From the simulation of Chung *et al.* (2007), it was also found that the shear stress induced in the cellular constructs increased with cell growth as the void pore sizes and overall permeability of the TEC decreased. This change occurs because of the increase in cell population dynamics, such as cell differentiation, proliferation, the migration and ECM production, although the influence of the increased shear stress on the cells was ignored. Chung *et al.* (2007) also verified the effect of media perfusion by including the time dependent porosity and permeability changes due to the cell growth.

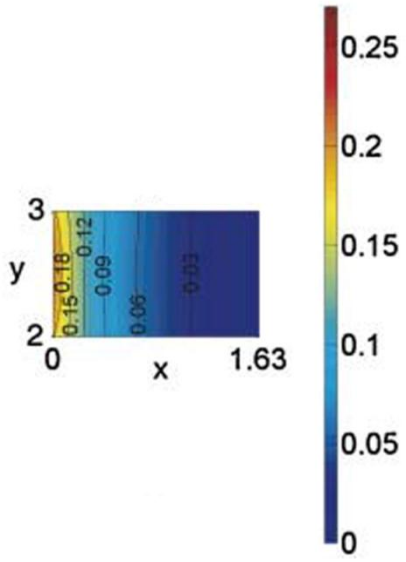

Figure 2.4: Contours of macroscopic viscous shear stresses (mPa) after 30 days of culture, at a Peclet number of 100 and 20 μm/s perfusion rates (Chung *et al.* 2007).

Hidalgo-Bastida *et al.* (2012) studied the flow in a perfusion bioreactor with circular and rectangular cross-sections. Their results demonstrated that in the circular cross-section bioreactor, the flow velocity and shear stresses changed significantly in the peripheral regions and the regions near the bioreactor inlet and outlet, as compared to the rectangular cross-section bioreactor. The authors adopted the following special form of the Navier-Stokes equation (Hidalgo-Bastida *et al.* 2012; Bruneau *et al.* 2008):

$$\frac{\partial V}{\partial t}+\left(V\cdot\nabla\right)V-\frac{1}{\mathrm{Re}}\Delta V+\frac{V}{K}+\nabla P=0 \tag{2.12}$$

This equation is valid in the fluid, porous and solid regions with different values of the permeability K. Generally, this type of alternative strategy, which is both robust and cost effective, can be applied if the principal focus is on the design optimization of the bioreactor and the detailed velocity and shear stress fields within the TECs are not required (Hidalgo-Bastida *et al.* 2012).

A comprehensive 3-D tissue growth model is necessary to predict the overall tissue growth that includes the changes in permeability of the porous structure in the simulation. Cheng

et al. (2006) present a model to simulate the dynamics of a cell population based on the key processes of migration, cell-cell collision, and proliferation. One limitation of their model was the use of a highly porous structure and not coupling cell population dynamics with nutrient transport and the flow environment. Galbusera *et al.* (2007) modified Cheng *et al.*'s model to introduce oxygen transport and consumption. The new model accounts for cell population dynamics using a model based on cellular automata. The calculation of the velocity field was carried out by the LBM and the velocity field was employed for the calculation of convective oxygen transport. In this model, there was no implementation of the coupling between the velocity field and cell distribution. The authors obtained similar results as Chung *et al.* (2007) for the cell population dynamics.

The modeling approaches discussed above include tissue growth by coupling cell population dynamics with nutrient transport and consumption. However, the forces experienced by the cells due to the dynamic nutrient flow and the impact of the flow forces typically have not been considered. Lemon and King (2007) developed a multiphase model for the growth of biological tissue where the cells, water, and solid scaffolds are considered as different phases. Using this approach, the authors obtained a more realistic flow-induced stress calculation, but without the consideration of nutrient transport and consumption. Therefore, comprehensive and detailed 3-D tissue growth models still need to be developed which specifically incorporate realistic flow behavior, appropriate nutrient transfer and the effects of cell population dynamics. While computational modeling already plays an important role in the development of overall 3-D tissue growth models, the reliability and accuracy of the computational models and methods needs to be validated using experimental results. More specifically, the fluid flow simulation through and around the TEC obtained by CFD needs to be carefully validated by comparison to experiments.

2.4 *In Vitro* Investigation of Tissue Engineered Constructs by Experimental Methods

Information regarding the velocity and shear stress fields based on CFD techniques is clearly of value for culture system design. However, from the discussion in the previous section, the application of new and improved CFD techniques is required to obtain more realistic prediction of the flow behavior in TECs. Lagana *et al.* (2012) developed a miniaturized and optically accessible bioreactor for direct perfusion of 3-D TECs. The cell proliferation and tissue growth were quantified non-destructively by using a fluorescence video imaging method. In their study, CFD was also used to characterize the flow, although its experimental validation was not conclusive. Different optical velocity measurement techniques, such as particle image velocimetry (PIV), laser Doppler anemometry (LDA), synchrotron X-ray PIV techniques and Doppler Optical Coherence Tomography (DOCT) can play an important role. The measurement of fluid velocities within porous and multiphase media is a concern not only for tissue engineering but also for many other engineering applications. For this reason, research in the past two decades has aimed to better understand fluid flow phenomena in porous media using optical measurement techniques. The current review will focus on studies which have used PIV techniques and DOCT to obtain the flow information. LDA is another viable optical measurement technique. It can provide greater spatial resolution of the velocity field than is possible with PIV, but PIV is capable of providing multi-point flow diagnostics while LDA is single point measurement technique.

2.4.1 Particle Image Velocimetry (PIV)

PIV is a non-intrusive optical technique able to provide measurement of the instantaneous velocity vectors in a cross-section of the flow (Adrian 2005). Using PIV, the local 2-D velocity field can be obtained with high accuracy. This technique is suitable for laboratory investigation of both laminar and turbulent flow. A typical PIV set-up consists of a charge coupled device (CCD) camera, a high-power laser, an optical arrangement to convert the laser output light to a light sheet, tracer particles, and a synchronizer. The small seeding particles must be illuminated in a plane of the flow at least twice within a certain time interval. The plane is divided into many smaller fields of views (FOV). The positions of particles within a FOV during two consecutive

laser pulses are recorded by a double-frame CCD camera. The typical width of a FOV in the fluid is of the order of 100 mm, but both larger and smaller fields are possible (Adrian 1997; Raffel *et al.* 1998). The local flow velocity is then calculated from the displacement of the particles between the two light pulses. Sophisticated post processing is required to handle the large amount of data produced (Adrian 1997; Raffel *et al.* 1998).

Application of this measurement technique to porous structures is challenging, Northrup *et al.* (1991a) were the first to report use of PIV in conjunction with refractive index matching to measure fluid velocities within a complex porous structure. They developed a fluorescent PIV technique and measured the velocity vector field in a porous medium test bed made from 9.4 mm diameter polymethyl methacrylate (PMMA) balls for very low flow velocities (tens of microns per second). This method is known as index matched fluorescent PIV (FPIV), and the use of fluorescent particles along with proper refractive index matching allowed clear PIV images of the flowing fluid to be obtained in the porous medium test bed. Other similar experimental techniques such as particle streak velocimetry (PSV) and particle tracking velocimetry (PTV) have also been employed for measuring fluid velocities in porous media (Peurrung *et al.* 1995; Northrup *et al.* 1991b).

Non-intrusive velocity measurement is one of the major advantages of the PIV technique, since it does not need to insert any probes into the flow. PIV was mostly developed for relatively high Reynolds number (Re) or high speed flows, as well as for flows near walls and within very small structures where the flow would be disturbed by the presence of a probe (Raffel *et al.* 1998). In most cases the flow inside the porous TEC is relatively slow and the microarchitecture of the constructs is complex. For this reason, PIV techniques have not been extensively used for measuring the velocity field inside porous TECs, but rather for the characterization of the flow inside bioreactors, which typically has a higher Reynolds number. Standard PIV only measures the velocity components in a plane which is one of the major disadvantages of using a 2-D PIV system to study a 3-D flow field. Stereo-PIV (SPIV) can be used to measure all three components of velocity in a variety of flows. The technique uses two cameras, set at an angle to one another, to record two mappings of the flow field. Recombination of the mappings allows all three components of the velocity field to be measured. This technique has also been carried out in micro-channel geometries. Bown *et al.* (2006) used a flow device

consisting of a backward facing step in a wide micro-channel manufactured in glass. The flow passed from a 234 μm deep channel, over the step into a 466 μm deep channel. The flow was driven by a pressure gradient, which was generated by elevating the inlet reservoir a known distance above the outlet. The authors obtained all three components of the velocity field, and compared the three dimensional vector mappings of the flow field over the micro step with the result from CFD (Bown *et al.* 2006). The difference between the experimental and computational results was 3% for the in-plane velocity components and 7% for the out-of-plane velocity components. Across the entire channel, the CFD and PIV agreed within the 5% for the in-plane and 8% for the out-of-plane components. This 3-D or stereo PIV could be a viable technique for studying the 3-D velocity field within porous TECs.

Dusting *et al.* (2006) studied the flow in spinner-flask bioreactors both computationally and experimentally; the bioreactors were used for the production of articular cartilage tissues *in vitro* (Sucosky *et al.* 2004). Using the SPIV technique, the velocity and shear-rate fields were determined in the vicinity of the construct closest to the stir bar in a scaled-up modeled bioreactor, where the flow generated by the rotating stir bar is both turbulent and unsteady in the mean (Dusting *et al.* 2006). Fig. 2.5 shows the experimental set-up for Dusting *et al.*'s study.

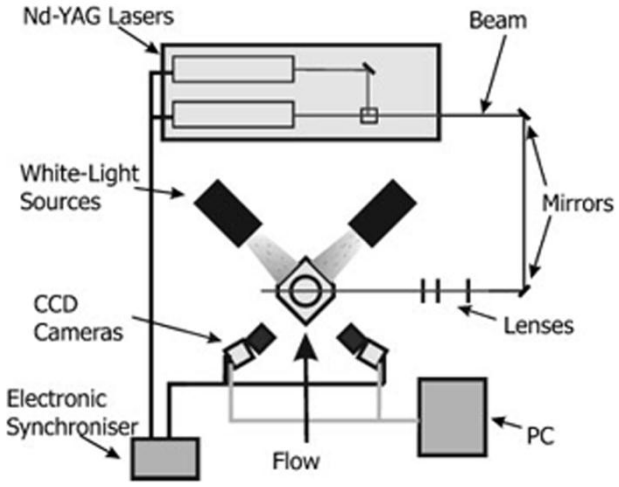

Figure 2.5: Annotated schematic of the SPIV configuration, viewed from above (Dusting *et al.* 2006).

Numerical computations were performed for the same model bioreactor and operating conditions using the commercial software package FLUENT. One major issue in the experimental simulation was obtaining high quality data from the optical-acquisition system which then affected the reliability of the PIV technique (Dusting *et al.* 2006). The model bioreactor was designed with plane external walls and compensation for the refraction of the curved inner wall of the vessel was accomplished by matching the refractive indices of the model bioreactor material and culture medium. The results obtained from the experiments and computations were in reasonable agreement. In the experiment, a Nd:YAG laser was used to generate a pulsed output beam with a wavelength of 532 nm. The resolution of the camera was 768 × 484 pixels and the desired FOV was 0.91 × 0.69 cm^2. The images obtained were analyzed by MATLAB programs. This study had one important limitation: the velocity and the shear stress profiles were only obtained in the vicinity of the TEC but not inside the TEC itself (Dusting *et al.* 2006). Also in this spinner-flask bioreactor the Reynolds number of the flow was 1758 and the flow was considered completely turbulent. Generally, in perfusion type bioreactors the Reynolds number is much lower, typically less than 1 (Isakssona *et al.* 2006). Thus, the time difference between two consecutive laser pulses must be large enough that the displacement of the particles can be differentiated in the CCD camera images.

2.4.2 Micro-PIV

A micron-resolution particle image velocimetry (micro-PIV) system would be most appropriate to obtain the velocity and shear stress field inside the porous TECs while culturing *in vitro*. Use of a micro-PIV system to measure instantaneous and ensemble-averaged flow fields in micron-scale fluidic devices was first reported by Santiago *et al.* (1998). Micro-PIV is a modification of PIV to work with microfluidic devices, and the set-up consists of similar components plus a microscope (upright or inverted) equipped with fluorescent filters. A number of major factors distinguish micro-PIV from PIV including: small seeding particles compared to the wavelength of the illuminating light; a requirement for fluorescence imaging in micro-PIV; the particles should be small enough to closely follow the fluid without disrupting the flow and large enough to dampen the effects of Brownian motion (Santiago *et al.* 1998; Mielnik *et al.* 2004). Different types of fluorescent polystyrene beads with specific gravities of approximately 1.05 g/cm^3 are available for micro-PIV applications. The diameters of the particles vary from tens of

nanometers to several microns. For such small particle sizes, Brownian motion may become a source of error in the measurement of particle displacement between images for very low velocities (Mielnik *et al.* 2004).

An important difference between PIV and micro-PIV systems is the flow illumination procedure. In PIV, the measurement is typically confined to a single plane within the fluid flow, which is illuminated by a thin sheet of laser light; in micro-PIV, the entire volume of the flow is illuminated as use of a laser light sheet is not feasible (Mielnik *et al.* 2004). Due to the illumination of the entire flow field the out-of-focus emitted light can result in high levels of background noise (Meinhart *et al.* 2000). One way to minimize the depth-of-focus problem is using confocal micro-PIV where the conventional PIV system uses a spinning disk with the confocal microscope (SDCM) (Lima *et al.* 2008). The SDCM has the ability to obtain in-focus images with an optical thickness less than 1 μm. Lima *et al.* (2008) studied the flow behavior of physiological saline (PS) and blood through a PDMS micro channel using a confocal micro-PIV system. This PIV system consisted of an inverted microscope with a 20× objective lens combined with a confocal scanning unit, a diode-pumped solid state laser, and a high-speed camera. Fluorescent tracer particles were seeded within the micro channel. A high-speed camera was used to record the PIV images. Fluid velocities up to 0.48 mm/s have been measured using a confocal micro-PIV system.

Provin *et al.* (2008) investigated a method to design the microstructure and geometry of a PDMS (polydimethylsiloxane) scaffold to allow high density cell cultures, then validated the method by measuring the flow distribution within the scaffold by micro-PIV. The scaffold thickness was 80 μm and an inverted fluorescent microscope with a mercury lamp and a 40 × objective lens was used in the micro-PIV system. Deionized water with 1 μm diameter tracer particles was used as the working solution. The camera resolution was 800×600 pixels, the analyzed area 500×460 pixels, and the resolution 0.35 μm/pixel. The velocity profile was taken between two pillars and on the central plane of the scaffold. The velocity profiles obtained by a companion numerical simulation were 8-20% higher than the experimental results.

De Boodt *et al.* (2010) conducted a study on the spatial and temporal flow characteristics inside a porous bone tissue engineered scaffold using both CFD and micro-PIV measurements. In their micro-PIV experiments, the bioreactor was filled with distilled water containing opaque polyamide particles, with an average diameter of 20 μm and a density of 1.03 g/cm^3. Images were captured with a cooled CCD camera mounted on a stereomicroscope. The stereomicroscope uses two separate optical paths with two objectives, two eyepieces and two intermediate lens elements which produce two distinct images with slightly different viewing angles to the left and right eyes. In this way it produces a three-dimensional visualization of the sample being examined. Each image of 600 × 800 pixels was preprocessed and, for every two subsequent images, a vector field was calculated with an optical flow algorithm in MATLAB.

In this study, the authors made a quantitative comparison between the CFD and the micro-PIV results for the fluid flow inside the TECs. The computational and experimental models were validated by comparing the results with the flow in a parallel plate set-up. The authors found that the average velocity inside the TEC simulated by CFD was 19% higher than the velocity measured by the micro-PIV (De Boodt *et al.* 2010). The average shear stress at the TEC wall (WSS) was 2.4 mPa based on the micro-PIV measurements and 3.3 mPa for the CFD simulations (27% difference). The authors mentioned that it is not known yet if the differences in the velocity and shear stress found in the study are large enough to influence the outcome of the biological experiments performed with the perfusion system (De Boodt *et al.* 2010). However, such comparative studies between CFD and experimental simulation are important to understand the reliability and accuracy of CFD models.

2.4.3 Synchrotron X-ray PIV

A recent development in velocity measurement within opaque structures is synchrotron X-ray PIV, or the combination of X-ray micro-imaging with the PIV technique (Kim *et al.* 2007; Fouras *et al.* 2007). Synchrotron X-ray micro-imaging has been used for imaging various internal structures (Kim *et al.* 2007), but typically no velocity information was obtained. However, PIV can measure the velocity field using a digital image processing technique. Applying PIV alone to opaque vessels or porous structures is challenging as it requires clear

optical access to the region of interest (Fouras *et al.* 2007). However, combining these two methods can overcome these limitations. Kim *et al.* (2007) used X-ray PIV to investigate the flow characteristics of blood. A non-monochromatic synchrotron beam (~10-60 KeV) was used from the Pohang (Korea) light source beam line. The blood flow was directly visualized in an opaque tube using the phase-contrast and interference based edge enhancement methods of synchrotron X-ray micro imaging without any tracer particles. The speckle patterns of the blood flow were obtained by using the X-ray beam and the PIV algorithm was applied on the blood pattern images to extract the velocity field information. Images were captured by a CCD camera with 1280×1024 pixel resolution and 6.7×6.7 μm^2 in physical pixel size. The FOV of the whole image was 642×514 μm^2 using a 10× objective lens to give 0.502 μm/pixel. A PIV algorithm based on the X-ray images enabled the instantaneous velocity field of the blood flow to be measured.

Fouras *et al.* (2007) measured the 3-D velocity field within a cylindrical tube using the X-ray PIV technique. A biomedical beam line was used with a 25 KeV X-ray beam, 25 mm in height and 40 mm in width. The flow pipe diameter was 15 mm and the Reynolds number of the flow was 10^{-4}. The pipe was filled with glycerin and silver coated hollow glass microspheres were used as the tracer particles.

To date, this technique has not yet been employed for velocity measurements in TECs, but it could be a viable technique for this particular application, especially since most TECs are made of opaque material.

2.4.4 Doppler Optical Coherence Tomography (DOCT)

Optical coherence tomography (OCT) is a non-invasive optical imaging technique which is able to obtain the volumetric image of the internal structure of 3-D specimens with high resolution (Jia *et al.* 2009). DOCT combines OCT with Doppler velocimetry, and is capable of producing simultaneous images of both tissue architecture and localized fluid flow. Using the DOCT technique, Jia *et al.* (2009) examined the localized fluid flow and shear stress within low- and high-porosity chitosan scaffolds and determined that the shear stress varied from one micro pore to another, e.g. with mean values of 0.49±0.3 and 0.38±0.2 $dyn \cdot cm^{-2}$. The drawback of using this technique is that the OCT imaging depth is limited to 3 mm for highly scattering biological tissues.

Table 2.2 summarizes the advantages and disadvantages of applying different experimental techniques to obtain the fluid flow information inside porous TECs.

Table 2.2: Advantages and disadvantages of different experimental techniques

Experimental Techniques	***Advantages***	***Disadvantages***	***References***
PIV	1. Non-intrusive velocity measurement. 2. Suitable for high Re flow measurement. Useful for the flow characterization inside the bioreactor which has a higher Re. 3. 3D or stereo PIV has the ability to measure all three components of the velocity field.	1. Needs clear optical access to the region of interest; transparent bioreactors and TECs are needed. 2. Difficult to measure the fluid velocity and shear stress field inside the small TECs.	Peurrung *et al.* (1995); Northrup *et al.* (1991); Bown *et al.* (2006)
Micro PIV	1. Suitable for microfluidic devices and low Re flow. 2. 3-D stereo micro-PIV is able to obtain the 3-D velocity fields at various depths in the TEC.	1. Needs clear optical access to the region of interest; transparent bioreactors and TECs are needed. 2. Volume illumination procedure results in high levels of background noise.	Mielnik *et al.* (2004); Meinhart *et al.* (2000); Lima *et al.* (2008)
Synchrotron X-ray PIV	1. Highly suitable for flow characterization in opaque porous structures. 2. Able to measure the 3-D velocity field.	1. Synchrotron beam line is required to obtain the X-ray micro-imaging.	Kim *et al.* (2007); Fouras *et al.* (2007)
DOCT	1. Non-invasive optical imaging technique. 2. 3-D flow information can be obtained.	1. Flow information can be obtained only at a certain depth due to the limitation in imaging depth.	Kim *et al.* (2007)

Some critical information such as the shear stress, hydrostatic stress, oxygen concentration and bioreactor type which were found to be favorable for cell and tissue growth in different studies has been summarized in Table 2.3.

Table 2.3: Summary of the culture parameters found to be favorable for the cell and tissue growth in various studies

Tissue type	*Reported shear stress, hydrostatic stress, mass transfer information favorable for cell and tissue growth*	*References*
Bone	A shear stress of 5×10^{-5} Pa correlated to the highest cell viability and proliferation at a flow rate of 0.01 ml/min in a perfusion bioreactor for human trabecular bone.	Porter *et al.* (2005)
	A shear stress of 0.015 Pa (0.013-0.018Pa) and flow rate of 3 ml/min can produce better engineered tissue in a perfusion bioreactor for culturing the human bone marrow-derived mesenchymal stem cells (hBMSCs).	Li *et al.* (2005)
	The macro average stresses increased from 0.2 mPa to 1 mPa at a perfusion rate of 20 mm/s with the overall cell volume fraction growing from 0.4 to 0.7.	Chung *et al.* (2007)
	MSC differentiation in a bone chamber was predicted under the effect of manually applied pressures of 1 MPa, 2 Mpa and 3 Mpa. Higher fibroblasts tissue formation occurs at 3 MPa; Chondrocytes and Osteoblasts differentiation was higher at 1 MPa.	Khayyeri *et al.* (2009)
	Characterization of the flow within a highly porous collagen based TEC was performed in perfusion bioreactor. In 2D, osteogenic differentiation is enhanced in the shear stress range of 0.1–1.5 Pa.	Bottaro *et al.* (2002)
	Human Osteosarcoma cells were cultured in an optically accessible perfusion bioreactor with an optically transparent TEC. The maximum flow rate was 25 ml/min and the shear stress range inside the TEC was 0-21 mPa. The number of cells increased from 15-43000 and tissue growth was 2% to 43% during culture time.	Galbusera *et al.* (2007)
Cartilage	In a controlled mechanical stimulation it was found that 2 MPa compressive hydrostatic stress enhanced cartilage growth.	Tagil *et al.* (1999)
	Primary bovine calf chondrocytes were seeded on fibrous polyglycolic	Gutierrez

acid meshes and cultured in spinner flask bioreactor. TECs exposed to mixing in the bioreactor contained higher percentages of collagen, and synthesized and released more GAG.	*et al.* (2007)
The convective oxygen transport was found favorable for the cell growth in a perfusion bioreactor. Also oxygen concentration within the range of 0.17-0.2 nmol/mm^3 was found favorable for the cell growth.	Bruneau *et al.* (2008)

2.5 Recommendation for Future Research

One of the major purposes for investigating the culture of TECs inside bioreactors is to develop a comprehensive tissue growth model which can be used to design the optimal environment for the growth of tissues. To achieve this goal, further research is required to develop improved models, to obtain local information inside the TEC and to validate the CFD results and simulation by experimental techniques.

Improved Models:

The capability of CFD to predict fluid flow and mass transfer at the pore level inside the TEC, as well as to provide information about the impact of the dynamic flow environment on cells in the culture process, has already been demonstrated. The cell growth model adopted in most studies is only a function of nutrient concentration. On the other hand, the mechanoregulation theories developed for the *in vivo* experiment of bone tissue engineering is only a function of mechanical environment. From the description of different studies given in the previous sections, it is clear that the cell differentiation, proliferation and migration during the *in vitro* culture process depend on mechanical environment, i.e. the flow induced shear stress on the cells and the nutrient supply to the cells inside the porous TECs. Recently, models have been developed to relate the biomass growth to both the nutrient transport and local shear stress field. However, such models still need to be verified by comparison to biological experiments. A cell growth model based on velocity and shear stress would require accurate flow information at the local pore level in order to provide realistic predictions of cell growth.

Use of Resolved Scale Method to provide local information:

For CFD flow simulation two different approaches have been used so far. Volume averaging has been used to obtain average flow information inside porous structures. The alternate approach is to obtain detailed flow information throughout the porous structure. Although knowledge of the average fluid flow inside the TECs can help to improve the flow environment in a bioreactor, the information obtained by this approach is macroscopic and disregards the effect of TEC micro-architecture on the local velocity field. The significance of the variation in flow forces acting on the cells due to the micro-architecture of the TECs is not resolved. Local information would be required to design the most suitable flow environment inside the bioreactor. As mentioned by Singh *et al.* (2009), in most studies, cells are only considered to be attached to the pore walls; however, cells can also occupy in spaces between the pore walls. Local flow information for a fully-resolved pore geometry would be required to determine the flow forces acting on cells located in the free pore spaces as well as those cells attached to the pore walls. Detailed knowledge of the flow forces acting on the cells is essential for developing improved cell growth models.

A closely related issue is the impact of flow forces on cell differentiation, proliferation, collision and migration as they contribute to the overall tissue growth. Local flow information could provide insight into the mechanical interaction between cells and the surrounding environment, such as the impact on the cells of cell-cell collisions and cell collisions with the construct wall. This information may also help to determine the mechanism of mechanical signal transduction to and from the cells during the culture process (Cioffi *et al.* 2006). To obtain local flow information, refined grids would need to be used in the resolved scale simulation approach. Some of the computational studies to date may not have used a sufficient number of nodes to accurately determine the effect of the micro-architecture on the local flow field. The design of a TEC with an optimized micro-architecture would also be a valuable outcome of comprehensive resolved scale studies.

Validation of CFD results using experimental techniques:

Validation of CFD predictions for the velocity fields inside TECs by experimental means is also an important issue for tissue engineering. In most cases, the computational models and/or codes

are validated using analytical or experimental results for comparatively simple flows, such as Poiseuille flow, Couette flow, or lid-driven cavity flow. Too often these flows are two-dimensional with simple geometries. Validating computer codes using such simple flows and then applying them to predict the flow through porous media with complex geometry and boundary conditions may not be appropriate. However, given recent developments in experimental techniques, it is now possible to perform experiments using flow conditions and geometries more representative of actual tissue constructs. Different PIV techniques such as stereo and micro-PIV can be used to verify the velocity field inside porous constructs. Novel synchrotron X-ray PIV techniques could be considered for constructs with limited or no optical access. Visualization of the flow in an actual TEC during the culture process is possible via x-ray imaging. The x-ray images could be analyzed to gather the velocity information, which in turn could be used to validate CFD simulations.

2.6 Conclusion

CFD is the most efficient way to analyze and characterize the flow fields inside TECs cultured *in vitro*. The results obtained using CFD models can significantly inform the design of bioreactors by revealing the flow patterns and nutrient transfer through the porous construct. This paper reviews various studies of the hydrodynamic environment inside bioreactors using both CFD models and experimental methods for *in vitro* culture of the constructs, and highlights the impact of such analysis on the tissue engineering field. This review also indicates significant opportunity still exists for future research by applying both CFD and experimental techniques. Improved computational methods are also needed to capture more accurate, yet comprehensive flow information during the culture process. Recent advances in experimental techniques have created the opportunity to apply those techniques to both validate the computational models and provide experimental insight into the culture process. Further computational and experimental studies will help to better understand the tissue growth inside bioreactors, and facilitate the development of comprehensive 3-D tissue growth models.

Acknowledgements

The authors wish to acknowledge the financial support from both the Natural Science and Engineering Research Council of Canada (NSERC) and the Saskatchewan Health Research Foundation (SHRF).

Chapter 3

Prediction of cell growth rate over scaffold strands inside a perfusion bioreactor

Md. Shakhawath Hossain, D.J. Bergstrom, X.B. Chen

(Published in: Biomech. Model. Mechanobiol., 2015, vol. 14(2), pp. 333-344)

Abstract

Mathematical and computational modelling of the dynamic process where tissue scaffolds are cultured in perfusion bioreactors is able to provide insight into the cell and tissue growth which can facilitate the design of tissue scaffolds and selection of optimal operating conditions. To date, a resolved scale simulation of cell growth in the culture process, by taking account of the influences of the supply of nutrients and fluid shear stress on the cells, is not yet available in the literature. This paper presents such a simulation study specifically on cartilage tissue regeneration by numerically solving the momentum, scalar transport and cell growth equations, simultaneously, based on the lattice Boltzmann method. The simulation uses a simplified scaffold that consists of two circular strands placed in tandem inside a micro-channel, with the object of identifying the effect of one strand on the other. The results indicate that the presence of the front strand can reduce the cell growth rate on the surface of the rear strand, depending on the distance between them. As such, the present study allows for investigation into the influence of the scaffold geometry on the cell growth rate within scaffolds, thus providing a means to improve the scaffold design and the culture process.

3.1 Introduction

In tissue engineering the scaffold-guided dynamic cell culture process plays an important role in the development of artificial tissues which can replace damaged tissues or organs (Blitterswijk 2008). The tissue scaffolds, which are made of biomaterials and seeded with cells, are typically placed inside bioreactors to facilitate cell growth prior to their implantation into animal models or human patients. Bioreactors provide nutrients and flow induced mechanical stimuli, i.e. shear stresses, to the cells to improve the overall growth of the cells and tissues (Porter *et al.* 2005; Sacco *et al.* 2010; Hossain *et al.* 2012). Among the different types of bio-reactors, perfusion bio-rectors are the most promising compared to other non-perfusion bioreactors (Porter *et al.* 2005). In the perfusion-type bioreactors, the fluid with nutrients flows through the porous scaffolds, thus supplying in a timely way the cells with nutrients. Typically, the scaffolds are made of arrays of circular strands and the diameter of those circular strands varies from 0.1 to 1.0 mm and the distance between two strands ranges from 0.1 to 1.0 mm (Yan *et al.* 2011). A number of studies are reported in the literature to optimize the scaffold design from a biochemical point of view, i.e. the biocompatibility and cell adhesion capability of the scaffold materials (Milan *et al.* 2009). However, the design of the scaffold is also important from a biomechanical point of view so as to provide adequate nutrient transport and favorable shear stress to the cells attached on the scaffold strands. The diameter of the scaffold strands, distance between the strands and orientation of the strands can affect the fluid flow through the scaffold and hence influence the shear stress generated on and nutrient supply to the cells (Yan *et al.* 2012; Singh *et al.* 2005; Singh *et al.* 2007). Improved scaffold design would enhance the cell and tissue growth during the culture process.

In the previous studies, bioreactors and scaffold architectures were designed mainly based on empirical knowledge and experience, e.g. the flow rate inside the bioreactor was selected based on a trial and error method (Singh *et al.* 2009). For improvement, computational fluid dynamics has been recently used to obtain knowledge of the fluid velocity, shear stress and nutrient concentration distribution inside the tissue scaffolds (Porter *et al.* 2005, Coiffi *et al.* 2006; Chung *et al.* 2007) as well as cell attachment (Spencer *et al.* 2013). Cell growth rates and cell volume fractions have also been predicted and are in good qualitative agreement with the experimental data (Sacco *et al.* 2011). To obtain information on cell growth during the culture

process the governing equations including the momentum, convection-diffusion equation and cell growth equation need to be solved in a coupled fashion. For this, the Monod-Contois kinetics equation has been widely used to describe the cell growth as a function of the nutrient concentration. Sacco *et al.* (2011) modified the Monod-Contois cell growth equation to include the influence of shear stress on the biomass growth. In this cell growth equation the nutrient concentration, shear stress field and cell growth are coupled in a consistent fashion. They determined model parameters from experimental data and then performed a computational analysis using the volume averaging method (VAM). Although the VAM provides the average stresses and concentration within the porous scaffold, it does not describe the local stress and concentration distributions. Another drawback of the aforementioned study is that it considers only one nutrient supplied for cell growth. A more realistic cell growth model should include multiple nutrients and the mechanical stimuli induced on the cells. In this context, Lendenmann and Egli (1997) developed a model describing the growth rate as a function of the individual concentrations of several carbon substances to study bacterial growth. Nava *et al.* (2013) also developed a modified Monod-Contois growth model and performed a resolved scale simulation, in which the growth of the tissue was modeled using a moving boundary approach. However no information can be found from the study regarding the optimization of the culture condition and design of the scaffold. The above discussion argues that a comprehensive resolved scale study with a realistic cell growth model is essential for investigating the cell culture process for improved tissue construct development.

In perfusion bioreactors, the fluid velocity inside the bioreactor is low and typically the Reynolds number based on the scaffold strand diameter is less than 1 (Yan *et al.* 2011). For numerical simulation of flow over complex boundaries, the lattice Boltzmann method (LBM) has become an attractive methodology due to its simple stream and collide procedure, easiness in implementation of the boundary conditions in a Cartesian co-ordinate system where the boundary is aligned with the numerical gird and the local nature of the calculation (Premnath *et al.* 2012). Among various two-dimensional (2D) and three-dimensional (3D) LBM models the D3Q19 multiple relaxation time (MRT) LBM has proven to be an efficient model to simulate 3D flows (d'Humieres *et al.* 2002). However, LBM typically uses a uniform Cartesian grid and the implementation of the boundary conditions on a curved surface is a challenge. To implement the boundary conditions on a curved surface, Bouzidi *et al.* (2001) proposed an interpolation based

bounce-back scheme. To perform the mass transfer analysis, Flekkoy (1993) developed a Bhatnagar-Gross-Krook LBM model for both 2D and 3D simulations. This method has since been used in various applications including studies on packed bed bioreactors (Sullivan *et al.* 2005), biofilm growth in porous media (Schulenburg *et al.* 2008), a flow bed bioreactor for cartilage cell growth using multi-phase LBM (Hussein *et al.* 2008), the shear stress distribution for a 3D poly-lactic acid scaffold using the structure image obtained from high resolution micro-computed tomography (Voronov *et al.* 2010) and 3D biofilm growth in random porous media (Pintelon *et al.* 2011). For the development of the 3D biofilm model, Pintelon *et al.* (2011) used the MRT LBM to simulate the pore scale hydrodynamics and single relaxation time LBM to solve the advection-diffusion-reaction equation. Recognizing the biofilm permeability, Pintelon *et al.* (2011) used the MRT LBM to simulate the hydrodynamics, which allowed consideration of a broader range of biofilm permeability without the loss of numerical stability. LBM has also proved to be reliable for simulating the convection-diffusion transport of nutrient inside a bioreactor (Sayed *et al.* 2010). The MRT LBM model has also been used to solve the convection-diffusion equation governing the isotropic and anisotropic diffusion (Yoshida *et al.* 2010; Li *et al.* 2013). For the in vitro tissue culture process the culture medium is typically water with oxygen and glucose as nutrients. The molecular diffusivity of oxygen and glucose is several orders of magnitude lower than that of water and as such the Peclet (Pe) number of the flow inside the bioreactor is typically several orders of magnitude higher. Such a liquid system can also be characterized by the Schmidt (Sc) number, which is the ratio of kinematic viscosity and molecular diffusivity. The D3Q7 MRT LBM mass transfer model has been shown to be effective for flows with high Pe and Sc numbers (Yoshida *et al.* 2010).

In this study, a resolved-scale simulation of fluid flow and mass transfer over two circular strands of a tissue scaffold has been performed. As part of a comprehensive study of the flow and transport process through a porous tissue scaffold, this study considers a simplified scenario where the scaffold modeled by only two circular strands in tandem is cultured inside a perfusion bioreactor. The primary objective of the study is to understand the influence of the front strand on the cell growth on the rear strand, specifically looking into the low velocity region between the strands, the local shear stress and wall mass transfer rates. A cell growth equation, which considers multiple nutrients as well as the shear stress induced on the cells, has been adopted to describe the cell growth on the strand surfaces specifically for cartilage tissue

regeneration. The culture medium for the tissue culture process primarily includes water with oxygen and glucose as nutrients. The flow and mass transfer analysis has been performed for a Reynolds number of Re_D = 1.0, which represents typical conditions for the in vitro culture process in the perfusion bioreactor. The distance between the strands is varied to study the influence of the gap between the strands on the cell growth.

3.2 Mathematical model

3.2.1 Flow equations

To perform the resolved-scale simulation, the governing equations that describe single-phase incompressible flow over the circular strands inside a confined channel are the continuity and momentum equations,

$$\frac{\partial u_i}{\partial x_i} = 0 \tag{3.1}$$

$$\rho \frac{\partial u_i}{\partial t} + \rho u_j \frac{\partial u_i}{\partial x_j} = -\frac{\partial p}{\partial x_i} + \frac{\partial}{\partial x_j}\left(\mu \frac{\partial u_i}{\partial x_j}\right) \tag{3.2}$$

where, ρ and μ represents the density and dynamic viscosity. Solving the above equations numerically, gives the velocity, u_i, and pressure, p, fields. From the velocity information, the viscous stress tensor, τ_{ij}, can be obtained by using the following constitutive relation for a Newtonian fluid,

$$\tau_{ij} = \mu\left(\frac{\partial u_i}{\partial x_j} + \frac{\partial u_j}{\partial x_i}\right) \tag{3.3}$$

3.2.2 Nutrient transport equations

The single-phase mass transfer over circular strands inside a confined channel is governed by the convection-diffusion equation,

$$\frac{\partial C_\sigma}{\partial t} + u_i \frac{\partial C_\sigma}{\partial x_i} - \frac{\partial}{\partial x_i}\left(D_\sigma \frac{\partial C_\sigma}{\partial x_i}\right) = 0 \tag{3.4}$$

where C_σ and D_σ are the concentration and diffusion coefficient of nutrient species σ, i.e. oxygen and glucose. At the surface of the strand oxygen and glucose are consumed by the thin layer of cells. In this study, the consumption rate, R_σ, is assumed to be a function of the local nutrient concentration C_σ, which is described by the Michaelis-Menten kinetics,

$$R_\sigma(C_\sigma) = \frac{R_{m\sigma} C_\sigma}{K_{m\sigma} + C_\sigma} \tag{3.5}$$

where $R_{m\sigma}$ and $K_{m\sigma}$ represent the maximal consumption rate and half-saturation constant of nutrient σ, respectively.

3.2.3 Cell growth equations

For the cell growth, the Monod growth kinetics modified by Contois has been widely used in the literature (Galban *et al.* 1999), i.e.

$$r_g(\epsilon_c, C_\sigma) = \frac{k_g C_\sigma}{k_{s\sigma} \rho_c \epsilon_c + C_\sigma} \tag{3.6}$$

where r_g and k_g are the cell growth rate and the maximum specific growth rate respectively, $k_{s\sigma}$ is a dimensionless parameter representing the Contois saturation constant of nutrient σ, ρ_c is the reference cell density, and ϵ_c is the cell volume fraction.

To account for the mechanical stimuli, Sacco *et al.* (2011) modified equation (3.6) by assuming that the maximum specific growth rate is a linear function of the shear stress induced on the cells, i.e.

$$k_g = k_{g0}(\alpha + \beta\tau) \tag{3.7}$$

where k_{g0} is the maximum growth rate in a static condition. In the work of Sacco *et al.* (2011), the values of the parameters α and β were determined from the experiments performed at inlet velocities ranging from 0.00072 m/s to 0.00884 m/s, where the median shear stress values were determined within the range of 0.0046 Pa to 0.056 Pa.

A cell growth equation that considers the growth rate as a function of multiple nutrients is given by (Lendenmann *et al.* 1997):

$$r_g(C_\sigma) = \frac{k_g \sum(k_{g0} C_\sigma)/k_s}{k_g \rho_c + \sum(k_{g0} C_\sigma)/k_s} \tag{3.8}$$

This equation indicates that the cell growth rate will be a sum of the growth rates for the individual nutrients (Zinn *et al.* 2004). In the present study the model has been modified using Sacco *et al.*'s shear stress dependent maximum specific growth rate, i.e.:

$$r_g(\tau, C_\sigma) = \frac{k_g(\tau) \sum(k_{g0} C_\sigma)/(k_{s\sigma}\varepsilon)}{k_g(\tau) \rho_c + \sum(k_{g0} C_\sigma)/(k_{s\sigma}\varepsilon)} \tag{3.9}$$

In the equation (3.9), ε represents the ratio of the thickness of the cells to the diameter of the scaffold strand. In this model, only the beneficial effect of shear stress on cell growth has been included. Further experimental studies need to be performed to validate the model and also to determine the shear stress range within which the effect on cell growth remains beneficial.

3.3 Numerical method

3.3.1 LBM for fluid flow

In this study a D3Q19 MRT LBM model is used to simulate the fluid flow. In this model a cubic lattice with 19 discrete lattice points is used to define the 3D space. The discretized MRT LBM equation can be written as (d'Humières *et al.* 2002; Voronov *et al.* 2010):

$$|f(x_i + e_\alpha \delta t, t + \delta t)\rangle - |f(x_i, t)\rangle = -M^{-1} S \left[|m(x_i, t)\rangle - |m^{eq}(x_i, t)\rangle\right] \pm |F\rangle \tag{3.10}$$

In the equation above, $|\cdot\rangle$ is used to represent the column vectors and $|f\rangle$ is the distribution functions (DF) at each lattice point. The left hand side of the equation (3.10) represents the streaming process and the right hand side is the collision process. In the streaming process, the particle population streams to their adjacent location from x_i to $x_i + e_\alpha \delta t$ with a velocity e_α along each characteristic direction; and in the collision process, particles interact with each other at each node and as a result, change their velocity direction accordingly.

In equation (3.10), $|m\rangle$ is the moment vector, $|m^{eq}\rangle$ is the equilibrium moment vector, M is the transformation matrix and S is the diagonal collision matrix. The components of S are the relaxation parameters using different relaxation time scales. The formulation for $|m\rangle$ and $|m^{eq}\rangle$, as well as the values of M and the relaxation parameters are given in reference (d'Humières *et al.* 2002). $|F\rangle$ is a forcing term. In the present simulation, a pressure gradient is specified by adding the forcing term to the distribution functions at the inlet in the streamwise direction and subtracting the forcing term at the outlet (Voronov *et al.* 2010).

The kinematic viscosity ν can be obtained using the following relationship (d'Humières *et al.* 2002),

$$\nu = \frac{1}{3}\left(\frac{1}{s_\nu} - \frac{1}{2}\right)\frac{\delta x^2}{\delta t} \tag{3.11}$$

where s_ν is the relaxation parameter. The hydrodynamic properties, i.e. the density ρ, velocity $\vec{u}$, and pressure P can be obtained by,

$$\rho = \sum_{\alpha=0}^{18} f_\alpha \,, \rho\vec{u} = \sum_{\alpha=0}^{18} f_\alpha \vec{e}_\alpha \,, P = {c_s}^2 \rho \tag{3.12}$$

where $c_s = 1/\sqrt{3}$, representing the speed of sound of the model.

3.3.2 Boundary condition for circular geometry

In the LBM for straight walls, the bounce-back boundary condition is the simplest and most efficient approach to implement the no-slip boundary condition. The bounce-back link scheme has the second-order accuracy for straight walls (Zhang *et al.* 2007). Such a bounce-back scheme typically uses a uniform Cartesian grid, so implementation of the curved geometry of the strand surface is a challenging task for the LBM. In this study the immersed boundary method (IBM) for curved walls developed by Bouzidi *et al.* (2001) based on both an interpolation and bounce-back scheme is adopted for use, which is called the interpolation based bounce-back (IBB) boundary condition. In this scheme, the following linear interpolation equations are used for the curved geometry where q is the distance from the curved surface of interest to the nearest node:

If $q < 0.5$

$$f_{i'}(x_i, t + \delta t) = 2q f_i^c(x_i, t) + (1 - 2q) f_i^c(x_i - e_\alpha, t) \quad (3.13)$$

If $q \geq 0.5$

$$f_{i'}(x_i, t + \delta t) = \frac{1}{2q} f_i^c(x_i, t) - \frac{(1-2q)}{2q} f_{i'}^c(x_i, t) \quad (3.14)$$

In these equations, f on the left-hand side refers to the values after collision and propagation, and f^c on the right hand side refers to the values taken after collision and before propagation.

3.3.3 LBM for mass transfer simulations

In this study, a D3Q7 MRT LBM model is used to simulate the mass transfer. The model is analogous to the so-called athermal MRT LBM scheme and solves the convection-diffusion equation (CDE). In this model, a cubic lattice with only 7 discrete lattice directions is used to define the 3-D space. The discretized MRT LBM equation can be written as (Yoshida *et al.* 2010),

$$|g(x_i + e_\alpha \delta t, t + \delta t)\rangle - |g(x_i, t)\rangle = -M^{-1} S \left[|m(x_i, t)\rangle - |m^{eq}(x_i, t)\rangle\right] \quad (3.15)$$

The macroscopic variable or concentration can be obtained by solving the discretized equation and using the following relationship,

$$C_\sigma = \sum_{\alpha=0}^{6} g_\alpha \quad (3.16)$$

The formulation of the moment vectors, the values of M and the relaxation parameters are given by Yoshida *et al.* (2010). The diffusion coefficients are related to the relaxation parameters and for the isotropic case are given by the following relation (Yoshida *et al.* 2010; Li *et al.* 2013),

$$D_\sigma = \frac{1}{4}\left(\frac{1}{s_D} - \frac{1}{2}\right)\frac{\delta x^2}{\delta t} \quad (3.17)$$

where s_D is the relaxation parameter.

3.3.4 Boundary conditions for mass transfer

To implement the concentration boundary condition of the CDE, a general bounce-back scheme proposed by Zhang *et al.* (2012) is adopted in this study. Using this scheme a concentration boundary condition of the form $b_1 \frac{\partial C}{\partial n} + b_2 C_\sigma = b_3$ can be easily implemented. This formulation can be used to implement both Dirichlet and Neumann boundary conditions at the channel walls for a Cartesian grid.

If $b_1 = 0$ and, $b_3 \neq 0$, the macrovariable at the wall becomes a Dirichlet type boundary conditions. To implement such a boundary condition, Zhang *et al.* (2012) proposed the following treatment for the distribution functions entering from the fluid nodes to the solid,

$$g_{i'}(x_f, t + \delta t) = -g_i^c(x_f, t) + 2\omega_i C_{w\sigma} \tag{3.18}$$

For $b_1 \neq 0$, $b_2 = 0$ and, $b_3 \neq 0$, $b_1 \frac{\partial C_{w\sigma}}{\partial n} + b_2 C_{w\sigma} = b_3$ becomes a Neumann type boundary condition i.e., $\frac{\partial C_{w\sigma}}{\partial n} = b_3/b_1$. Here, $C_{w\sigma}$ represents the concentration value at the wall. Implementation of this type of boundary condition requires the calculation of the concentration gradient. Using a finite difference relation, the concentration gradient can be expressed as (Zhang *et al.* 2012),

$$\frac{\partial C_\sigma}{\partial n} = \frac{C_{f\sigma} - C_{w\sigma}}{-0.5\, \boldsymbol{n} \cdot \boldsymbol{e_i}\, \delta x} \tag{3.19}$$

where, $C_{f\sigma}$ is the concentration at the fluid node next to the solid surface and n is the interface normal vector. Using this relationship, the concentration at the solid surface can be obtained from the following equation (Zhang *et al.* 2012):

$$C_{w\sigma} = C_{f\sigma} + 0.5\, \boldsymbol{n} \cdot \boldsymbol{e_i}\, \delta x\, (b_3/b_1) \tag{3.20}$$

To model the reaction on the surface of the circular strand, the consumption rate, R was calculated at the surface of the strands. The concentration values were specified at the surface of the strands using linear extrapolation based on previous time steps and subsequently used to

calculate the value of R, which was then used to calculate the distribution functions following the procedure described by Yoshida *et al.* (2010).

3.4 Results and discussions

In Hossain *et al.* (2014), the fluid flow and mass transfer over a single circular strand inside a bioreactor was predicted using the MRT LBM and the results were validated by comparison with published experimental data. Building on the aforementioned study, the present analysis will focus on the fluid flow, mass transfer and cell growth rate over two circular strands placed in tandem inside a perfusion bioreactor.

In the present simulation, the length, width and height of the bioreactor are $L = 21R$, $W = 0.5R$ and $H = 4R$, respectively, where R is the radius of the strand. The strand spanned the entire width of the channel, so that the strand aspect ratio (AR) was AR = 2.1 and the blockage ratio (BR) was BR = 0.5. The origin of the coordinate frame was positioned $10R$ downstream from the channel inlet and on the center of the channel. The center of the front strand was located at $x/R = -2$. The position of the rear strand was varied to study the influence of the front strand on the rear strand, specifically, on the shear stress, mass concentration and cell growth rate on the surface of the rear strand. For the first case, the center of the rear strand was located at $x/R = 2$ giving a center-to-center distance between the two strands of $s = 4R$. For the second case, the rear strand was located at $x/R = 1$ so that the center-to-center distance between the two strands became $s = 3R$. The number of nodes used for both cases was 250×6×48 in the x, y and z directions, respectively. The grid was uniform with a spatial increment of δx = 0.04 mm and the simulation used a time step of δt = 0.266 ms. The diameter of the strand was D = 0.96 mm. The relaxation parameter value was set to s_ν= 1.0 to yield a kinematic viscosity of $\nu = 1\times10^{-6}$ m^2/s. The flow inside the channel was driven by the pressure difference specified between the inlet and outlet planes. The Reynolds number for the simulation was 1.0, which represents the flow condition inside a typical bioreactor and was calculated using the equation, $Re_D = \frac{UD}{\nu}$, where U is the bulk velocity at the inlet of the channel. The present simulation considers an inlet bulk velocity of 0.00104 m/s. A bounce-back no-slip boundary condition was applied on the channel upper and lower walls, while an IBB BC was used to implement the curved wall of the strand on the uniform mesh. A periodic boundary condition is applied at the side walls. It was assumed that the

cells are attached uniformly to the scaffold surface and the thickness of the attached cells is negligible compared with the cylinder diameter. It was also assumed that the nutrient consumption due to the biochemical reaction occurs only at the surfaces of the cylinders. Section views of the strands in the bioreactor together with the mesh used in the numerical simulation are presented in Figure 3.1.

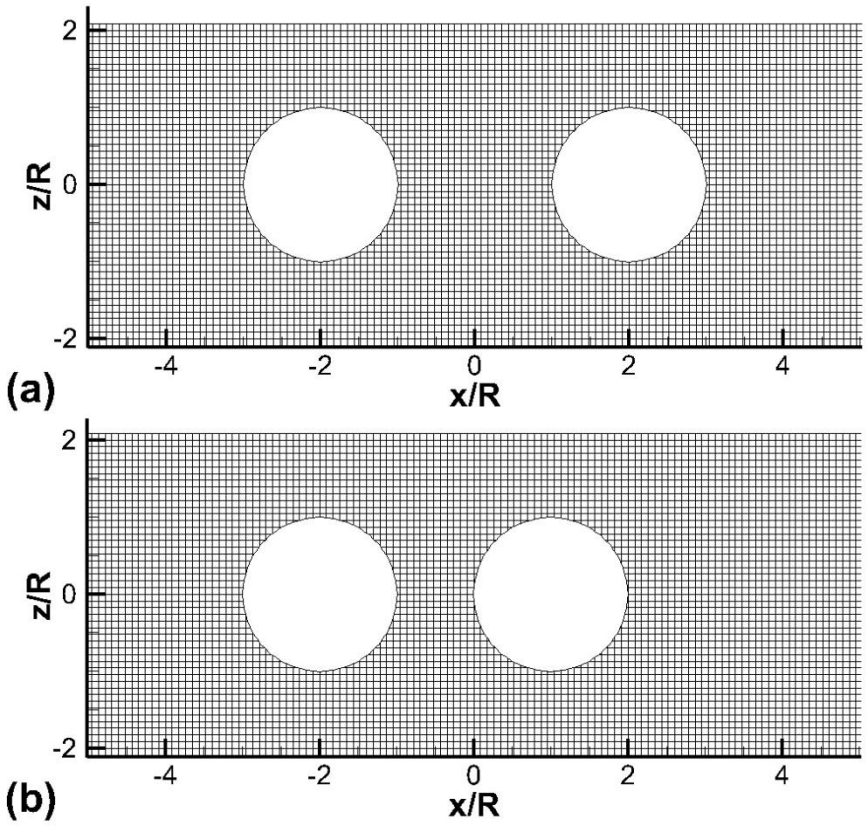

Figure 3.1: Side view of the strands in the bioreactor channel with the mesh used for the numerical simulation: (a) $s = 4R$, (b) $s = 3R$

For the mass transfer simulation, the inlet values of the both oxygen and glucose concentrations were assumed to be 6.4×10^{-3} kg/m^3 and the nutrients were transported by the incoming fluid through the bioreactor. A Michaelis-Menten kinetics reaction was specified at the strand surface. The boundary condition applied at the side walls and at the outlet of the bio-reactor was a zero concentration gradient normal to the boundary surface. Two values of s_D = 1.928 and 1.963 were used to specify diffusivity values corresponding to oxygen $D_o = 2\times10^{-9}$

m^2/s and glucose $D_g = 1\times10^{-9}$ m^2/s; the corresponding Schmidt numbers were 500 and 1000 and the corresponding Peclet numbers were Pe = 500 and 1000. The consideration of Schmidt number in such low Reynolds number flow is important since at high Sc convection dominates over diffusion (Dani *et al.* 2006). The values of the model parameters for cartilage tissue regeneration are given in Table 3.1.

Table 3.1: Values of the model parameters used in the simulations

Definition	Value	Reference
Inlet oxygen concentration, C_o	6.4×10^{-3} kg/m^3	Sacco *et al.* (2011)
Inlet glucose concentration, C_g	6.4×10^{-3} kg/m^3	This work
Oxygen diffusivity, D_o	2.0×10^{-9} m^2/s	Sacco *et al.* (2011)
Glucose diffusivity, D_g	1.0×10^{-9} m^2/s	Lin *et al.* (2013)
Maximum specific cell growth rate, k_{g0}	1/(2×24×3600) [1/s]	Sacco *et al.* (2011)
Contois cell saturation constant for oxygen, k_{so}	4.2×10^{-3}	Sacco *et al.* (2011)
Contois cell saturation constant for glucose, k_{sg}	2.3×10^{-3}	Chung *et al.* (2010)
Reference cell density, ρ_c	1 kg/m^3	Sacco *et al.* (2011)
Oxygen maximal consumption rate, R_{mo}	3.9×10^{-5} kg/(m^{3}s)	Sacco *et al.* (2011)
Oxygen half saturation constant, K_{mo}	3.2×10^{-3} kg/m^3	Sacco *et al.* (2011)
Glucose maximal consumption rate, R_{mg}	3.9×10^{-5} kg/(m^{3}s)	Chung *et al.* (2010)
Glucose half saturation constant, K_{mg}	6.3×10^{-3} kg/m^3	Chung *et al.* (2010)
Reference cell density, ρ_c	1 kg/m^3	Sacco *et al.* (2011)
α	0.8761	Sacco *et al.* (2011)
β	0.1045	Sacco *et al.* (2011)
ε	0.001	This work

Figure 3.2a) and 3.2b) show the velocity vectors on the *x*-*z* plane at the centerline of the channel, $y/R = 0$ for $s = 4R$ and $s = 3R$, respectively. For clarification only is the region close to the cylindrical strand shown for all the velocity and mass transfer results described in this section. In Figure 3.2, for a cleaner presentation of the vector field, only one of two vectors is plotted along the x- direction. The vector field is symmetric about the centerline of the channel ($z/R = 0$) for both cases. From Figure 3.2 it is evident that for both cases the flow begins to sense the obstruction presented by the front strand at approximately $x/R = -4$ and as a result, it is directed toward the narrow passages formed between the front strand and the channel sidewalls. Even though this is a low Reynolds number flow, there is significant acceleration of the fluid around the front strand. A maximum velocity of approximately $u/U = 2.6$ is observed midway between the front strand shoulder and channel walls. No evidence of flow recirculation or reverse flow is evident downstream of the front strand. Figure 3.2a) indicates that the fluid velocity field begin to recover by $x/R = 0$, which is the mid-point between the strands. The flow is then directed towards the narrow passages formed by the rear strand and channel side walls in a similar fashion to the flow around the front strand. Significant acceleration of the fluid around the rear strand is also observed. Figure 3.2b) shows that if the rear strand is located closer to the front strand, the velocity is much reduced in the region between the two strands. In the region bounded by $z/R = -0.5$ and $z/R = 0.5$, the velocity magnitude is less than $0.05U$.

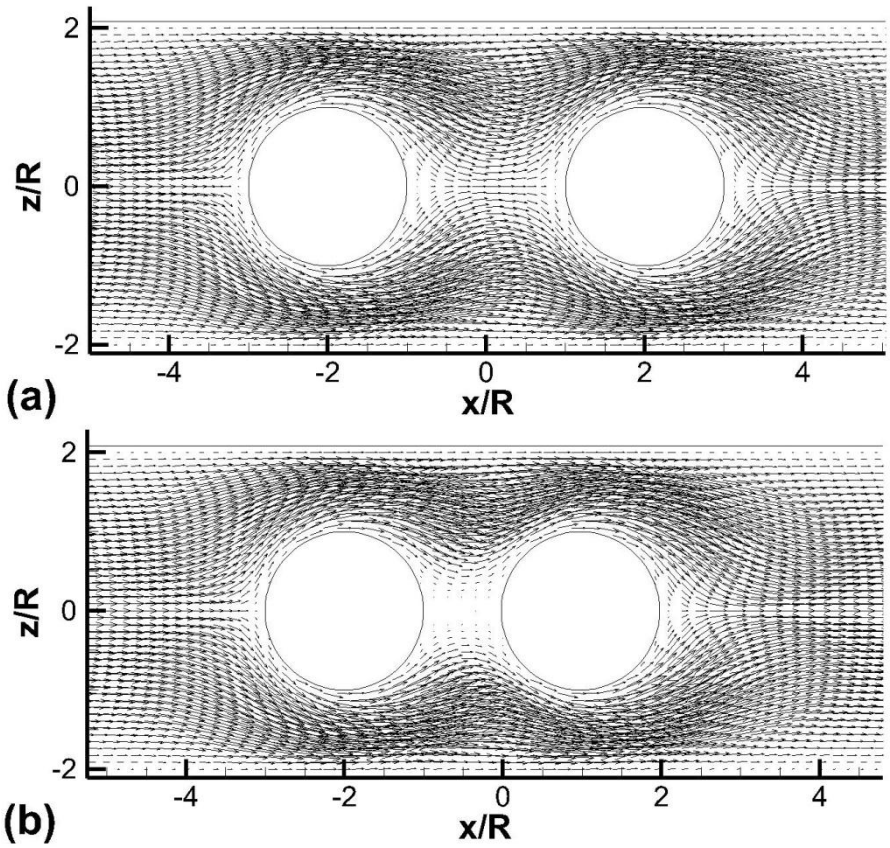

Figure 3.2: Velocity vectors at $y/R = 0$ (a) $s = 4R$, (b) $s = 3R$

Figure 3.3a) and 3.3b) show the shear stress contours on the x-z plane at the centerline of the channel, $y/R = 0$, for $s = 4R$ and $s = 3R$, respectively. To calculate the shear stress values from the constitutive relation for the fluid, the strain rate tensor was calculated locally using the non-equilibrium moments within the MRT LBM framework by following Yu *et al.* (2006). The contours indicate symmetric behavior about the line $z/R = 0$ for both $s = 4R$ and $s = 3R$. The values of the shear stress in the x-z plane vary by almost one order of magnitude. Low shear stress zones are observed in the center region of the channel, while the highest shear stress values of approximately 0.15 N/m^2, occur at the channel walls and strand shoulder. The lowest surface shear stress values are found on the upstream and downstream faces of the strands where the flow stagnates for both $s = 4R$ and $s = 3R$.

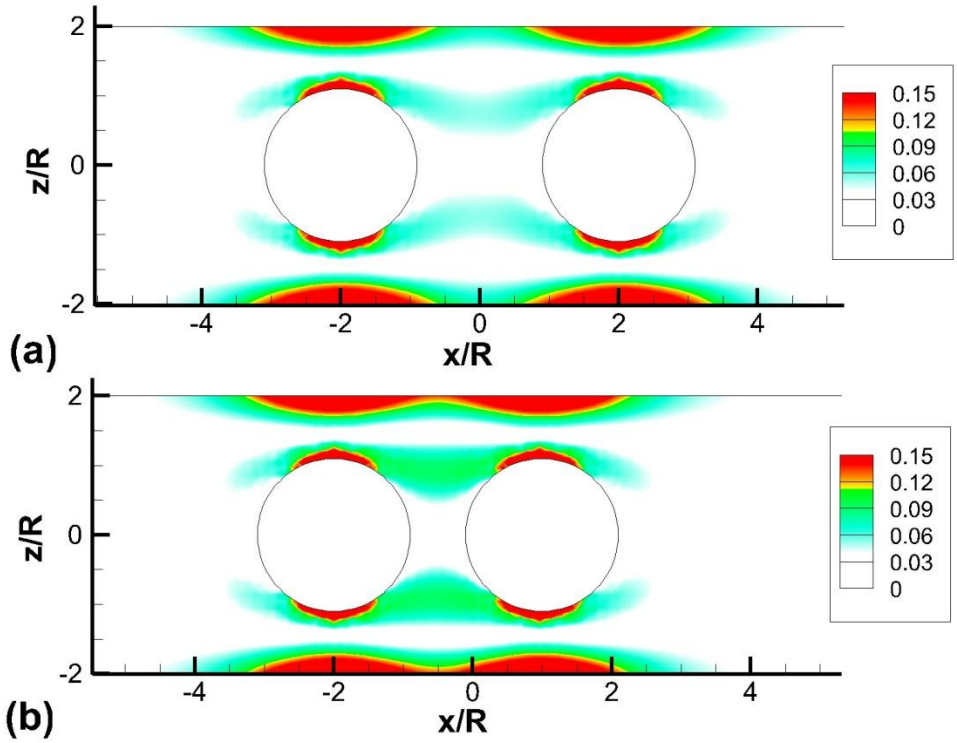

Figure 3.3: Shear stress (Pa) contours at y/R = 0 (a) $s = 4R$, (b) $s = 3R$

In tissue engineering knowledge of the shear stress field is important for the *in vitro* culture process since modest levels of shear stress can stimulate cell growth. On the other hand, excessively high shear stress values can cause cell death (Sacco *et al.* 2011). Note that knowledge of the shear stress on the surface of the strand is the most important issue, since the cells are initially attached only on the surface of the strand. In the present simulation the surface shear stress was calculated based on the linear extrapolation of the velocity field with the results shown in Figure 3.4a) for Re_D = 1.0. For clarity, part of the downstream section is enlarged and also shown in Figure 3.4b). In Figure 3.4, lines have been used to represent the shear stress profiles for s = 4R and symbols have been used for $s = 3R$. It is evident that the surface stress profiles are similar on both strands for both separation distances. The maximum surface stress occurs slightly upstream of the strand shoulder for both the front and rear strand for both $s = 4R$ and $s = 3R$. Both the front and rear strand profiles show slightly lower shear stress values for $s = 3R$ than $s = 4R$ on the downstream surface of the strand and the differences are approximately

10-15%. The profile on the rear strand for s = 3R also shows 5-7% lower values on the upstream surface compared to the other shear stress profiles. Overall, for the present flow conditions, it can be concluded that the values of the shear stress contours and surface shear stress do not vary significantly when the center to center distance between the strands changes from 4R to 3R.

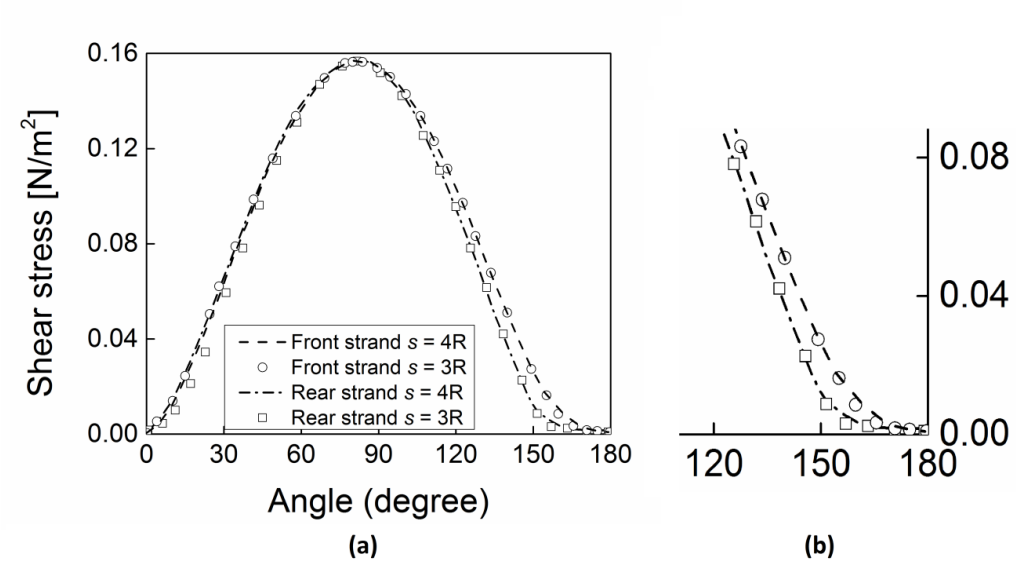

Figure 3.4: (a) Shear stress profiles at the surface of the strands, (b) enlarged view of the shear stress profiles near the rear stagnation point

Figure 3.5a) and b) show the steady state oxygen concentration distribution for a Schmidt number of Sc = 500 for s = 4R and s = 3R, respectively. The concentration values are normalized using the inlet oxygen concentration. The contour distribution in Figure 3.5a) is asymmetric at the upstream and downstream surfaces for both front and rear strands and indicates that the mass flux on the upstream surfaces of the strands is greater than on the downstream surfaces. The supply of oxygen on the upstream surface of the rear strand is also lower than the upstream surface of the front strand. Although the high initial scalar (nutrient) concentration moving from the channel inlet towards the strands is transported into the region between the strands, the convective transport is not high enough to provide a similar mass flux on the upstream surface of both front and rear strands. This is partly due to the fact that the cells attached on the surfaces of the strands are consuming nutrients.

Figure 3.5b) indicates that if the center to center distance between the strands is reduced from 4*R* to 3*R*, the normalized concentration values become close to zero in the region between the strands, i.e. from *z/R* = - 0.5 to *z/R* = 0.5. Recall from Figure 3.2b), the velocity values were also close to zero in this region. Hence, for the present flow conditions, the convective transport clearly fails to supply significant amounts of the scalar to this region. Increasing the Reynolds number Re_D might improve the scalar transport. However, this will also increase the surface shear stress values and any values higher than those required for cell sustainability might become problematic for tissue cell growth. Comparison between Figure 3.5a) and 3.5b) clearly indicates that increasing the distance between the strands will improve the scalar transfer.

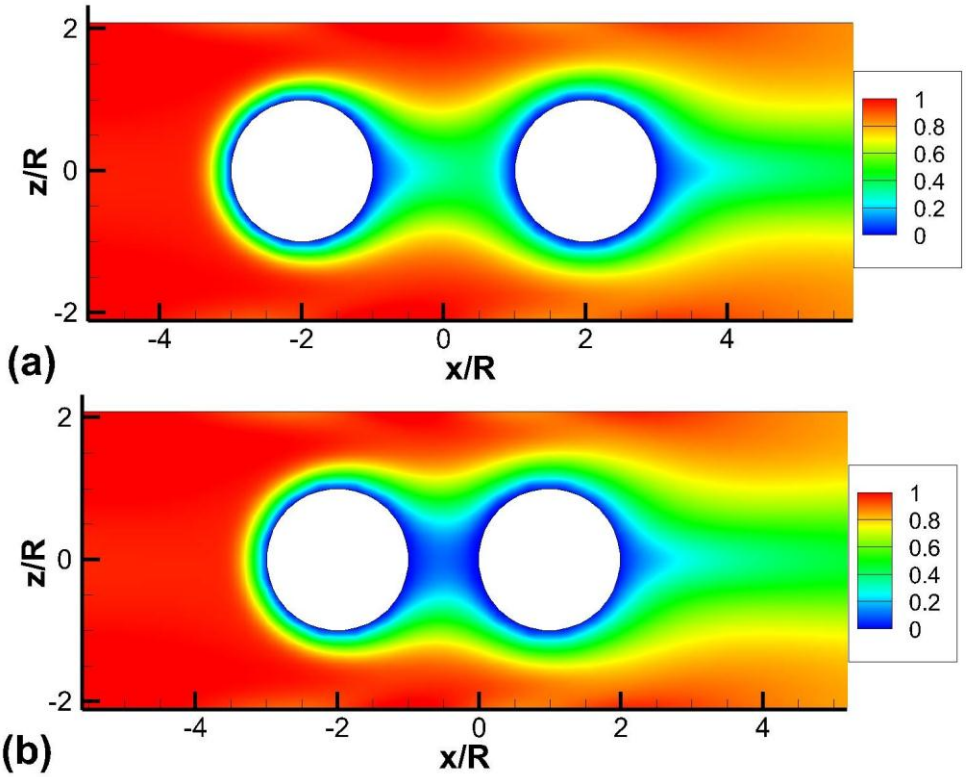

Figure 3.5: Normalized oxygen concentration contours at y/R = 0 (a) *s* = 4R, (b) s = 3R

Figure 3.6a) and b) show the steady state glucose concentration distribution for a Schmidt number of Sc = 1000 for *s* = 4R and *s* = 3R, respectively. An adequate supply of glucose is also required for the growth of cells, especially for the Chondrocytes growth (Chung *et al.* 2010). In general, the distributions of the glucose concentration contours are very similar to those given in

Figure 3.5 for oxygen. However, if the magnitude of the concentration contours for both nutrients is compared, it is evident that the transport of glucose is more effective than that for oxygen. This is because glucose has a higher Schmidt number than oxygen. The higher Schmidt number implies a decrease in the scalar diffusivity, so that the relative influence of convection increases.

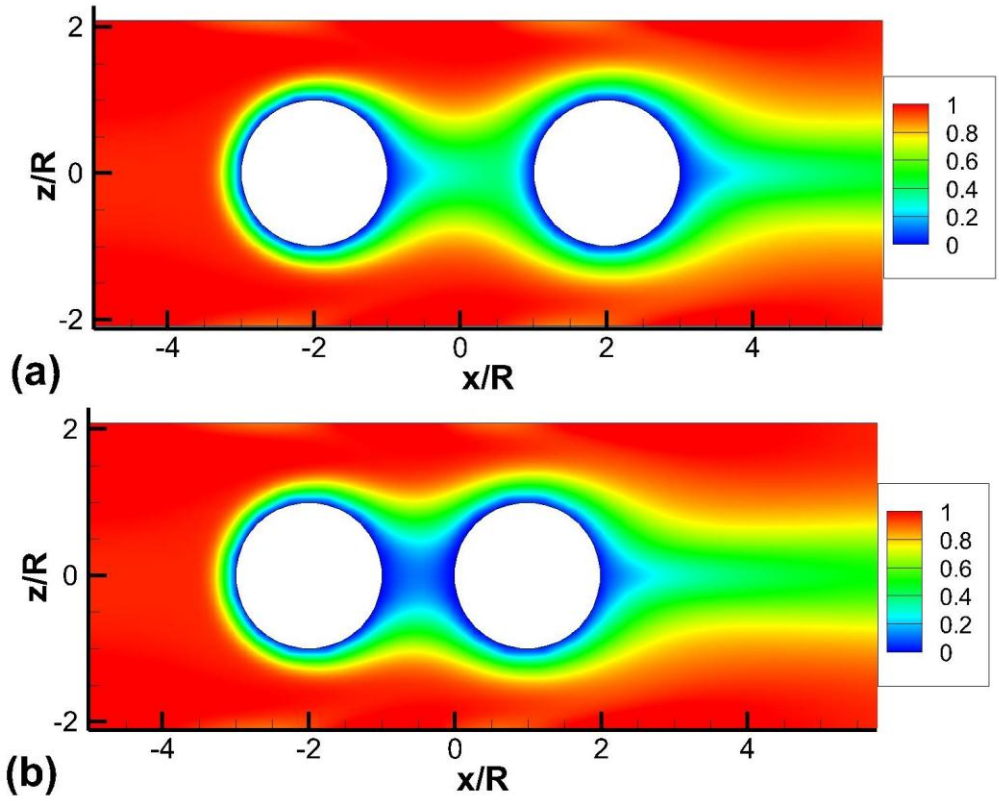

Figure 3.6: Normalized glucose concentration contours at y/R = 0 (a) *s* = 4R, (b) *s* = 3R

Figure 3.7 shows the normalized oxygen concentration profile at the both front and rear strand surfaces for both $s = 4R$ and $s = 3R$. Recall that it was assumed that the cells were attached at the surface of the strand and that the nutrient consumption by the cells is defined by a Michaelis-Menten kinetics type reaction. The concentration profiles for the front strands for both $s = 4R$ and $s = 3R$ show that the maximum concentration values occur at the front stagnation point where the normalized value is 0.073. The values start to decrease at about 45° and reduce to values of 0.013 and 0.009 at the downstream stagnation point for $s = 4R$ and $s = 3R$,

respectively. The concentration values for both profiles are similar up to 75°. Thereafter, the profile for s = 3*R* exhibits lower values than the profile of *s* = 4*R*. The rear strand concentration profiles are different than the front strand profiles. For the rear strand the maximum normalized concentration occurs slightly upstream of the strand shoulder and the normalized value is 0.041. The difference in maximum normalized concentration between the front and rear strands is about 43% which is significant. The profile for the rear strand for *s* = 4*R* shows higher values than for *s* = 3R up to 75°. The values are similar on the surfaces of the rear strands from 75° to 180°. From the normalized concentration profile of the rear cylinder for *s* = 3*R*, it can also be found that the concentration value is zero at the upstream stagnation point.

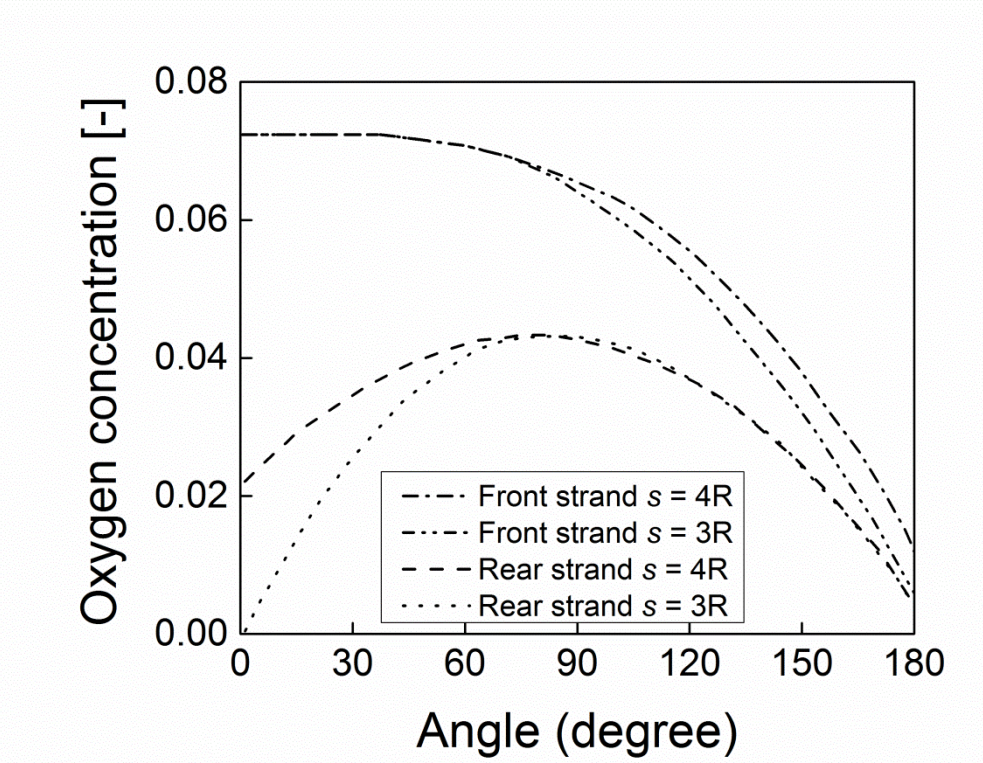

Figure 3.7: Normalized oxygen concentration profiles over the strand surfaces

Similar concentration profiles are observed for glucose in Figure 3.8. The maximum concentration values occur at the upstream stagnation point for the front strands and the normalized value is approximately 0.084. Similar to the oxygen concentration profiles the profile for *s* = 3*R* exhibits lower values on the downstream surface of the front strand compared to the profile of *s* = 4*R*. The profile of the rear strand for *s* = 4*R* shows higher values than for *s* = 3*R* up

to 75°; the values are similar on the surfaces of the rear strands from 75° to 180°. The difference in maximum normalized concentration between the front and rear strands is about 46% which is significant. The normalized concentration profile of the rear strand for $s = 3R$ indicates that the concentration value is zero at the upstream stagnation point. A comparison between Figure 3.7 and 3.8 shows that the transport of glucose to the strand surface is in general higher than for oxygen for the same value of Re_D. Comparing the maximum normalized concentration values at the front strand between oxygen and glucose indicates a 13% higher value for glucose. Similarly for the rear strand, the maximum normalized concentration is about 18% higher for glucose. From the concentration profiles on the strand surfaces for both nutrients, it is evident that the cells attached on the downstream face of the front strand and the rear strand will obtain significantly less nutrients than the cells on the upstream surface of the front strand, which will lead to lower cell growth in these regions.

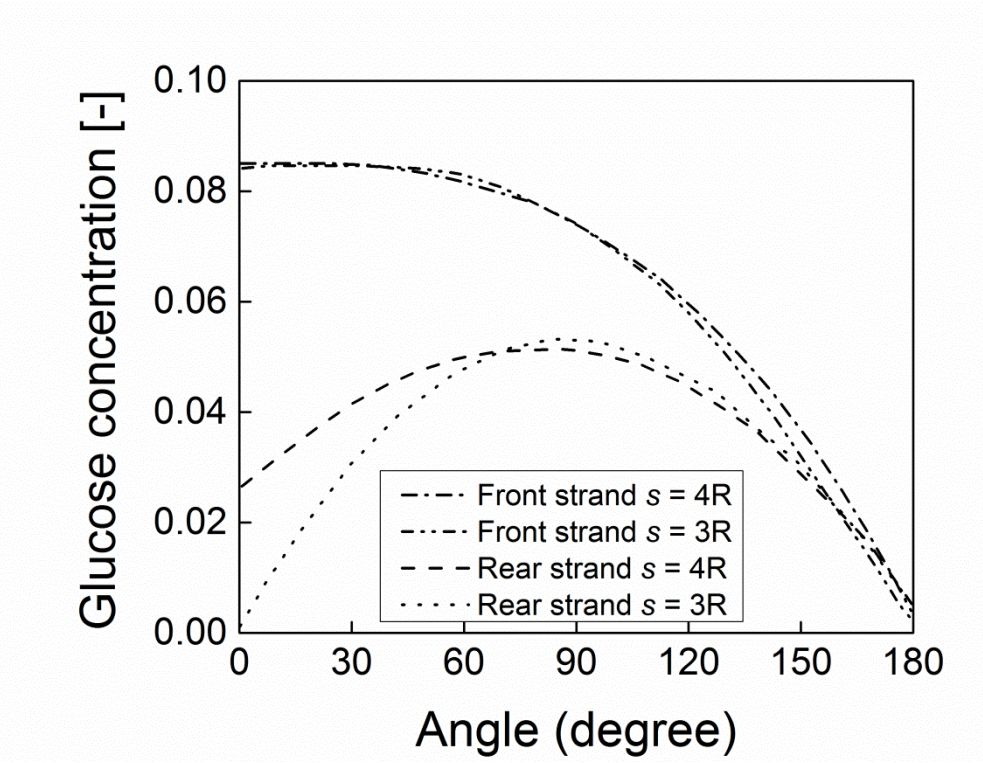

Figure 3.8: Normalized glucose concentration profiles over the strand surfaces

Figure 3.9 shows the cell growth rate on the strand surfaces using Lendenmann and Egli's (1997) cell growth equation, i.e., Equation 3.8, which considers both nutrients but does not

include the effect of shear stress. A constant value of k_g is used in Equation 3.8 and the value of k_g is assumed to be equal to k_{g0}. The growth rate profiles are found to be similar, as was the case for the oxygen and glucose concentration profiles. The growth rate profiles for the front strands are much higher than for the rear strands. For the front strands the maximum growth rate is about 1.0×10^{-6} s^{-1} and occurred at the front stagnation points for both $s = 4R$ and $s = 3R$. The profile for the rear strand for $s = 4R$ shows higher values than for $s = 3R$ up to a location of 75°. The growth rate profiles presented in Figure 3.9 clearly indicate the influence of the nutrient concentration profiles.

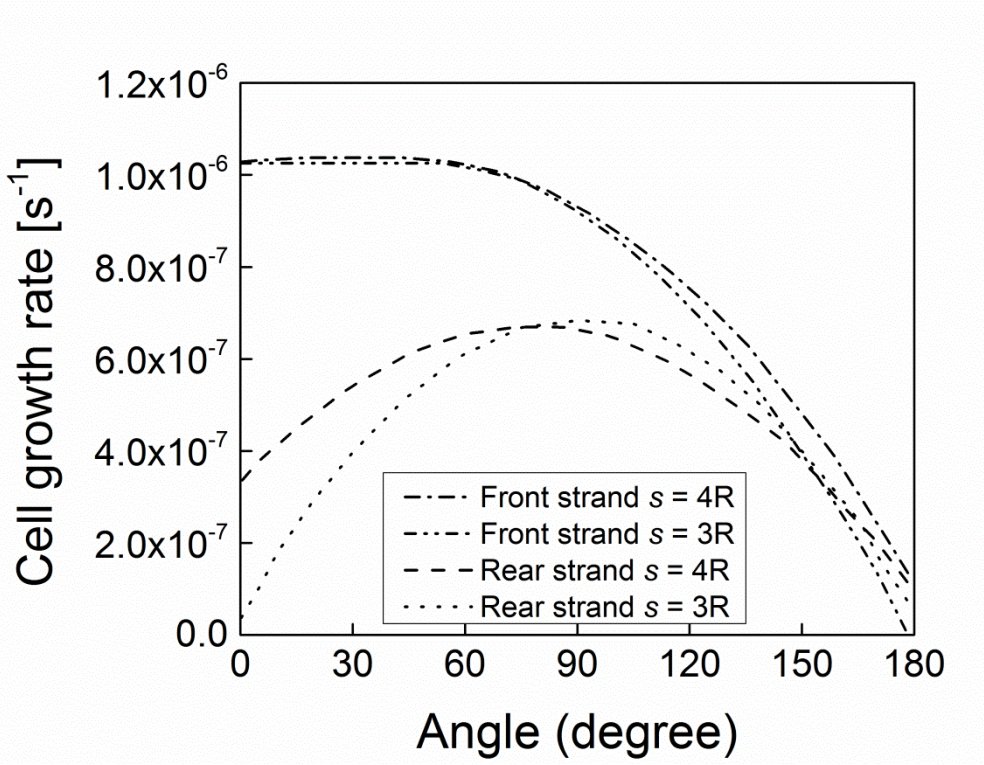

Figure 3.9: Cell growth rate over the strand surfaces using the model of Lendenmann and Egli (1997)

Figure 3.10 shows the cell growth rate on the strand surfaces based on the shear stress acting on the surface and transport of both nutrients using the modified Lendenmann and Egli's (1997) cell growth equation, i.e., Equation 3.9. For the front strands, the cell growth rate is clearly much higher on the upstream face of the strand compared to the downstream face. Both profiles show the maximum growth rate occurs at θ = 50° and the growth rate gradually

decreases to a minimum value at the downstream stagnation point. Recall that the maximum growth rate occurred at the upstream stagnation point; the value thereafter gradually decreased to reach a minimum value at the downstream stagnation point when Lendenmann and Egli's (1997) cell growth equation (i.e., Equation 3.8) was used. The increase of the cell growth rate from the upstream stagnation point to about 50° reflects the effect of the increasing shear stress levels, which develop between the upstream stagnation point and the shoulder of the strand (see Figure 3.4) in the modified Lendenmann and Egli's growth model. The cell growth rate profile on the rear strand for s = 4R indicates the maximum cell growth rate occurs between 60° and 95°. The maximum cell growth rate occurs between 75° and 105° on the rear strand surface for s = 3R. The cell growth rate profile on the rear strand surface for s = 3R also indicates that the cell growth rate is minimum (close to zero) at both the upstream and downstream stagnation point. The average cell growth rate on the front and rear strand surfaces for s = 4R are 7.20×10^{-7} s^{-1} and 4.85×10^{-7} s^{-1}, respectively, and for s = 3R are 7.13×10^{-7} s^{-1} and 4.33×10^{-7} s^{-1}, respectively. The predictions obtained from both the modified Lendenmann and Egli's model are in agreement with the results of Sacco *et al.*'s (2011) model for a similar inlet velocity. In Sacco *et al.*'s (2011) model the net cell growth rate for the porous scaffold was about 6.0×10^{-7} s^{-1} with an inlet velocity of 0.0022 m/s. The higher average cell growth rate in Sacco *et al.*'s (2011) study is mainly due to the higher inlet velocity. For s = 4R, the average cell growth rate on the rear strand surface decreases by approximately 32% compared to the front strand. For s = 3R, the reduction of the average cell growth rate on the rear strand is somewhat higher, about 39%. Although the average cell growth rate on the front strand for both cases are almost similar, a 10% decrease can be seen on rear strand surface for s = 3R compared to s = 4R.

The predictions for the cell growth rate examined in the present simulation clearly indicate that decreasing the distance between the strands can decrease the average cell growth rate. It should be noted that decreasing the distance between the strands within a scaffold can increase the mechanical strength of the scaffold and also increase the average cell growth rate per unit volume of the scaffold. From the present simulation it was found that the average cell growth rate per unit radius based on the cell growth rate on the surfaces of both the front and rear strand are 1.01×10^{-7} s^{-1} and 1.14×10^{-7} s^{-1} for s = 4R and 3R, respectively. Increasing the distance between the strands will increase the porosity of a tissue scaffold. It is known that highly porous tissue scaffolds will provide less mechanical support for the cells (Murphy *et al.* 2013).

Therefore, it is important to obtain an optimal distance between the strands during the culture process to provide higher nutrient transport to the cells on the strand surfaces, meanwhile possessing adequate mechanical support for cells.

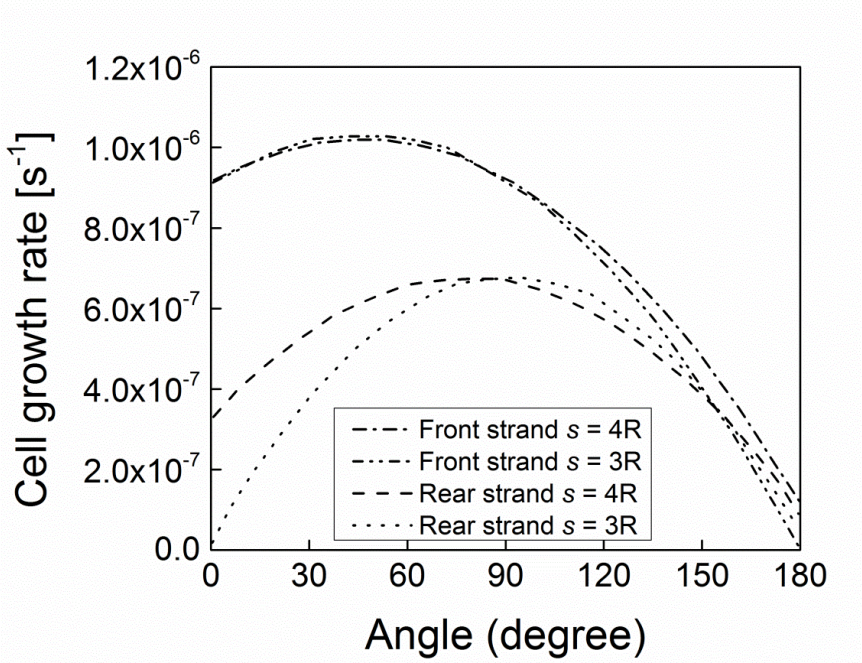

Figure 3.10: Cell growth rate over the strand surfaces using the modified model of Lendenmann and Egli (1997)

3.5 Conclusions

In this study a resolved-scale simulation of fluid flow and mass transfer has been performed to predict the cell growth rate at the surfaces of two tissue strands placed in tandem within a channel representative of a perfusion bioreactor. The distance between the strands was varied to study the influence of the front strand on the cell growth rate at the surface of the rear strand. The simulations were performed for a center to center distance of s = 4R and s = 3R between the strands, respectively. The cell growth equation used in the present study considers multiple nutrients as well as the shear stress level induced on the cells. The coupled fluid flow and mass transfer simulation was performed using the MRT LBM. With the numerical methodology that was previously validated, the simulations were performed at a Reynolds number of 1.0. For s = 4R, the velocity field almost recovers in the region between the strands;

and for *s* = 3R, the region between the strands from z/R = -0.5 to 0.5 is almost stagnant. At the present flow condition, the shear stress profiles of both the front and rear strand show lower values for *s* = 3R than *s* = 4R on the downstream surface of the strand and the differences are approximately 10-15%.

The mass transfer over the circular strand was predicted for oxygen and glucose with Schmidt numbers of Sc = 500 and 1000, respectively. A uniform concentration of nutrients was assumed at the inlet and Michaelis-Menten kinetics was assumed at the strand surface where the cells are typically seeded. The supply of the nutrients to the front strands is much higher compared to the supply to the rear strands for both orientations of the strands. When the distance between the strands is reduced from 4R to 3R, the scalar concentration level becomes almost zero in the region between the strands from z/R = -0.5 to 0.5. From the prediction for the velocity field it is seen that in this region of stagnant velocity the convective transport would not be able to supply sufficient nutrients. The supply of nutrient to the rear strand also reduces to a great extent if the distance between the strands is reduced. Comparison between the concentration contours and surface profiles of glucose and oxygen shows that increasing the Schmidt number decreases the diffusive transport and hence increases the effect of convection, with the overall result of enhanced wall mass transfer rates. Hence, better nutrient transport is observed to occur for glucose than for oxygen.

The cell growth rate is also found to be a maximum on the upstream face of the front strand at about θ = 50°for both s = 4R and 3R. The growth rate is significantly lower on the downstream face of the front strand since the convection at this Reynolds number is not sufficient to provide enough nutrients for producing a homogeneous cell growth rate on both upstream and downstream of the strands. Also due to the reduced nutrient transport to the rear strand, the cell growth rate is much lower on the rear strands. The cell growth rate obtained from the modified Lendenmann and Egli's duel nutrient controlled cell growth equation by including the shear stress dependent maximum specific cell growth rate clearly reveals the influence of surface shear stress on the cell growth rate. A 32% and 39% reduction occurs in the average cell growth rate at the rear strand surface compared to the surface of the front strand for *s* = 4R and 3R, respectively. The cell growth rates at the front strand surface are almost similar for both cases. However, at the rear strand surface 10% reduction in the cell growth rate occurs as the

distance between the strands is reduced from 4R to 3R. The results presented in this study suggest that an optimized distance between the strands is required for designing scaffolds. The optimization should consider the shear stress levels acting on the cells, nutrient transport to the cells, the density of cell seeding on the scaffold strands and mechanical support provided to the attached cells and growing tissues. The resolved scale numerical modeling approach using LBM adopted in the present study has been demonstrated to be an effective technique for obtaining insight into the culture process. Although the cell growth rate obtained in the present study using the modified cell growth model are in agreement with the results of other models documented in the literature, additional data from biological experiments is required to assess the accuracy of the model.

As a continuous study of the present one, the authors will apply the developed model to a more complicated (as compared to the one used in the present study) tissue scaffolds for simulation studies. It is believed that the present study has laid down a solid base to perform such a comprehensive study of the flow and transport through tissue scaffolds in perfusion bioreactors.

Acknowledgements

The authors wish to acknowledge the financial support of the Natural Science and Engineering Research Council of Canada (NSERC) and the Saskatchewan Health Research Foundation (SHRF).

Chapter 4

Modelling and simulation of the chondrocyte cell growth, glucose consumption and lactate production within a porous tissue scaffold inside a perfusion bioreactor

Md. Shakhawath Hossain, D.J. Bergstrom, X.B. Chen
(Published in: Biotech. Rep., 2015, vol. 5, pp. 55-62)

Abstract

Mathematical and numerical modelling of the tissue culture process in a perfusion bioreactor is able to provide insight into the fluid flow, nutrients and waste transport, dynamics of the pH value, and the cell growth rate. Knowing the complicated interdependence of these processes is essential for optimizing the culture process for cell growth. This paper presents a resolved scale numerical simulation, which allows one not only to characterize the supply of glucose inside a porous tissue scaffold in a perfusion bioreactor, but also to assess the overall culture condition and predict the cell growth rate. The simulation uses a simplified scaffold that consists of a repeatable unit composed of multiple strands. The simulation results explore some problematic regions inside the simplified scaffold where the concentration of glucose becomes lower than the critical value for the chondrocyte cell viability and the cell growth rate becomes significantly reduced.

4.1 Introduction:

In tissue engineering, the development of the artificial tissues largely depends on the supply of an adequate amount of nutrients, including oxygen and glucose to the cells during the culture process (Blitterswijk 2008). The *in vitro* cell culture process inside a bioreactor under dynamic flow conditions has shown significant potential for the development of artificial tissues to replace damaged or injured tissues (Blitterswijk 2008). During such a dynamic cell culture process, the cells are seeded on artificial three-dimensional (3D) scaffolds constructed of biocompatible polymers which are then placed inside the bioreactor to provide nutrients and flow-induced mechanical stimuli, such as shear stress, to the cells to promote cell growth and tissue generation (Porter *et al.* 2005; Chung *et al.* 2007; Sacco *et al.* 2011; Hossain *et al.* 2012). Freed *et al.* (2004) found that the growth rate of cartilage cells (chondrocytes) decreased in a static culture process as the cell density increased. The reason for this might be that the increased cell density inside the scaffold decreases the permeability, which in turn limits the supply of glucose and thus chondrocyte growth. For a well-mixed culture condition, however, the regenerated cartilage was capable of resurfacing small joints, e.g. the trapezium bone at the base of a human joint (Freed *et al.* 2004). Among the various bioreactors, perfusion bioreactors are the most promising as compared to other non-perfusion bioreactors (Pörtner *et al.* 2005; Rodrigues *et al.* 2011; Yan *et al.* 2012). In perfusion-type bioreactors, the fluid is directed to flow through the bioreactor and porous scaffold. Typically the inlet velocity inside the perfusion bioreactor varies between 0.1 to 1 mm/s (Yan *et al.* 2011; Nava *et al.* 2013). The study of Davisson *et al.* (2002) demonstrates the positive effects of perfusion on cartilage growth inside a scaffold.

Besides the supply of nutrients to the cells, perfusion bioreactors also play an important role in removing the waste products or products of metabolism, such as CO_2 and lactate in order to retain a viable cell culture condition. During the culture process the chondrocyte cells produce a significant amount of lactate due to the presence of glycolysis (Blitterswijk 2008). The lactate production rate is also related to the metabolism of oxygen (Lin *et al.* 2013). The metabolism of a single glucose molecule yields two lactic acid molecules. On the other hand, three molecules of oxygen are required to oxidize one lactate molecule (Sengers *et al.* 2005; Boubriak *et al.* 2006).

As the glucose consumption rate for chondrocyte cells is substantially higher than the oxygen consumption rate, the oxidation of lactic acid molecules can be ignored and only the production of lactate due to glycolysis was considered to perform the simulation (Lin *et al.* 2013). It was also found that glucose is the main nutrient for the chondrocyte cell to develop the intervertebral disc tissue (Horner *et al.* 2001; Bibby *et al.* 2002). Even at high oxygen concentrations, disc cells mainly rely on glycolysis and hence produce lactate (Jackson *et al.* 2011). A rising level of lactate can decrease the pH level and hamper the cell growth (Blitterswijk 2008). Typically the disc cells cannot survive at a pH level lower than 6.0 for an extended period of time (Horner *et al.* 2001; Bibby *et al.* 2002). In a similar fashion, chondrocytes exhibit higher metabolic activity if the pH value is greater than 7.0 and even slight changes in the pH level (pH 6.6) are found to retard energy metabolism of the cells (Wu *et al.* 2007). A number of experimental and computational studies have investigated the correlation among nutrient consumption, lactate production and pH value during the culture process (Lin *et al.* 2013, Zhou *et al.* 2008). Such studies provide important information on the *in vitro* cell culture process, e.g. a glucose concentration of 0.3 mM and pH value of 6.8 is considered critical for chondrocyte cell viability (Zhou *et al.* 2008).

Most of the studies investigate the influence of pH and waste products on the cell culture process to date are limited to the static culture process. However, Zacharof *et al.* (2013) studied the cell growth dynamics of *Lactococus lactis* inside a stirred-tank bioreactor and found that the growth is highly dependent on the substrate consumption and pH value of the medium. To predict the volumetric cell productivity, Zacharof *et al.* (2013) developed a cell growth model by taking into account the influence of the produced lactate and pH value. Zhou *et al.* (2008) studied the interdependence among oxygen, glucose, lactic acid, and pH value for the cartilage culture process. Their study was performed in static, perfusion and suspended culture systems. The results indicated that the perfusion and suspended culture systems produced a higher cell density than the static culture system. In Zhou *et al.*'s (2008) study, the perfusion was modeled for the medium alone and the flow within the tissue scaffold was not considered. Another major drawback of the aforementioned studies (Zhou *et al.* 2008; Zacharof *et al.* 2013) is that they do not consider the influence of the shear stress on the cell growth rate. In the studies of Sacco *et al.* (2011), Nava *et al.* (2013) and Hossain *et al.* (2014) the Monod-Contois cell growth equation was modified to incorporate the influence of the shear stress. On the other hand, the cell growth

predicted in those studies does not consider the influence of the lactate production during the culture process. As such, a comprehensive resolved scale simulation of the transport inside a complex porous tissue scaffold with a realistic cell growth model is desirable for improving our understanding of the cell culture process in perfusion bioreactors.

Mathematical and computational modelling of *in vitro* tissue culture process in perfusion bioreactors is capable of providing the nutrient concentration distribution (Lin *et al.* 2013). The developed mathematical models can be used in the simulation to obtain both the nutrient and waste product distribution. However, performing a resolved-scale simulation is difficult due to the complicated geometry of the scaffold, even though the local fluid velocity in perfusion bioreactors is typically very small. Recently, the multiple relaxation time lattice Boltzmann method (MRT LBM) has become an attractive numerical method for simulating flow and mass transfer with complex boundaries (Mei *et al.* 2013). This method has been used to optimize the bioreactor culture condition and scaffold microarchitecture for the culture process (Porter *et al.* 2005), simulate packed bed reactors (Sullivan *et al.* 2005), simulate biofilm growth in a 3D porous media (Schulenburg *et al.* 2008), and develop a 3D biofilm growth model applicable to random porous media (Pintelon *et al.* 2011). The D3Q7 MRT LBM mass transfer model is especially suitable for solving the mass transfer equation for high Peclet number flows (Yoshida *et al.* 2010). In the perfusion culture process the culture medium is typically water and the molecular diffusivity of the nutrients is a few orders of magnitude lower than the kinematic viscosity of water. Even though the Reynolds number is typically within the creeping flow regime, the Peclet number inside the bioreactor is always a few orders of magnitude higher.

This study presents a resolved-scale simulation of fluid flow and mass transfer through a generic scaffold made from strands with a thin layer of chondrocyte cells attached at the strand surface. Such simple unit scaffolds have been widely used in the literature to analyze the mechanical properties of the scaffolds and regenerated tissue (Hollister 2005), to design porous scaffold microstructure (Chen *et al.* 2011) and to predict the cartilage tissue growth (Nava *et al.* 2013). The simulation in the present study investigates the shear stress values, the glucose consumption and lactate generation and the pH values at the surface of the strands. Transport of both glucose and lactate by the fluid flowing through the bioreactor and scaffold are also studied. Finally, the Chondrocyte cell growth rate has been predicted for cartilage tissue regeneration, by

adopting a growth model which takes into account the shear stress acting on the cells, glucose consumption, and lactate production.

4.2 Mathematical model:

In the present simulation a simplified scaffold structure, which consists of a single pore – or generic cell – as shown in Figure 1, is modelled within a perfusion bioreactor. To perform the simulation and develop the model the following assumptions are made:

1. The culture medium or the fluid inside the bioreactor is Newtonian.
2. The Reynolds number inside the bioreactor is low and the flow is incompressible. The effect of viscous heat dissipation is neglected.
3. A thin layer of chondrocyte cells are assumed to be attached at the surface of the strands.
4. The thickness of the chondrocyte cell layers is assumed to be negligibly thin compared to the diameter of the strands. Hence it is assumed that the biochemical reactions, such as the Michaelis-Menten kinetics and Monod growth kinetics, occur only on the surface of the strands. Also, the attached cell layers do not have any influence on the flow field.
5. The main component of the nutrient (substrate) is glucose and the main product of the glycolysis is lactate. The concentration distributions of the glucose and lactate are predicted by the model. Other nutrients (i.e. oxygen) are not considered.
6. The scaffold strands and attached cell layers are rigid and impermeable to the fluid. No-slip boundary conditions are applied at the strands surface.
7. To calculate the cell growth rate, the initial stage of the culture process was considered.

4.2.1 Flow equations

The governing equations for the flow are the continuity and momentum equations, which represent the conservation of mass and momentum, respectively:

$$\frac{\partial u_i}{\partial x_i} = 0 \tag{4.1}$$

$$\rho \frac{\partial u_i}{\partial t} + \rho u_j \frac{\partial u_i}{\partial x_j} = -\frac{\partial p}{\partial x_i} + \frac{\partial}{\partial x_j}\left(\mu \frac{\partial u_i}{\partial x_j}\right) \tag{4.2}$$

where, u_i are the velocity components, x_i and x_j are the spatial coordinates. The subscripts i and j run from 1 to 3. The variables u_i, x_i and x_j with the subscripts represents as follows: $x_1 = x, x_2 = y,\ x_3 = z$ and $u_1 = u, u_2 = v,\ u_3 = w$. In equation 4.2, ρ is fluid density, μ is dynamic viscosity and p is pressure. Solving the governing equations numerically yields the velocity and pressure fields. From the velocity information, the viscous stress tensor, τ_{ij}, can be obtained by using the following constitutive relation for a Newtonian fluid:

$$\tau_{ij} = \mu\left(\frac{\partial u_i}{\partial x_j} + \frac{\partial u_j}{\partial x_i}\right) \tag{4.3}$$

4.2.2 Nutrient transport equations

The governing equation for single phase mass transfer through a single pore of a tissue scaffold is the convection-diffusion equation (CDE)

$$\frac{\partial C_\sigma}{\partial t} + u_i \frac{\partial C_\sigma}{\partial x_i} - \frac{\partial}{\partial x_i}\left(D_\sigma \frac{\partial C_\sigma}{\partial x_i}\right) = 0 \tag{4.4}$$

where C_σ and D_σ are the concentration and diffusion coefficient of species σ, i.e. glucose (g) and lactate (l). At the surface of the strand glucose is consumed by the thin layer of cells with the consumption rate, R_g, which is assumed to be a function of the local glucose concentration C_g, is described by the Michaelis-Menten kinetics,

$$R_g(C_g) = \frac{R_{mg} C_g}{K_{mg} + C_g} \tag{4.5}$$

where R_{mg} and K_{mg} represent the maximum consumption rate and half-saturation constant of glucose, respectively. The values of all of the model parameters are given in Table 4.1.

During the consumption of glucose one molecule of glucose is broken down into two lactic acid molecules. Therefore the production of lactate can be expressed by the following equation:

$$R_l = -2 \times R_g \tag{4.6}$$

Table 4.1: Numerical values of the model parameters used in the simulations

Definition	Value	Reference
Inlet glucose concentration, C_g	5.56 mM	Zhou *et al.* (2008)
Glucose diffusivity, D_g	1.0×10^{-9} m^2/s	Lin *et al.* (2013)
Lactate diffusivity, D_l	1.4×10^{-9} m^2/s	Lin *et al.* (2013)
Maximum specific cell growth rate, μ_{max0}	1/(2×24×3600) 1/s	Sacco *et al.* (2011)
Glucose consumption rate k_{sg}	2.3 g/cm^3	Chung *et al.* (2010)
Lactate production rate k_{sl}	2.3 g/cm^3	This work
Glucose maximal consumption rate, R_{mg}	3.9×10^{-5} $kg/(m^3s)$	Chung *et al.* (2010)
Glucose half saturation constant, K_{mg}	6.3×10^{-3} kg/m^3	Chung *et al.* (2010)
α	0.8761	Sacco *et al.* (2011)
β	0.1045	Sacco *et al.* (2011)

4.2.3 pH equation

At a lower pH value (pH less than 7) the culture medium becomes acidic. The acidic environment can have an adverse effect on the matrix production and even on the cell viability (Sengers *et al.* 2005). The pH of the culture medium depends on the lactic acid concentration (Zhou 2005). Zhou *et al.*'s (2008) experiment developed the following linear relationship between the pH value and lactate concentration:

$$\text{pH} = 7.4 - 0.0406\, C(l) \tag{4.7}$$

4.2.4 Cell growth equations

For the cell growth, the Monod growth kinetics has been widely used in the literature, i.e.

$$\mu(C_\sigma) = \frac{\mu_{max}\, C_\sigma}{\rho_c\, k_{s\sigma} + C_\sigma} \tag{4.8}$$

where μ and μ_{max} are the cell growth rate and the maximum specific growth rate, respectively, ρ_c is the reference cell density and $k_{s\sigma}$ is a dimensionless parameter representing the Contois saturation constant of species σ. To account for the mechanical stimuli, Sacco *et al.* (2011) modified equation 4.8 by assuming that the maximum specific growth rate is a linear function of the shear stress induced on the cells, i.e.

$$\mu_{max} = \mu_{max0}(\alpha + \beta\tau) \tag{4.9}$$

where μ_{max0} is the maximum growth rate in a static condition. In the work of Sacco *et al.* (2011), the values of the parameters α and β were determined from experiments

A cell growth equation that considers the inhibition effect of the lactate and the influence of the pH of the media is given by Zacharof *et al.* (2013),

$$\mu = \frac{(\mu_{max} * C_g)\,(k_{sl} + C_l)}{(k_{sg} + C_g) * C_l} \tag{4.10}$$

In this equation, C_l represents the concentration of lactate. The k_{sg} and k_{sl} are the glucose consumption rate and lactate production rate respectively. In the present study the model has been modified using Sacco *et al.*'s shear stress dependent maximum specific growth rate, i.e.,

$$\mu\,(\tau, C_\sigma) = \frac{(\mu_{max}(\tau) * C_g)\,(\,k_{sl} + C_l)}{(\,k_{sg} + C_g) * C_l} \tag{4.11}$$

In this model, only the beneficial effect of shear stress on cell growth has been included. Further experimental studies are required to validate the model, to determine the shear stress range within which the effect on cell growth remains beneficial.

4.3 Methods

To perform the numerical simulation, only part of a tissue scaffold has been considered as shown in Figure 4.1. It is assumed that the scaffold is made of polystyrene and the geometric integrity of the scaffold remains unchanged during the culture process. The co-ordinate frame is located at the mid-point of the inlet plane. The simplified scaffold consists of two circular strands of radius R aligned in the flow direction. These two strands are located 0.7 R downstream of the inlet plane and the length of each strand is 7.8 R. The overall length of the channel in the streamwise direction (x) is 10 R. At 2.5 R from the inlet plane, two circular strands of radius R are positioned perpendicular to the flow, directly above and below the longitudinal strands as shown in Figure 4.1. These two strands will be referred to as the front strands in the following discussion. Similarly at 6.5 R downstream, two more strands are positioned perpendicular to the flow; these two strands will be referred to as the rear strands. The center-to-center distance between the two pairs of strands is 4 R. The width and height of the simplified scaffold is 4 R . Note that only one-half of each strand is included in the solution domain.

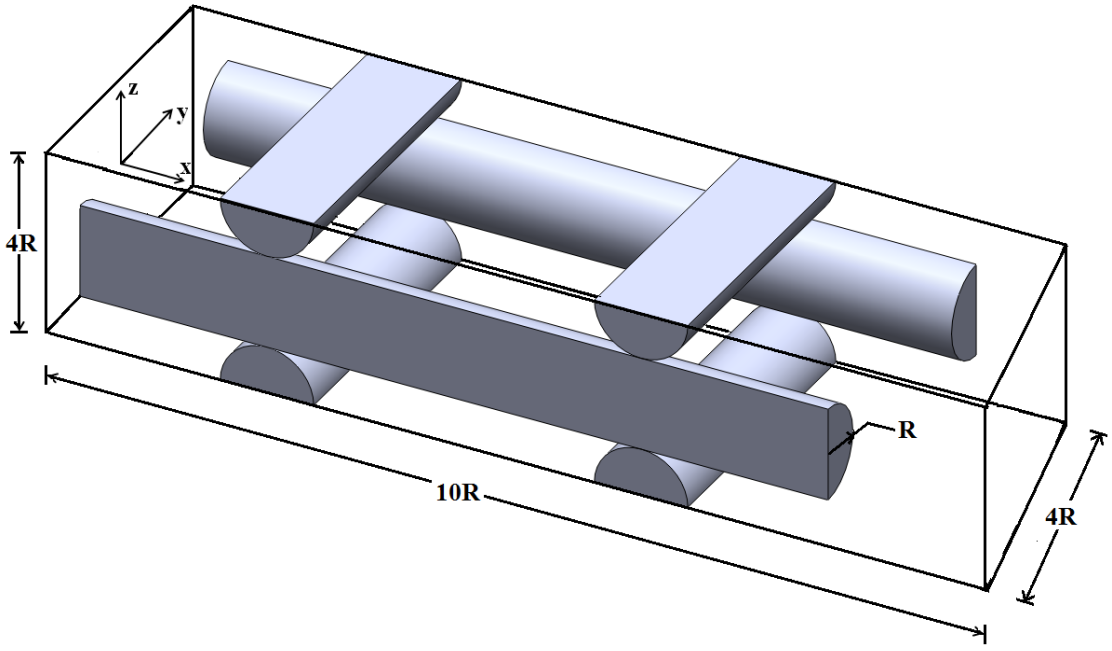

Figure 4.1: Geometry of the portion of the tissue scaffold considered by the simulation with strand radius $R = 0.46$ mm

In this study the fluid flow and mass transfer simulation has been performed using the D3Q19 and D3Q7 MRT LBM model respectively (Yoshida *et al.* 2010; d'Humières *et al.* 2002; Voronov *et al.* 2010). The details of the MRT LBM methods used in the present paper can be found in previous study of Hossain *et al.* (2013) and in Sullivan *et al.* (2005). The number of nodes used for the simulation was 115×46×46 in the *x*, *y* and *z* directions, respectively. The grid was uniform with a spatial increment of δx = 0.04 mm and the simulation used a time step of δt = 0.266 ms. The radius of each strand was R = 0.46 mm and the distance between the strands is $2R$ = 0.92 mm. The distance between the strands is selected based on the information available in the literature (Yan *et al.* 2011; Bawolin *et al.* 2010). The relaxation parameter value was set to s_v= 1.0 to yield a kinematic viscosity of ν = 1×10^{-6} m^2/s. The flow inside the channel was driven by the pressure difference specified between the inlet and outlet planes. The Reynolds number for the simulation was $Re_D = 0.21$ which models the flow condition inside a typical bioreactor and was calculated using the equation, $Re_D = \frac{UD}{\nu}$, where U is the bulk velocity at the inlet of the

channel. The present simulation considers an inlet bulk velocity of 0.23 mm/s. Periodic boundary conditions were applied at the side, upper and lower walls. An interpolation-based bounce-back (IBB) boundary condition was used to implement the no-slip condition on the curved wall of the strand on the uniform mesh (Zhang *et al.* 2012). It was assumed that the cells are attached uniformly to the scaffold surface and the thickness of the attached cells is negligible compared with the strand diameter. Hence, it was also assumed that the glucose consumption and lactate production due to the biochemical reaction occurs only at the surfaces of the strands.

For the mass transfer simulation, the inlet value of the concentration of glucose (5.56 mM) being convected by the incoming fluid is assumed to be uniform. The concentration boundary condition applied at the side walls was periodic. A zero concentration gradient normal to the boundary surface was implemented at the outlet of the bio-reactor using a general bounce-back scheme proposed by Zhang *et al.* (2012) was adopted. A Michaelis-Menten kinetics reaction was specified at the strand surface. To model the reaction on the surface of the circular strand, the consumption rate, R_σ was calculated at the surface of the strand. The concentration values were specified at the surface of the strands using linear extrapolation based on previous time steps and these values were subsequently used to calculate the value of R_σ, which was then used to calculate the distribution functions following the procedure described in Yoshida *et al.* (2010).

The mass transfer simulation was decoupled from the fluid flow simulation and the velocity field obtained by solving the flow equations was used to simulate the mass transport Sullivan *et al.* (2005). The decoupling allowed a different time step of δt = 0.005 ms to be used for the mass transfer simulation. The relaxation parameter value of s_D = 1.963 and 1.949 were used to specify diffusivity values corresponding to glucose, D_g = 1×10^{-9} m^2/s and lactate D_l = 1.4×10^{-9} m^2/s; the corresponding Schmidt numbers were 1000 and 714. Consideration of the Schmidt number in such low Reynolds number flow is important since for high Schmidt numbers convection is dominant relative to diffusion (Dani *et al.* 2006). The Peclet numbers of glucose and lactate were 211 and 151, respectively.

4.4 Results and discussion

The velocity vector fields on the x-z plane at y/R = 0 and on the x-y plane at z/R = 0, respectively are shown in Figure 4.2a) and 4.2b) respectively. For a cleaner presentation of the vector field, only one out of two vectors is plotted in the x-direction. Figure 4.2a) indicates that the velocity vector field is symmetric about the center line y/R = 0, as implied by the geometry. The flow is observed to accelerate through the gap between the front strands and a maximum velocity of u/U = 6.76 occurs at the center line. The fluid is again seen to accelerate while flowing between the rear strands and a maximum velocity of u/U = 6.80 occurs at the center line. No evidence of flow recirculation or reverse flow is evident downstream of the front and rear strands. A lower velocity region is observed between the front and rear strands and behind the rear strands at the top and bottom surfaces of the solution domain. In Figure 4.2b) the velocity vector field is also symmetric about the center line z/R = 0. A relatively high velocity region can be observed from x/R = 1.5 to 3.5 and also from x/R = 5.5 to 7.5. This is due to the acceleration of the fluid flowing between the front and rear strands placed across the flow. The magnitude of the velocity vectors is very low in the region behind the strands near the outlet plane.

The surface shear stress profiles are shown in Figure 4.3a) and the profiles are almost identical for both the front and rear strands. The maximum surface stress occurs slightly upstream of the strand shoulder for both the front and rear strands and the value of the maximum shear stress value is 0.04 N/m^2. The mean shear on the surface of the strand is approximately 0.02 N/m^2. In Raimondi *et al.*'s (2006) study for an inlet velocity of 0.221 mm/s the mean shear stress was observed to be 0.16 N/m^2 inside the bioreactor. The shear stress profile on the inside surface of the strand aligned in the streamwise direction is shown in Figure 4.3b). The value of the shear stress begins to increase at x/R = 1.0 and reaches the maximum value at x/R = 2.5. From x/R = 2.5, the value begins to decrease and the minimum shear stress value occurs at x/R = 4.5. The peaks in the shear stress profile are due to the presence of the front and rear strands with centers located at x/R = 2.5 and x/R = 6.5, respectively. Recall that the acceleration of the velocity vectors associated with the transverse strands was also evident in Figure 4.2b).

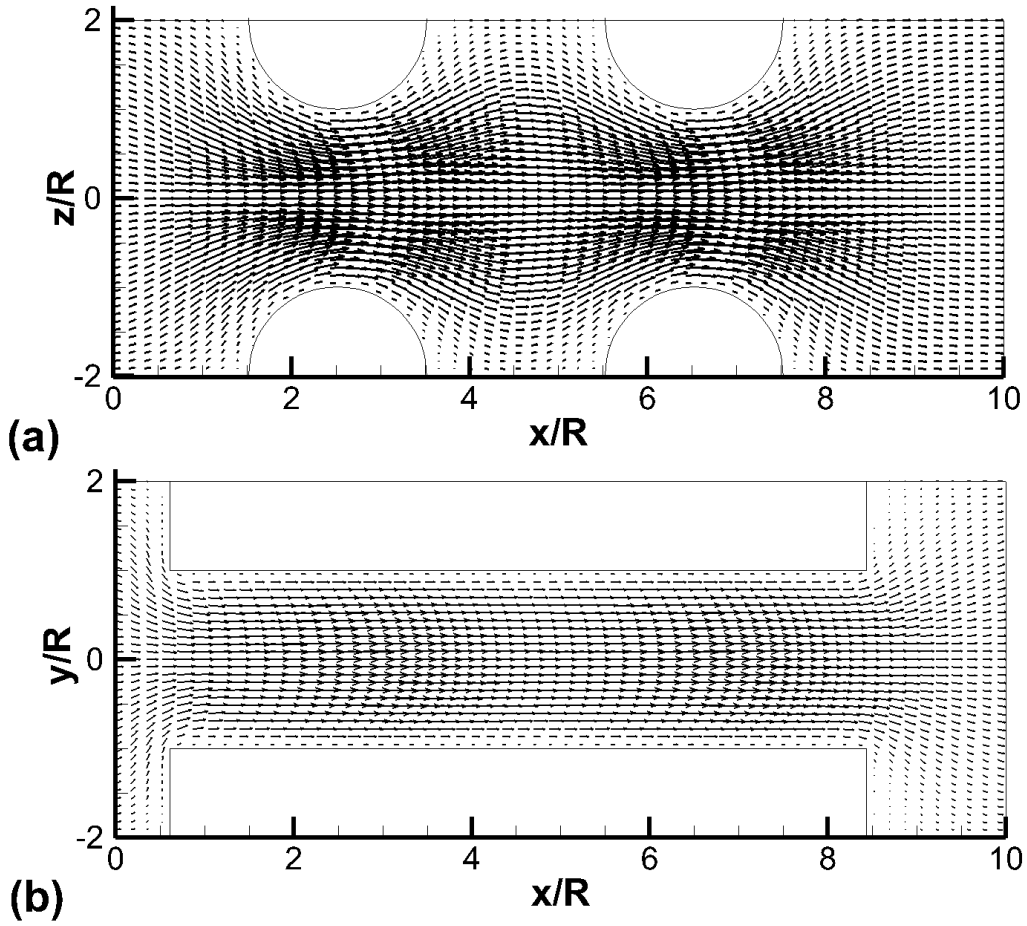

Figure 4.2: Velocity vector fields: a) on the *x*-*z* plane at *y*/*R* = 0, and b) on the *x*-*y* plane at *z*/*R* = 0

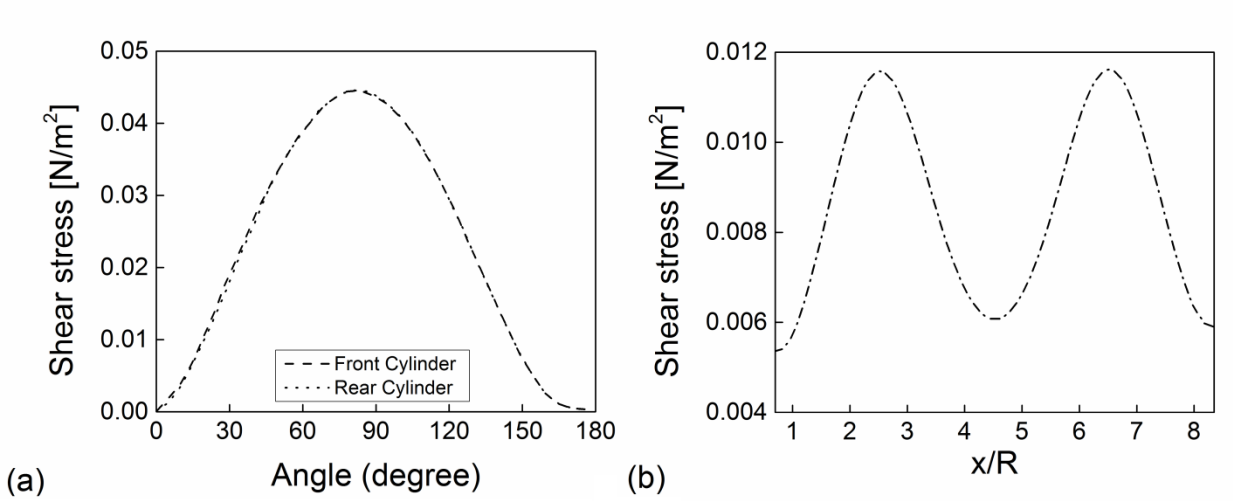

Figure 4.3: Shear stress profiles on: a) the surface of the front and rear strands at *y/R* = 0, and b) the strand shoulder along the streamwise direction at *z/R* = 0

The steady state glucose concentration distribution on the x-z plane at y/R = 0 and on the x-y plane at z/R = 0 is shown in Figure 4.4a) and 4.4b), respectively. Figure 4.4a) shows that, the higher glucose concentration, $C_g = 5.56$ mM, coming from the inlet can only reach up to *x/R* = 5 or halfway through the pore. At the surface of the strands the concentration values become much lower due to the consumption of glucose by the thin layer of cells. The concentration values are close to zero in the low velocity regions described in Figure 4.2a), i.e. between the front and rear strand and behind the rear strand. This clearly indicates that convective transport is important to supply glucose inside the porous structure. Figure 4.4b) shows that along the center line *y/R* = 0 a relatively high glucose concentration extends up to *x/R* = 5. A layer of lower concentration values can be observed on the strand surface, and the thickness of the layer increases along the streamwise direction. A region of very low concentration can be seen in the low velocity region behind the strands identified in Figure 4.2b). Overall, Figure 4.4a) and 4.4b) indicate that, for the present flow conditions, the convective transport fails to supply significant amounts of glucose to the region between the front and rear strands, the region behind the rear strands and the region behind the streamwise strands at the exit of the pore. Figure 4.5a) and 4.5b) show the steady state lactate concentration distribution on the *x-z* plane at *y/R* = 0 and on the x-y plane at *z/R* = 0, respectively. Lactate concentration is higher at the surface of the strands where glucose is consumed. Higher concentration of lactate can also be observed in the lower velocity regions.

The lactate contour distributions also indicate that, for the present flow conditions, the fluid velocity is not sufficient to entirely remove the lactate produced at the scaffold surface.

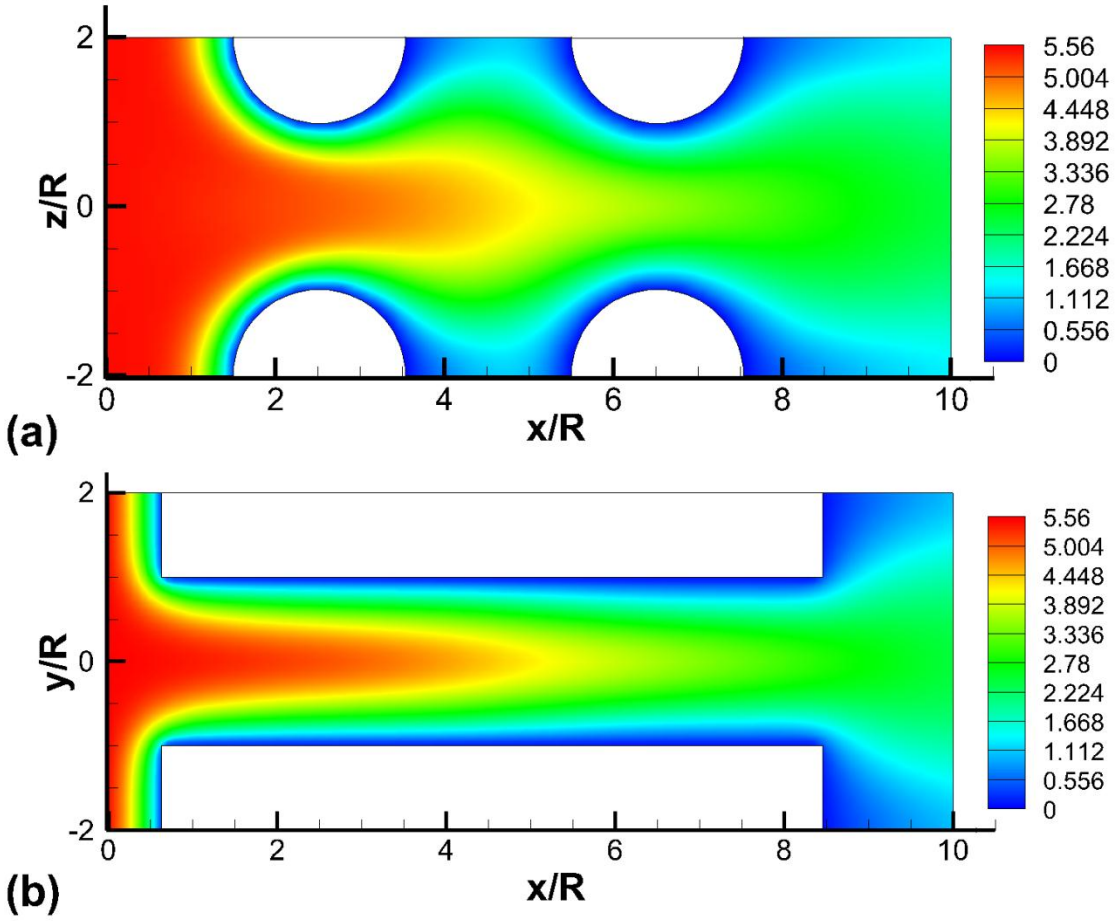

Figure 4.4: Glucose concentration (mM) fields: a) in the *x*-*z* plane at *y*/*R* = 0, and b) in the *x*-*y* plane at *z*/*R* = 0

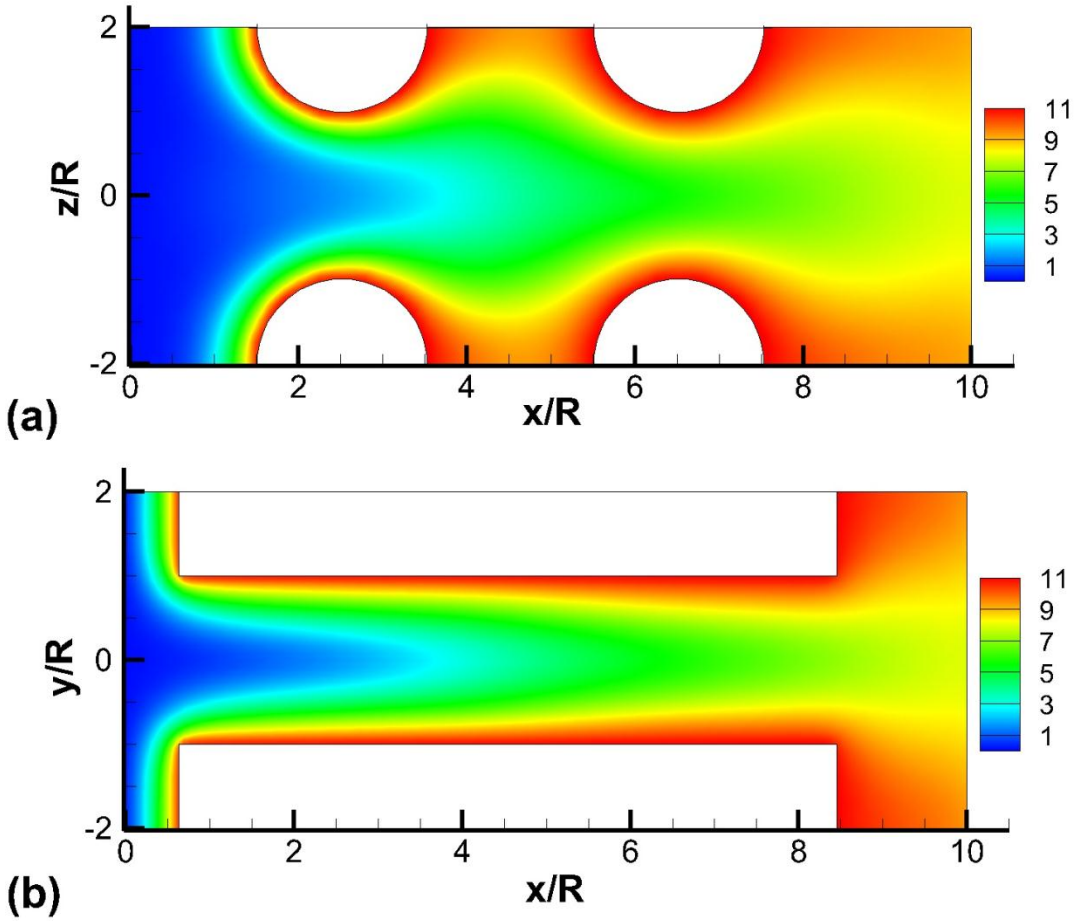

Figure 4.5: Lactate concentration (mM) fields: a) in the *x*-*z* plane at *y*/*R* = 0, and b) in the *x*-*y* plane at *z*/*R* = 0

Figure 4.6 investigates the glucose concentration on the surface of the strands. Figure 4.6a) shows the glucose concentration profile on both the front and rear strand surfaces at y/R = 0. Recall that the cells were attached to the surface of the strand and that the glucose consumption by the cells is defined by a Michaelis-Menten kinetics-type reaction. The concentration profile for the front strands shows that the maximum concentration value occurs near the front stagnation point where the maximum value is approximately C_g = 0.5 mM. The value begins to decrease near 45° and reduces to a value of about C_g = 0.02 mM at the downstream stagnation point. The rear strand concentration profile shows a markedly different

behavior than the front strand profile. For the rear strand, the maximum concentration occurs slightly upstream of the strand shoulder and the value is approximately C_g = 0.2. The difference in the maximum glucose concentration between the front and rear strands is approximately 60%, which is significant. From the concentration profiles predicted for the strand surfaces, it is evident that the cells attached to the downstream face of the front strand and to the surface of the rear strands will be supplied with a glucose concentration that is lower than the critical value (0.3 mM). As such, a lower cell growth can be expected for these regions. Figure 4.6b) shows the glucose concentration at the inner surface of the strands aligned in the streamwise direction. A maximum and minimum concentration value can be observed at the front and rear end points, with values of C_g = 0.85 and 0.21, respectively. In the region from *x/R* = 4.5 to 8.5, the concentration values fall below the critical value of C_g = 0.3 mM, and hence cell viability is threatened.

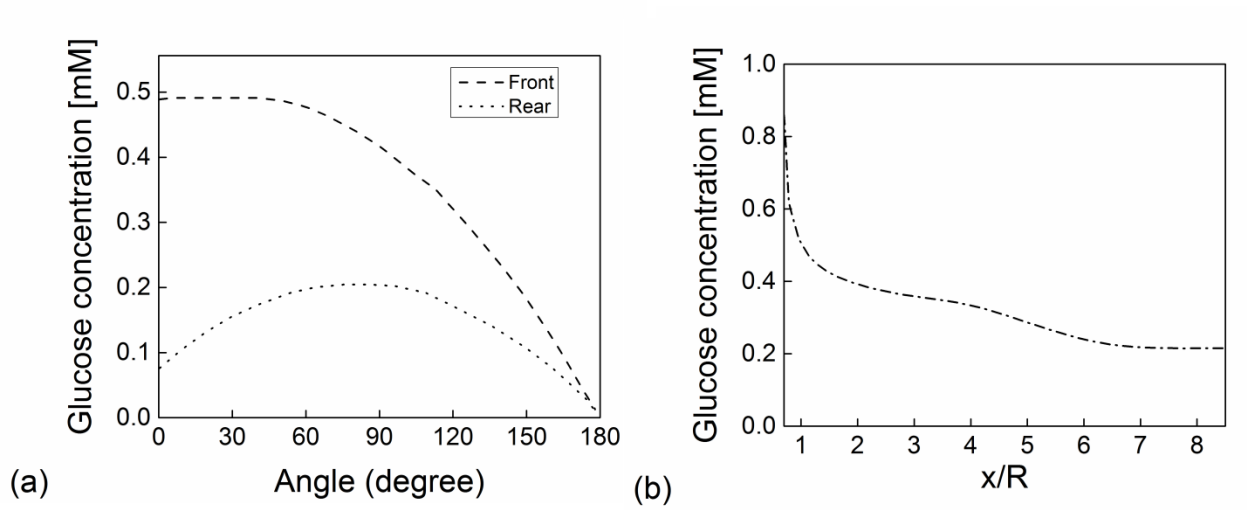

Figure 4.6: Glucose concentration profiles on: a) the surface of the front and rear strands at *y/R* = 0, and b) the inner shoulder of the strand in the streamwise direction at *z/R* = 0

Figure 4.7a) shows the lactate concentration profile on both the front and rear strand surfaces at *y/R* = 0. The concentration profiles of lactate show the opposite behavior to the glucose profiles. The maximum and minimum values are observed at the downstream and upstream stagnation points, respectively. For the front strand, the minimum concentration value is C_l = 10.25 mM. A maximum value of C_l = 11.20 mM can be observed at the downstream

stagnation point. For the rear strand, the maximum lactate concentration value is C_l = 11.20 mM which can be observed at the downstream stagnation point. Figure 4.7b) shows the lactate concentration on the inner surface of the strand aligned in the streamwise direction. The minimum value of C_l = 9.5 mM is found at the front end. The lactate concentration increases along the strand surface as the distance from the front end increases and reaches a maximum value of C_l = 10.8 mM at the rear end point of the strand. The accumulation of lactate inside the scaffold is particularly important as the pH level decreases with increasing lactate concentration. Figure 4.8a) shows the pH profile on both the front and rear strand surfaces at y/R = 0. The minimum pH value of 6.95 occurs at the rear stagnation point for both the front and rear strands, so that the pH value on both surfaces remains above the critical value of 6.8 for cell viability. Figure 4.8b) shows the pH on the inner surface of the strand aligned in the streamwise direction. The minimum pH value of 6.97 occurs at the rear end point of the strand.

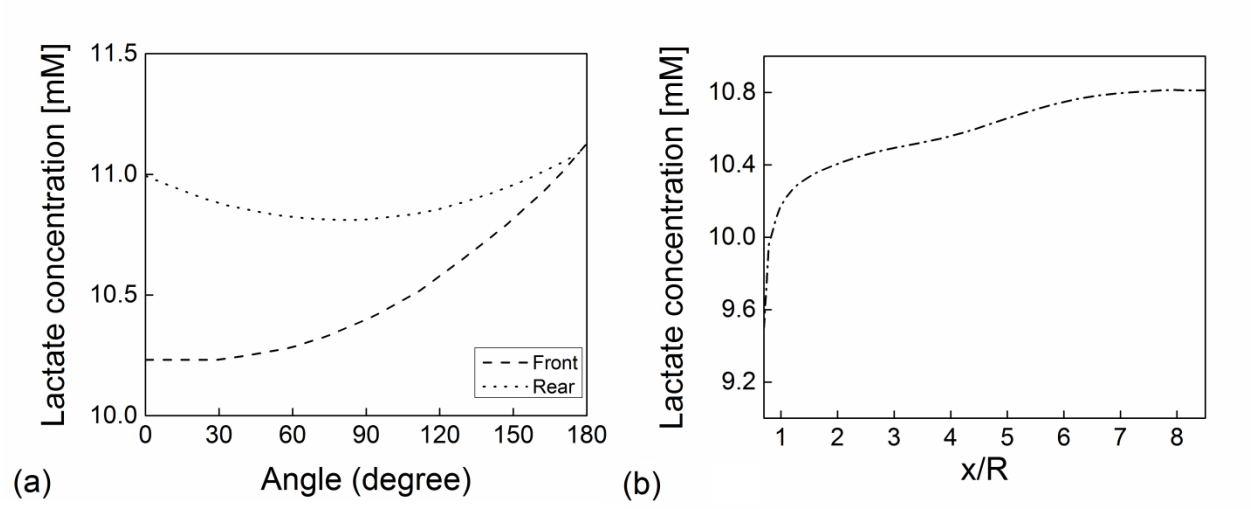

Figure 4.7: Lactate concentration profiles on: a) the surface of the front and rear strands at y/R = 0, and b) the inner shoulder of the strand in the streamwise direction at z/R = 0

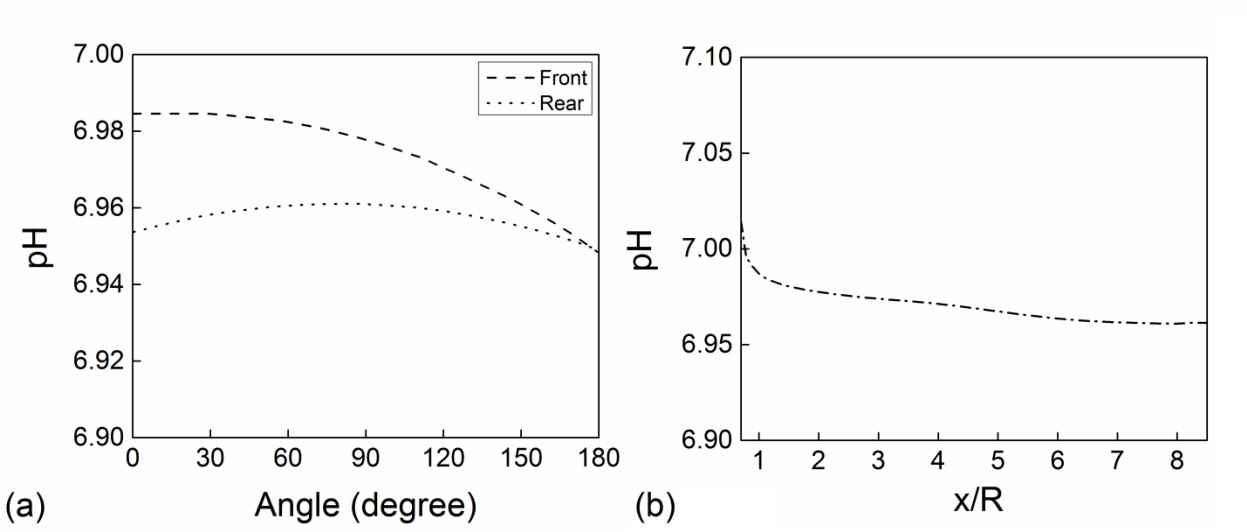

Figure 4.8: pH profiles on: a) the surface of the front and rear strands at y/R = 0, and b) the inner shoulder of the strand in the streamwise direction at z/R = 0

Figure 4.9 shows the cell growth rate normalized by maximum specific cell growth rate (μ_{max0}). Recall that the cell growth rate model adopted in this study (Equation 4.10) considers the shear stress acting on the surface, consumption of glucose and production of lactate. From Figure 4.9, it is evident that the cell growth rate profiles show similar behaviour as the glucose concentration profiles. This indicates the fact that, the most important factor in cell growth is the glucose supply. The cell growth rate is significantly higher on the upstream face of the front strand where the glucose supply was higher compared to the downstream face. The cell growth rate profile on the rear strand indicates that the maximum cell growth rate occurs at about θ = 75°. In Figure 4.9b), the maximum and minimum normalized cell growth rate is found at the front and rear end, respectively, of the strand aligned in the streamwise direction.

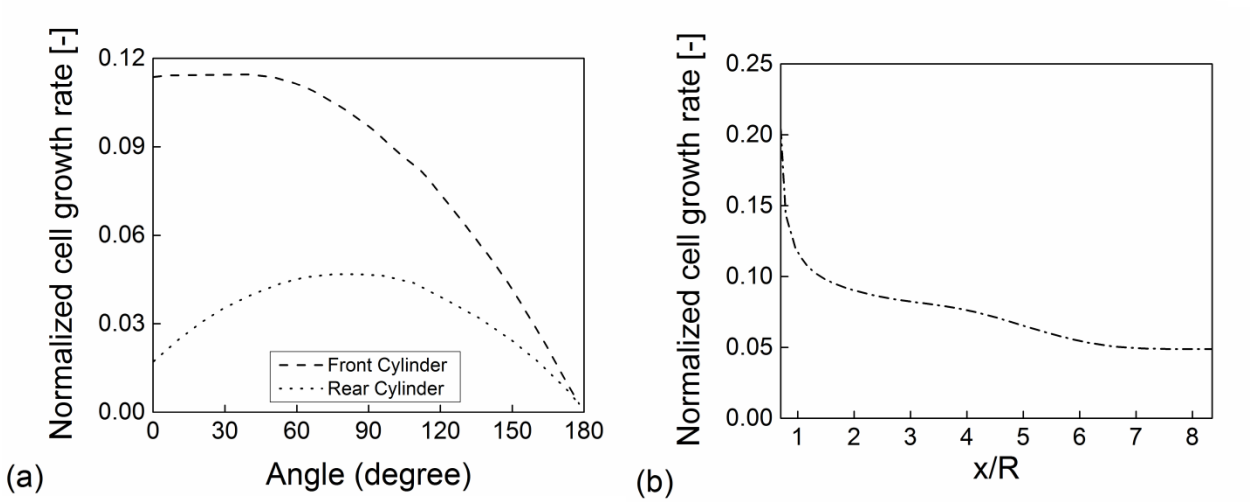

Figure 4.9: Cell growth rate profiles on: a) the surface of the front and rear strands at y/R = 0, and b) the inner shoulder of the strand in the streamwise direction at z/R = 0

4.5 Conclusions

In this study, a resolved scale simulation of the fluid flow and nutrient (glucose) transfer through a simplified tissue scaffold consisting of a repeatable unit/pore inside a perfusion bioreactor has been performed. In this simulation, it is assumed that: 1) the glucose concentration is uniform at the inlet, and 2) the glucose consumption occurred at the surface of the strands by a thin layer of chondrocyte cells following the Michaelis-Menten kinetics. The predictions for the glucose concentration show that at the flow conditions considered in the present study, the value of the glucose concentration becomes lower than the critical value of 0.3 mM on the downstream face of the front strand, on the surface of the rear strand and on the rear half of the inner surface of the strand aligned in the streamwise direction. The major reason for the lower concentration values in the regions described above is the lower velocity which means the convective transport is not high enough to overcome the nutrient consumption by the layer of cells attached on the surface.

The transport of waste products (lactate) through the porous structure has also been included in this simulation. The lactate concentration field shows that a higher lactate accumulation occurs in the regions where velocity is low. However, the decrease in the pH value

due to the production of lactate did not fall below the critical pH value required for a viable cell culture condition. The cell growth rate model adopted here considers the influence of shear stress at the surface of the strands, glucose consumption and lactate generation as well as the pH of the culture medium. The maximum cell growth rate occurred at the front region on the surface of the strand aligned in the streamwise direction. The cell growth rates are much lower on the rear surface of the front strand and on the entire surface of the rear strand. The lower cell growth rate in the regions mentioned above is primarily due to the reduced supply of glucose. The influence of the shear stress on the cell growth rate was assumed to be favorable for the present flow conditions.

The simulation results presented in this paper, particularly the detailed information regarding the fluid flow and nutrient transport inside the porous scaffold, would be essential to understanding the perfusion culture process. From the results, it is evident that, to improve the cell growth rate the supply of glucose should be increased inside the scaffold. The existence of regions with a glucose concentration lower than the critical value might not be observed in a volume-averaged analysis. The improvement in the glucose supply can be achieved by increasing the inlet glucose concentration and inlet velocity. However, increasing the inlet velocity will also increase the shear stress levels acting on the cells, so that it would be prudent to first check whether the higher levels of shear stress are within the cell viability range. Increasing the inlet glucose concentration might increase the amount of lactate production due to the higher consumption rate of glucose, which could cause the pH value of the medium to fall below the critical value. As such an optimization would be required to determine the appropriate inlet condition to ensure both an adequate supply of nutrients and favorable shear stress level for promoting cell growth inside the scaffold. The computational framework presented in this study can be a viable tool to obtain the optimal parameters. Increasing the distance between the strands and reducing the diameter of the strands can also increase the transport of glucose inside the scaffold. However, these parameters should be selected through a detail analysis of the scaffold's mechanical strength. In the future, the authors intend to perform a simulation for a complete porous structure with higher distance between the strands, a higher inlet glucose concentration and flow rate. Such a simulation will be useful for assessing the influence of the higher lactate production and shear stress values on the cell growth rate using the model adopted in the present study.

Acknowledgements

The authors wish to acknowledge the financial support of the Natural Science and Engineering Research Council of Canada (NSERC) and the Saskatchewan Health Research Foundation (SHRF).

Chapter 5

Computational modelling of the scaffold-free chondrocyte regeneration: a two-way coupling between the cell growth and local fluid flow and nutrient concentration

Md. Shakhawath Hossain, D.J. Bergstrom, X.B. Chen

(Published in: Biomech. Model. Mechanobiol., 2015, DOI: 10.1007/s10237-015-0666-0)

Abstract

The *in vitro* chondrocyte cell culture process in a perfusion bioreactor provides enhanced nutrient supply as well as the flow-induced shear stress that may have a positive influence on the cell growth. Mathematical and computational modelling of such a culture process, by solving the coupled flow, mass transfer and cell growth equations simultaneously, can provide important insight into the biomechanical environment of a bioreactor and the related cell growth process. To do this, a two-way coupling between the local flow field and cell growth is required. Notably, most of the computational and mathematical models to date have not taken into account the influence of the cell growth on the local flow field and nutrient concentration. The present research aimed at developing a mathematical model and performing a numerical simulation using the lattice Boltzmann method to predict the chondrocyte cell growth without a scaffold on a flat plate placed inside a perfusion bioreactor. The model considers the two-way coupling between the cell growth and local flow field and the simulation has been performed for 174 culture days. To incorporate the cell growth into the model, a control-volume based surface growth modelling approach has been adopted. The simulation results show the variation of local fluid velocity, shear stress and concentration distribution during the culture period due to the growth of the cell phase, and also illustrate that the positive influence of the shear stress resulted in a 20 percent increase in the overall cell volume fraction.

5.1 Introduction

The artificial cartilage or chondrocyte cell culture process in a perfusion bioreactor can be used to develop cartilage tissue to replace or repair damaged joint cartilage (Galban and Locke 1999). The perfusion bioreactor has shown promise in the development of the tissue engineered cartilage in both the scaffold-based (Sacco *et al.* 2011; Chung *et al.* 2007) and scaffold-free approaches (Li *et al.* 2014, Gilbert *et al.* 2014). The dynamic flow condition in a perfusion bioreactor provides enhanced nutrient transport, increases the cell proliferation rate and obtains a more even cell distribution (Liu *et al.* 2013). The flow induced shear stress within the cell viability range can also modulate the cell physiology and improve the cell growth (Sacco *et al.* 2011). To obtain the full benefit of the dynamic cell culture process it is essential to select the optimal culture parameters, including the flow rate inside the bioreactor and inlet nutrient concentration. Increasing the flow rate through the bioreactor will improve the nutrient transport inside the bioreactor and increase the shear stress acting on the cells. However, excess shear stress can cause cell death, thus leading to the development of poor tissue constructs (Sacco *et al.* 2011). In the past, the input culture parameters were typically selected based on the empirical knowledge and previous experience (Singh *et al.* 2009). In the last decade, mathematical modelling and numerical simulation have been used to quantify the biophysical environment inside the bioreactor, thus providing insights into the fluid flow, shear stress, nutrient distribution and overall cell growth (Porter *et al.* 2005, Cioffi *et al.* 2006; Chung *et al.* 2007; Hossain *et al.* 2012). Such insights have been used to improve the overall culture condition (Rodrigues *et al.* 2011).

Chung *et al.* (2007) developed a mathematical model to predict the overall tissue growth for a porous tissue scaffold. This model solved the volume-averaged momentum, convection-diffusion-reaction and cell growth equations in a coupled fashion. To describe the cell growth, the Monod-Contois (M-C) kinetics was used and modified as a function of the nutrient concentration. Sacco *et al.* (2011) used a similar model with a modified M-C cell growth kinetics to include the influence of shear stress on the biomass growth. Both of the aforementioned studies obtained their computational results using the volume-averaged method (VAM). Although the VAM provides the average shear stress, concentration and cell volume distribution within the porous scaffold, it does not provide specific or local information. Nava *et al.* (2013)

performed a resolved scale simulation for a simplified scaffold, in which the growth of the tissue was modeled using a moving boundary approach. Nava *et al.* (2013) imposed a similar moving boundary condition to that used by Galban and Locke (1997) at the fluid biomass interface. An arbitrary Lagrangian-Eulerian technique was implemented for the mesh movement and the fluid-biomass interface was a function of the local nutrient concentration and shear stress values. To enable realistic tissue growth modelling, implementation of such moving boundary condition is of critical importance. Typically the cell and tissue growth rate is very slow (Sacco *et al.* 2011, Hossain *et al.* 2014) so that the change in the cell-fluid interface due to the growth might not influence the external fluid flow and nutrient distribution during the initial culture period. However, as the culture period becomes longer, the increase in overall cell and tissue growth will influence the flow pattern and subsequent nutrient transport inside the bioreactor and scaffold. Hence, the movement and change in the cell-fluid interface and its influence on the external environment needs to be considered and a two-way coupling between the cell growth and local flow field should be included in the model. Nava *et al.* (2013) presented comprehensive velocity, nutrient and shear stress distributions inside the simplified scaffold structure. However, the influence of the tissue growth on the biophysical environment was not explained in detail. A major challenge in performing such a resolved-scale simulation with a moving boundary condition is that due to the complex geometry of the tissue scaffold and cell growth, a large number of computational nodes is required. At each time step the field variables throughout the solution domain need to be recalculated. This makes the computational procedure both complex and time consuming, and it may cause an issue of convergence as reported by Nava *et al.* (2013), who experienced convergence issues after five simulated culture days. Another major disadvantage of the aforementioned studies is that the scaffold-based culture process which might introduce biocompatibility issues (Hunziker 2001; Nagai *et al.* 2008). However, to date, only a few experimental studies can be found in the literature with a scaffold-free approach (Li *et al.* 2014, Gilbert *et al.* 2014; Marlovits *et al.* 2003). Typically, the duration of the culture period in those experimental studies varied between 21 to 90 days. Realistic mathematical and computational modelling of such a culture process could potentially save a significant amount of time and effort.

For large-scale complex flow problems, the lattice Boltzmann method (LBM) has become an attractive methodology due to its simple stream and collide procedure, and the local

nature of the calculation (Premnath *et al.* 2009). This method has been successfully used in various applications including a packed bed bioreactor (Sullivan *et al.* 2005) and a flow bed bioreactor for cartilage cell growth considering multi-phase flow (Hussein *et al.* 2008).The method has also been successfully applied to predict the cell growth rate at the surface of circular tissue strands (Hossain *et al.* 2015). Schulenburg *et al.* (2009) and Pintelon *et al.* (2010, 2011) developed a biofilm growth model using a LBM platform. The multiple relaxation time (MRT) LBM was used to simulate the pore scale hydrodynamics while the single relaxation time LBM was used to solve the advection-diffusion-reaction equation. The biofilm growth was calculated separately at a different time scale, and in the flow and nutrient transport simulation the change in geometry due to the biofilm growth was implemented in between the time steps. Pintelon *et al.* (2011) obtained the simulated biofilm growth after 14 culture days and the simulation results compared well with the experimental studies. However, the 3D biofilm growth model in the aforementioned studies did not consider the influence of flow-induced shear stress on the biofilm growth and the biofilm attachment on the solid surface was random.

In this study, a mathematical model has been developed and a numerical simulation has been performed using the MRT LBM to obtain the chondrocyte cell growth on a flat plate placed inside a perfusion bioreactor which is typically considered a scaffold-free culture approach. The chondrocyte growth was modelled within the LBM framework on a uniform Cartesian grid. On this basis, the influence of the local shear stress and nutrient distribution on the chondrocyte growth was simulated, thus enabling examination of the dynamic two-way coupling between the chondrocyte growth and the local flow field/nutrient distribution. The overall chondrocyte growth process was simulated over a total of 174 culture days to provide insights that would be impractical by using experiments.

5.2 Mathematical model

5.2.1 Flow equations

The flow concerned in the *in vitro* cell culture process in a perfusion bioreactor can be treated as a single-phase flow inside a confined channel. The governing equations for such a flow includes the continuity and momentum equations,

$$\frac{\partial u_i}{\partial x_i} = 0 \tag{5.1}$$

$$\rho \frac{\partial u_i}{\partial t} + \rho u_j \frac{\partial u_i}{\partial x_j} = -\frac{\partial p}{\partial x_i} + \frac{\partial}{\partial x_j}\left(\mu \frac{\partial u_i}{\partial x_j}\right) \tag{5.2}$$

where ρ and μ represents the density and dynamic viscosity. The velocity fields, u_i, and pressure field, p, can be obtained by solving equation (5.1) and (5.2). The viscous stress tensor, τ_{ij}, can be evaluated from the velocity information by,

$$\tau_{ij} = \mu\left(\frac{\partial u_i}{\partial x_j} + \frac{\partial u_j}{\partial x_i}\right) \tag{5.3}$$

5.2.2 Nutrient transport equations

The single phase mass transfer inside a confined channel is governed by the convection-diffusion equation,

$$\frac{\partial C_g}{\partial t} + u_i \frac{\partial C_g}{\partial x_i} - \frac{\partial}{\partial x_i}\left(D_g \frac{\partial C_g}{\partial x_i}\right) = 0 \tag{5.4}$$

where C_g and D_g are the concentration and diffusion coefficient of glucose.

In this study, R_g, is the the consumption rate of glucose and is assumed to be a function of the local glucose concentration C_g. The consumption rate, R_g, is described by the Michaelis-Menten (M-M) kinetics,

$$R_g(C_g) = \frac{R_{mg} C_g}{K_{mg} + C_g} \tag{5.5}$$

where R_{mg} and K_{mg} represent the maximal consumption rate and half-saturation constant of glucose, respectively. The present study does not consider the diffusion of glucose through the cell layer.

5.2.3 Cell growth model

Typically, cell growth can occur by consuming nutrients from the media and due to the positive influence of the mechanical stimuli i.e. shear stress. The cell growth can be modelled by the Monod growth kinetics modified by Contois (Galban *et al.* 1999), i.e.

$$r_g(C_g) = \frac{k_g C_g}{k_s + C_g} \tag{5.6}$$

where r_g and k_g are the cell growth rate and the maximum specific growth rate respectively, k_s is the saturation coefficient of glucose.

Nava *et al.* (2013) included the influence of the shear stress and modelled the time evolution of the cell layer thickness, r, using the following phenomenological law:

$$\frac{\partial r}{\partial t} = \frac{k_c C_g}{k_d + C_g} \cdot g(\tau) \tag{5.7}$$

where k_c is the maximum cell layer growth velocity and k_d is the cell layer growth corrective factor. $g(\tau)$ is considered as a modulation function which incorporated the influence of the shear stress acting on the surface of the cell layer and is described by the following relation (Nava *et al.* 2013),

$$g(\tau) = \begin{cases} 0.6 + 4\tau & \tau \epsilon\ [0, 0.1)\ \text{Pa} \\ 1 & \tau \epsilon\ [0.1, 0.6]\ \text{Pa} \\ 2.5(1 - \tau) & \tau \epsilon\ (0.6, 1]\ \text{Pa} \end{cases} \tag{5.8}$$

The equation indicates a positive influence of the cell growth as the values approaches from 0 Pa to 0.1 Pa and a harmful influence as the values approaches from 0.6 Pa to 1.0 Pa. For the values of $\tau > 1.0$, the value of $g(\tau)$ is considered 0.

In this study, the method similar to Nava's approach outlined above was adopted to include the shear stress into the cell growth model. Thus, Equation (5.6) becomes,

$$r_g(C_g, \tau) = \frac{k_g C_g}{k_s + C_g} \cdot g(\tau) \tag{5.9}$$

5.3 Numerical method

5.3.1 LBM for fluid flow

The D3Q19 MRT LBM model has been adopted in this study to simulate the fluid flow. This model considers 19 discrete lattice points within a cubic lattice to define the 3D space. The discretized MRT LBM equation can be written as (d'Humières *et al.* 2002; Voronov *et al.* 2010):

$$|f(x_i + e_\alpha \delta t, t + \delta t)\rangle - |f(x_i, t)\rangle = -M^{-1} S \left[|m(x_i, t)\rangle - |m^{eq}(x_i, t)\rangle\right] \pm |F\rangle \quad (5.10)$$

Equation (5.10) can be solved in two steps, i.e., the collision and streaming steps. In equation (5.10), $|\cdot\rangle$ represents the column vectors, $|f\rangle$ is the distribution functions (DF), $|m\rangle$ is the moment vector, $|m^{eq}\rangle$ is the equilibrium moment vector, M is the transformation matrix and S is the diagonal collision matrix. The components of S are the relaxation parameters using different relaxation time scales. The formulation for $|m\rangle$ and $|m^{eq}\rangle$, the values of M and the relaxation parameters and detail solution procedure of equation (5.10) are given in reference (d'Humières *et al.* 2002). $|F\rangle$ is the forcing term. The pressure gradient can be specified using this forcing term. In this simulation, the forcing term is added to the DFs at the inlet and subtracted from the DFs at the outlet to specify the pressure gradient (Voronov *et al.* 2010, Hossain *et al.* 2014).

The kinematic viscosity ν can be obtained using the following relationship (d'Humières *et al.* 2002),

$$\nu = \frac{1}{3}\left(\frac{1}{s_\nu} - \frac{1}{2}\right)\frac{\delta x^2}{\delta t} \quad (5.11)$$

where s_ν is the relaxation parameter. The hydrodynamic properties, i.e. the density ρ, velocity $\vec{u}$, and pressure P can be obtained by,

$$\rho = \sum_{\alpha=0}^{18} f_\alpha \,, \rho\vec{u} = \sum_{\alpha=0}^{18} f_\alpha \vec{e}_\alpha \,, P = {c_s}^2 \rho \quad (5.12)$$

where c_s is the sound speed of the model with a value of $c_s = 1/\sqrt{3}$ (Premnath *et al.* 2009).

5.3.2 LBM for mass transfer simulations

In this study, a D3Q7 MRT LBM model is adopted to perform the mass transfer simulation. In this model, a cubic lattice with only 7 discrete lattice directions is used to solve the convection-diffusion equation (CDE) in 3-D space. The discretized MRT LBM equation can be written as (Yoshida *et al.* 2010),

$$|g(x_i + e_\alpha \delta t, t + \delta t)\rangle - |g(x_i, t)\rangle = -M^{-1} S \left[|m(x_i, t)\rangle - |m^{eq}(x_i, t)\rangle\right] \quad (5.13)$$

The concentration values can be obtained by solving the discretized equation and using the following relationship,

$$C_\sigma = \sum_{\alpha=0}^{6} g_\alpha \quad (5.14)$$

The formulation of the moment vectors, the values of M and the relaxation parameters are given by Yoshida *et al.* (2010). The diffusion coefficients are related to the relaxation parameters and can be obtained by the following relation (Yoshida *et al.* 2010),

$$D_\sigma = \frac{1}{4}\left(\frac{1}{s_D} - \frac{1}{2}\right)\frac{\delta x^2}{\delta t} \quad (5.15)$$

where s_D is the relaxation parameter.

5.3.3 Cell growth simulations

The cell growth has been incorporated into the simulation by using a control volume (CV) approach reported by Kang *et al.* (2004). In this approach, the cell phase is defined by a number of CVs each with an initial mass m_0. The mass of the CVs at the cell-fluid interface increases with the growth of the cells. The cell growth rate was determined using equation (5.9) at each time step. From the cell growth rate, the increase in the mass of the CVs over each time step was calculated by:

$$m = m_0 + r_g \rho_c \delta x \delta y \delta z \delta t_c \quad (5.16)$$

In equation (5.16), δx ,δy, and δz, are the CV dimension and for the two-dimensional flow considered here $\delta x = \delta z$, and $\delta y =$ unit length, m is the mass of the CV, ρ_c is the

reference cell density and δt_c is the time step for the cell growth simulation. Whenever the mass, m, becomes higher than the threshold value, m_{max}, the cell phase grows by adding a new cell or solid node. The new solid node is selected from the surrounding nodes belonging to the fluid phase based on a uniform probability. The overall algorithm uses the following steps:

1. Identify the CVs at the cell-fluid interface having an initial mass of m_0;

2. Update the mass at those CVs at each time step;

3. Selection of a new CV from the surrounding fluid nodes if the mass of a CV exceeds the threshold value, m_{max},;

Note that, the old CV is still located at the cell-fluid interface and the aforementioned algorithm will be applied until all the surrounding nodes of the old CV become solid nodes. However the old CV will have a new mass whenever the mass exceeds the threshold value and a new solid node is selected.

5.4 Computational procedure and flow conditions

A summary of the overall computational algorithm is described in Fig. 5.1. The fluid velocity and shear stress values are obtained by solving the continuity and momentum equations. The fluid velocity is used to perform the mass transfer simulation with the reaction boundary condition at the interface between the cell layer and fluid phase. The glucose concentration and the shear stress value at the cell-fluid interface are then used to calculate the cell growth rate. The geometry of the overall solution domain is then updated following the algorithm described in Section 3.3 before the next time step to incorporate the change in cell phase.

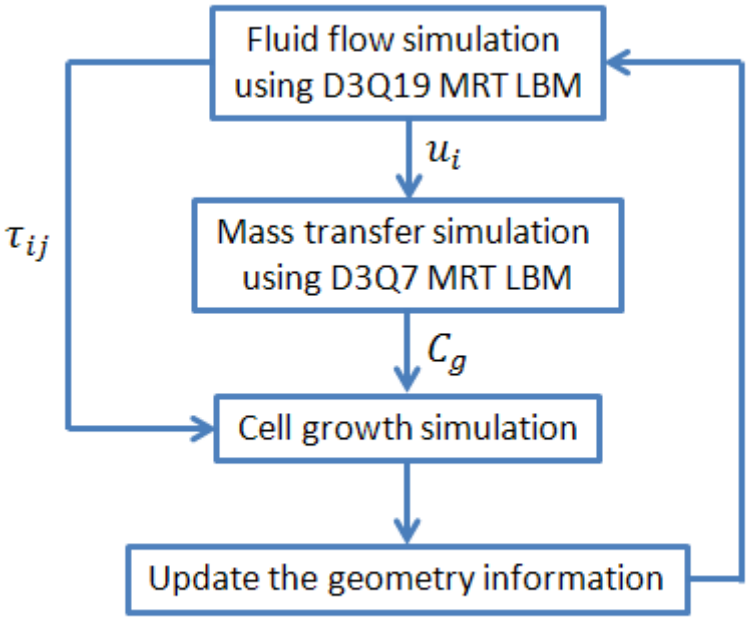

Figure 5.1. The overall algorithm which combines the fluid flow, mass transfer and cell growth simulation.

A major issue in this calculation is that the time scales for the fluid flow, mass transfer and cell growth processes are very different. Specifically, the cell growth rate occurs at a much slower rate compared to the fluid flow and mass transfer process. To include the cell growth simulation within the LBM framework, the computational efforts could become large. Picioreanu *et al.* (2000) used separate time steps for the biofilm growth, mass transfer and fluid flow in order to achieve a realistic calculation speed for performing the biofilm growth simulation. In a similar way, separate time steps have used in this study for chondrocyte cell growth, glucose transport and fluid flow simulation. Since the cell growth is the slowest process, the largest time step is required for the cell growth simulation. It should be noted that, in this computational approach the local flow field and scalar component do not interact with the cells at the same time scale. Typically, the fluid flow inside the perfusion bioreactor is very slow with the Reynolds number of $Re < 10$. For this range of Reynolds number, at the cell growth time scale the influence of cell growth on the local fluid flow and scalar distribution occurs gradually. Hence,

the use of larger time steps for the cell growth simulation does not significantly influence the accuracy of the result.

In the present study, the simulation was performed for a two-dimensional (2D) channel or bioreactor using the computational domain as shown in Fig. 5.2. The overall length and height of the channel were 6 mm and 1.84 mm respectively. A compact uniform chondrocyte cell layer was attached on the surface of the base plate from X = 2 mm to X = 4 mm as shown in Figure 5.2. The thickness of the attached cell layer was 0.01 mm. The number of nodes used for the numerical simulation was 100 and 47 in the X- and Z- directions respectively. For the fluid flow simulation the grid was set uniformly with a spatial increment of δx = 0.04 mm and the simulation used a time step of δt = 0.266 ms. The value of the relaxation parameter was set to s_ν= 1.0 to yield a kinematic viscosity of ν = 1×10^{-6} m^2/s. Inside the 2D channel, the fluid flow was in the streamwise x-direction, which was driven by the pressure difference specified between the inlet and outlet planes. The Reynolds number for the simulation was Re =3.0, which represents the flow condition inside a typical bioreactor and was calculated using the equation, $Re_H = \frac{UH}{\nu}$, where H is the height and U is the bulk velocity at the inlet of the channel. The present simulation considers an inlet bulk velocity of 0.0016 m/s. A bounce-back no-slip boundary condition was applied on the channel upper and lower walls and at the interface between the cell and fluid phases. The cell phase is assumed to be impermeable in the present simulation. A periodic boundary condition is applied at the side walls as a fully three-dimensional code is used to perform the 2D simulation.

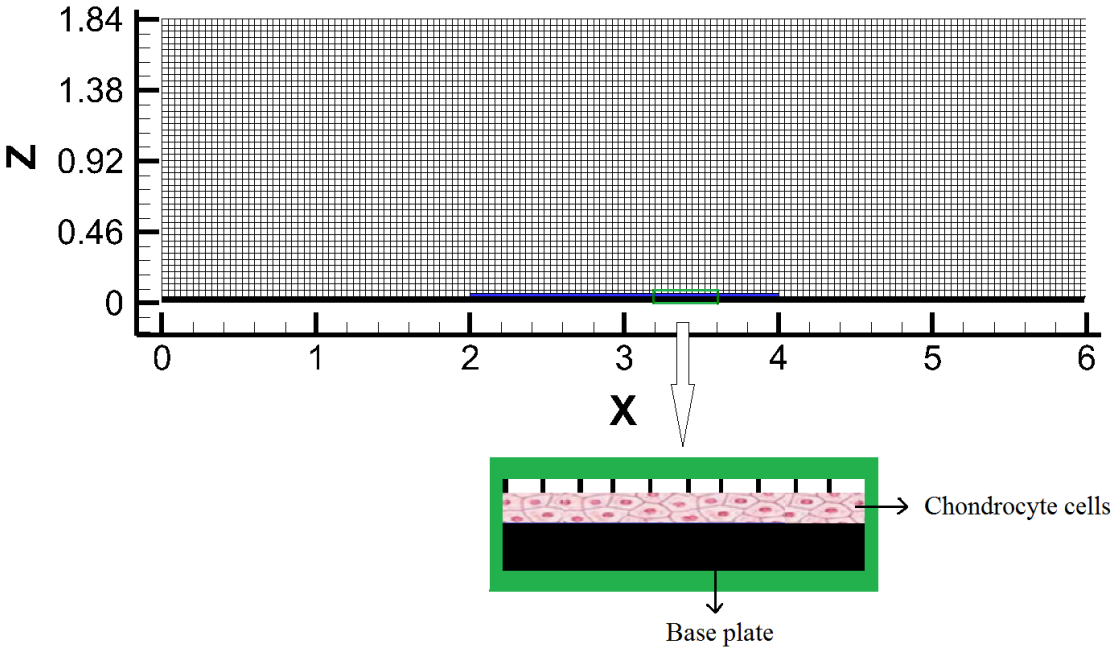

Figure 5.2 Schematic of the computational domain with enlarged view of the lower bioreactor plate where the chondrocyte cells are attached

At the inlet of the bioreactor, a uniform glucose concentration, i.e., $C_g = 4.5 \times 10^{-3}$ g/cm^3, was assumed to be transported by the incoming fluid. The velocity field obtained from the flow equations was used in the mass transfer simulation. A different time step of δt = 50 ms to be used for the mass transfer simulation; the value of δx was same as for the flow simulation. An M-M reaction kinetics reaction was specified at the interface between the cell layer and fluid phase. The boundary condition applied at the side walls and at the outlet of the bio-reactor was a zero concentration gradient normal to the boundary surface. The value of s_D = 1.963 was used to specify the glucose diffusivity value of glucose, D_g = 2×10^{-9} cm^2/s. For the cell growth simulation, initially the CVs at the cell-fluid interface were inoculated with m_0 = 3.3×10^{-10} g. The threshold value was defined as m_{max} = 1.6×10^{-5} g and the cell growth simulation used a time step of δt_c = 13s. Table 5.1 shows the numerical values of the model parameters used in the simulation.

Table 5.1: Numerical values of the model parameters used in the simulations

Definition	Value	Reference
Inlet glucose concentration, C_g	4.5×10^{-3} g/cm^3	This work
Glucose diffusivity, D_g	2.0×10^{-6} cm^2/s	Lin *et al.* (2013)
Cell growth rate constant, k_g	5.8×10^{-6} g/cm^3/s	Sacco *et al.* (2011)
Saturation coefficient for glucose, k_s	2.3×10^{-3} g/cm^3	Chung *et al.* (2010)
Glucose maximal consumption rate, R_{mg}	3.9×10^{-5} kg/(m^{3}s)	Chung *et al.* (2010)
Glucose half saturation constant, K_{mg}	6.3×10^{-3} kg/m^3	Chung *et al.* (2010)
Reference cell density, ρ_c	1 g/cm^3	Sacco *et al.* (2011)

5.5 Results and discussion

In our previous studies (Hossain *et al.* 2014, 2015), the fluid flow, mass transfer and cell growth rate was predicted over the circular strands inside perfusion bioreactor using the MRT LBM and the results were validated by the previously-published experimental data. Building on the aforementioned study, the present analysis focuses on the fluid flow, mass transfer and cell growth over a flat plate using a scaffold-free approach inside a perfusion bioreactor, where the surface geometry over the plate varies as the cells grow.

Figure 5.3 shows the streamwise u-velocity contours at three different culture times. The contour fields indicate the local magnitude of streamwise velocity inside the bioreactor at different times during the culture process. The velocity components are zero at the bioreactor walls and at the cell-fluid interface. All the contour profiles show a maximum value in the region between the bioreactor upper wall and the growing cell surface. In Figure 5.3a), the maximum u-

velocity after 70 culture days was 0.003 m/s. The cell growth causes a constriction in the channel between the surface of the cells and upper bioreactor wall. As the region becomes narrower, the magnitude of the u-velocity increases. After 105 and 174 culture days the maximum u-velocity becomes 0.0037 and 0.0045 m/s, respectively. The higher velocity region above the surface of the growing cell phase is important since the magnitude of the shear stress will increase with an increase in velocity components. Figure 5.4 shows the shear stress contours at three different culture times. In Figure 4a), after 70 culture days higher shear stress values are found at the upper surface of the growing cells. The maximum shear stress value was $\tau = 0.01$ Pa, which is found at edges of the growing cell surface. After 105 and 174 days, a similar contour distribution is observed with higher shear stress values i.e. $\tau = 0.015$ and 0.025 Pa, respectively. In this simulation, the shear stress values remained within the range of cell viability and had a positive influence on the cell growth as described in Equation (5.8).

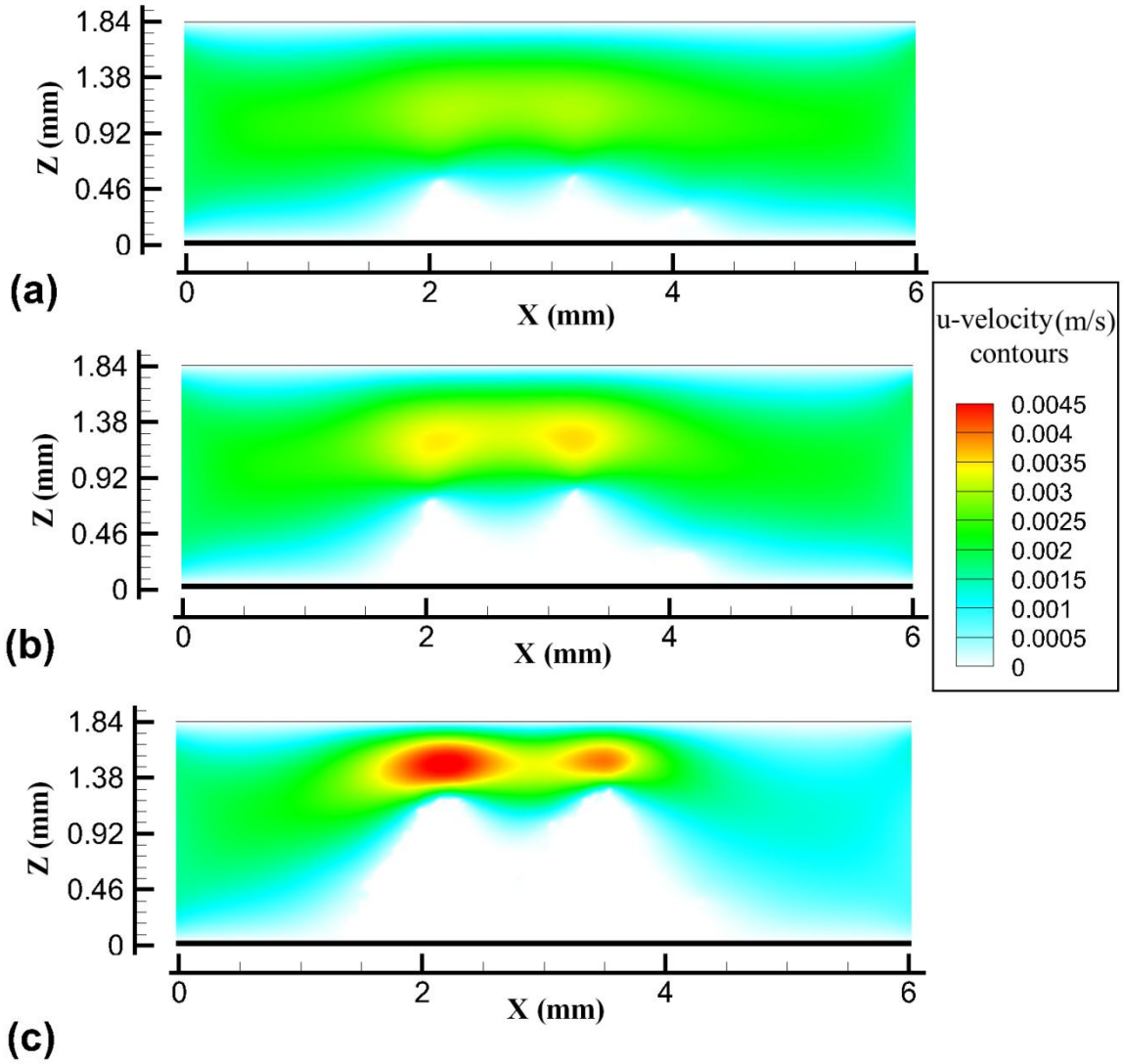

Figure 5.3: U-velocity (m/s) contours at three different culture period, a) 70 days, b) 105 days and c) 174 days

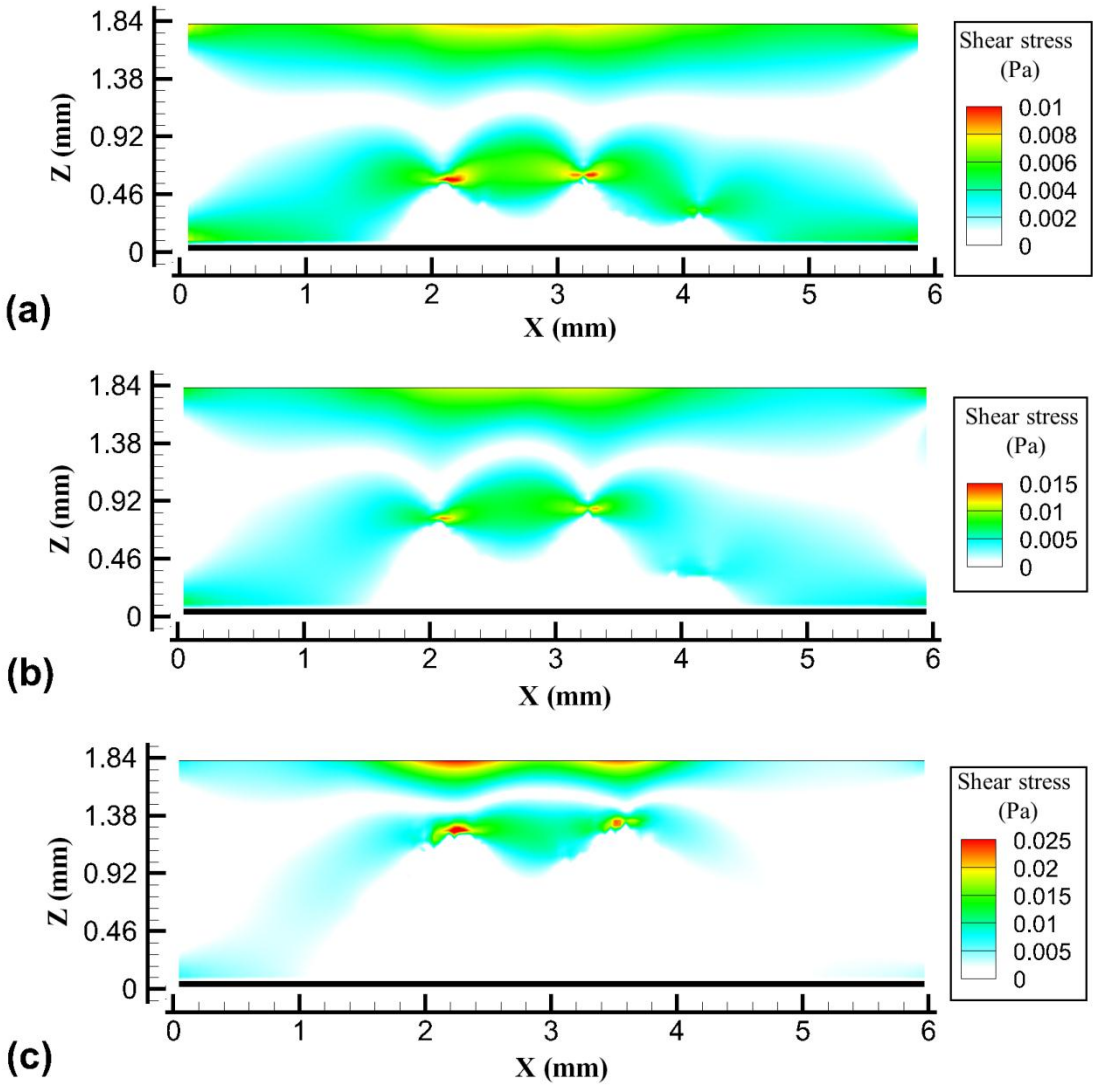

Figure 5.4: Shear stress (Pa) contours at three different culture period, a) 70 days, b) 105 days and c) 174 days

Figure 5.5 shows the normalized glucose concentration distribution overlaid on the velocity vector field inside the bioreactor. The concentration values are normalized using the inlet glucose concentration and for cleaner presentation of the vector field only every one out of three vectors are plotted in the streamwise direction. The relative size of the streamwise and wall-normal velocity components, u and w, respectively, is evident from the velocity vector field presented in Figure 5.5. Typically, the wall-normal component is less than the streamwise

component, but still finite so as to satisfy the continuity equation. Figure 5.5 also shows a strongly inhomogeneous concentration field inside the bioreactor: the concentration of the glucose at the downstream of the cell phase is much lower than the upstream side. This is mainly due to the fact that the growing cell phase consumes the glucose so that bulk transport of glucose is not large enough to provide a similar mass flux to the cells downstream of the constriction. Figure 5.5a) indicates that the value of the high initial (normalized) glucose concentration $C_g =$ 0.9 to 1.0 can penetrate up to 4.5 mm from the channel inlet after 70 days of culture. However, after 105 and 174 days of culture the high initial normalized glucose concentration can only penetrate up to 3.5 and 2.5 mm from the channel inlet, which is shown in Figure 5.5b) and 5.5c), respectively. This can be explained from the fact that a larger mass of the cell phase consumes more nutrients. On the other hand, recall from Figure 5.3 that the growing cell phase steadily tightens the constriction between the cell phase and upper bioreactor channel. Although, this increases the fluid velocity in that region which in turn increases the scalar transport at the cell-fluid interface, the convective transport does not become high enough to supply high level of glucose throughout the bioreactor. Hence the growing cell phase strongly reduces the transport of the glucose to the region downstream of the cell phase. A similar mass transport phenomenon was observed in Sergi *et al.*'s (2014) study of the surface growth effect on reactive capillary-driven flow.

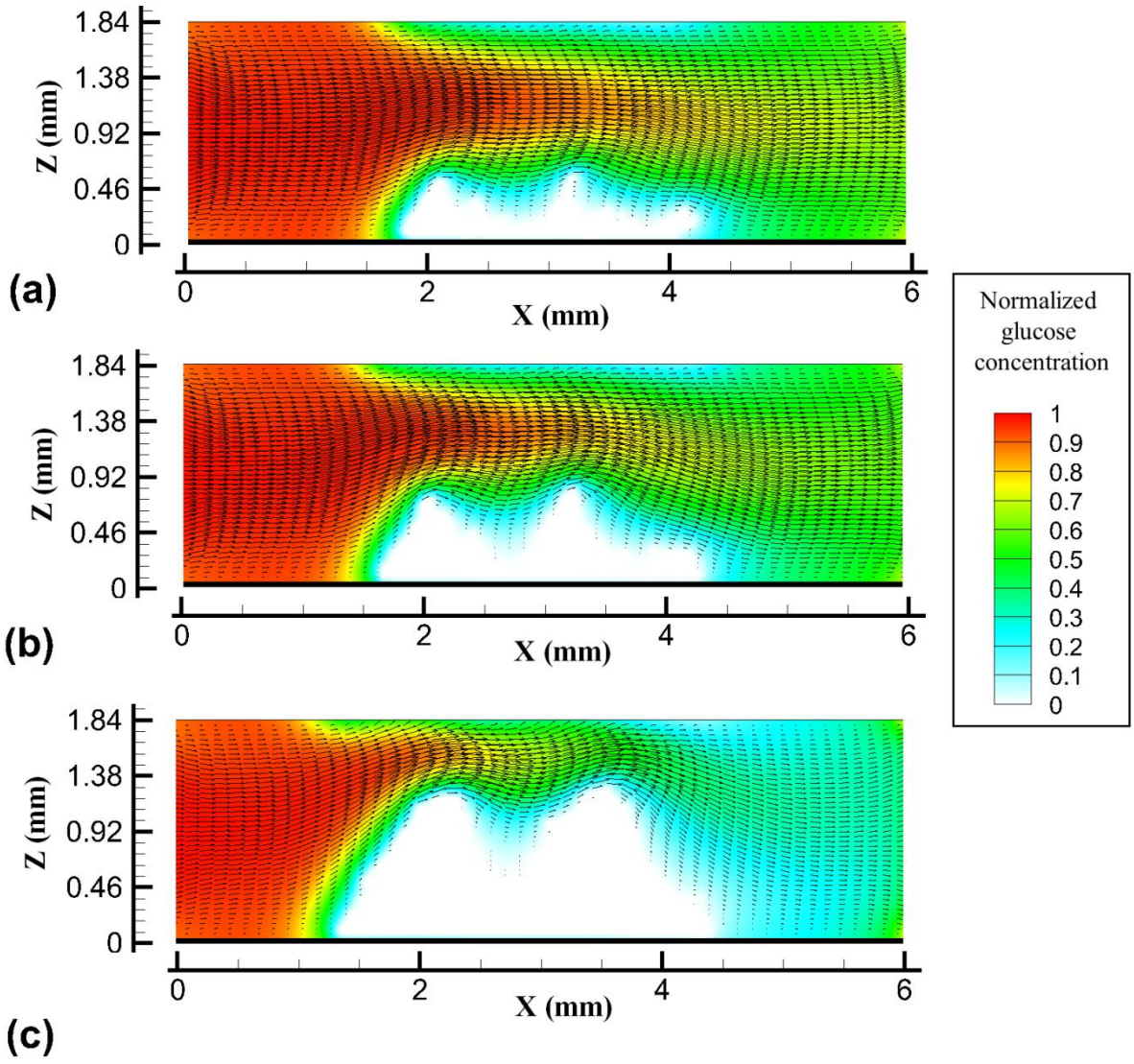

Figure 5.5: Velocity vector field and normalized glucose concentration contours at three different culture period, a) 70 days, b) 105 days and c) 174 days

Figure 5.6a) shows the chondrocyte cell growth at 174 culture days which includes the influence of the shear stress. The growth of the chondrocyte covers 2.05 mm^2 on the 2D surface and the overall cell volume fraction, ε_c , which represents the ratio between the area of cell phase and the area of the computational domain becomes 0.20. The increase in cell volume fraction is $\varepsilon_c = 0.0011$ per day. In Sacco *et al.*'s (2011) experimental study of cartilage growth for a 15 day culture period, the increase in cell volume fraction per day was approximately $\varepsilon_c = 0.001$ for an

inlet velocity of 0.0022 m/s. The difference in the results can be attributed to the use of a different geometry, inlet velocity, model parameters and length of the culture periods. The maximum height, $H_{\max}$ = 1.22 mm, of the cell phase occurs at X = 2.5 mm and X = 3.8 mm. The cell phase extends from X = 1.6 mm to X = 4.8 mm on the surface of the base plate and the mean height of the surface is approximately $H_{\text{mean}} = 0.92$ mm. Recall that initially the cells were seeded from X = 2 to 4 mm. Since the growth of the chondrocyte cells mainly depends on the supply of glucose, the growth rate in the region near X = 2 mm is higher due to the higher amount of glucose supplied. The higher growth rate in the region near X = 2 mm accounts for the peak located at X = 2.5 mm which subsequently reduces the glucose supply to the region immediately downstream of the peak. However, the flow recovers downstream of the first peak, and the higher level of glucose results in the development of a second peak at X = 3.8 mm. The primary reason for the lower cell growth in the region between the two peaks is the deficiency in glucose supply. Note that in this CV-based simulation approach the growth direction and organization of the growing cells is considered to be random. If the mass of the growing cells exceeds the threshold mass of a CV, a new CV is selected randomly from the surrounding fluid phase which then determines the growth direction. Typically, the local cell growth direction due to the cell division can also be random (Shimizu *et al.* 1995). As such the approach of the simulation realistically follows the actual cell growth direction. So, in summary, although the cell growth rate is random at the cell level, overall the growth rate responds to the level of glucose transport to the cell surface which then results in localized peaks such as in Figure 5.6.

Figure 5.6b) shows the chondrocyte cell growth without the influence of the shear stress after 174 culture days. To obtain the growth results in Figure 5.6b), $\tau = 0$ has been specified in equation 5.8. The growth of the chondrocyte covers 1.65 mm^2 and the corresponding cell volume fraction is $\varepsilon_c = 0.16$. The maximum cell height $H_{max} = 1.22$ mm, is observed at X = 2.8 mm. The cells phase extends from X = 1.6 mm to X = 4.8 mm on the surface of the base plate which is the same as in Figure 5.6a). The mean cell height is approximately, $H_{mean} = 0.75$ mm. A comparison between Figure 5.6a) and 5.6b) clearly indicates the significant influence of the shear stress on the overall chondrocyte growth. The cell growth model adopted in this study includes a modulation function, $g(\tau)$, which incorporated the influence of the shear stress acting on the cells. The value of the modulation function, g(τ), increases linearly with increasing shear

stress, for values less than 0.1 Pa. Recall that, in this present study the maximum shear stress value was found to be 0.025 Pa. Hence, for the present culture condition, shear stress always has a positive influence on the cell growth. The positive influence of the shear stress resulted in a 20 percent increase in the overall cell volume fraction compared to that obtained when the influence of shear stress was not included.

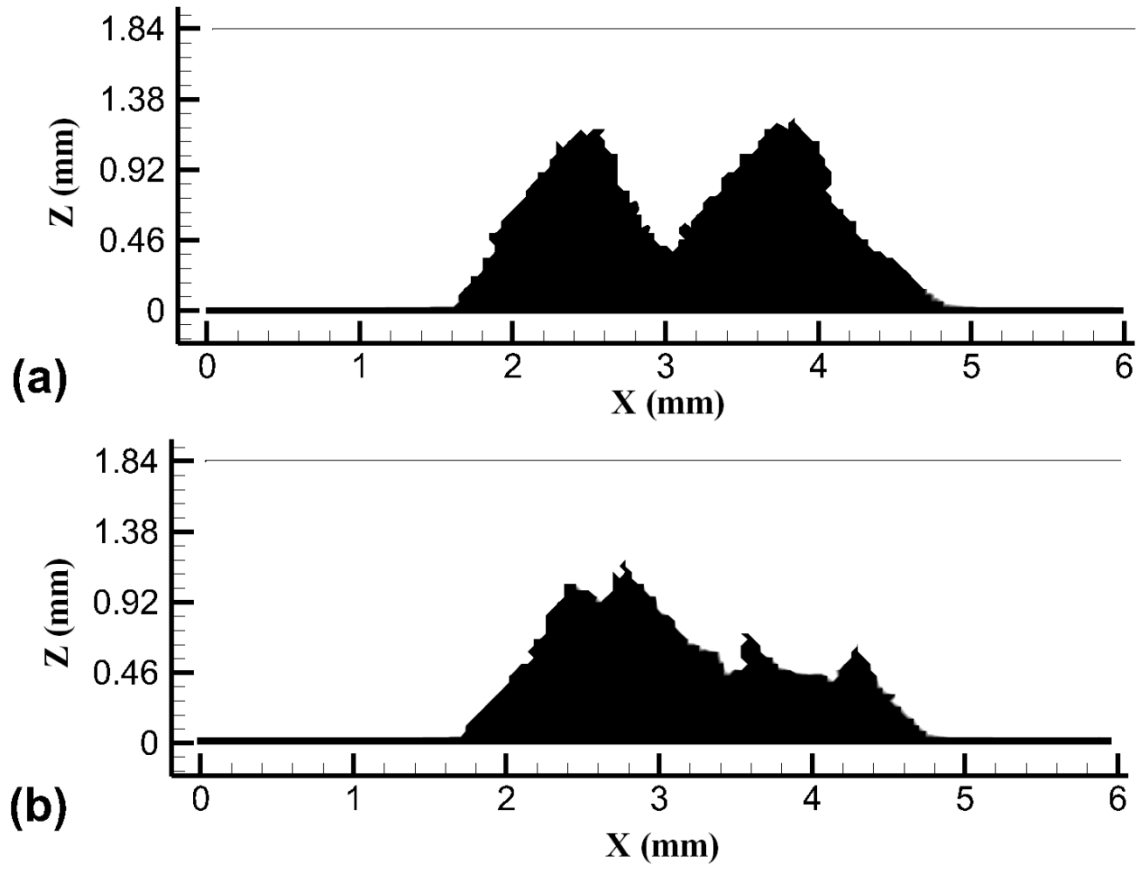

Figure 5.6: Overall cell growth inside the bioreactor a) including the influence of shear stress and b) without the influence of shear stress

5.6 Conclusions

In the present study a computational model has been developed to simulate the scaffold-free chondrocyte culture process over a flat plate placed inside a perfusion bioreactor. The model development considers the growth of the cell phase on the bioreactor plate attached to the channel wall and the influence of the growing cell phase on the local flow field and nutrient

concentration distribution. By including the two-way coupling between the cell growth and local flow field, a realistic cell growth model was resultant for the subsequent simulation studies. The simulation results indicate that for longer culture periods, the influence of the growing cell phase is significant on the local fluid velocity, shear stress and glucose concentration distribution. The growing cell phase is observed to affect the glucose transport. The increase in the maximum streamwise velocity and shear stress values are 50 percent and 150 percent, respectively, for culture periods ranging from 70 to 174 days. The results presented in this study, demonstrates that the shear stress is important to modulate the cell growth during the culture process. With the flow conditions examined in the present study, the shear stresses were found to result in an increase in the overall cell growth. Note that, the excess shear stress may cause the issues of cell detachment and cell damage.

The results from such realistic computational studies of cell growth are especially important since to perform experiments for extremely long culture periods is not feasible. Furthermore, to experimentally obtain various biophysical environmental information, such as, the local flow velocity, shear stress and concentration during the culture period, is difficult and in some cases impossible. In the present study, the lattice Boltzmann modelling approach was adopted and to incorporate the cell growth into the computational model a well-established control-volume based approach was included to model the surface growth. The modeling method appears to be a viable tool for the representation of cell growth and the resultant model can be readily extended to perform 3D cell growth studies. In the future, the authors intend to use the model to simulate the cell growth in the scaffold-based cell culture process, where the cell movement will also to be taken into consideration.

Acknowledgments

The authors wish to acknowledge the financial support of the Natural Science and Engineering Research Council of Canada (NSERC) and the Saskatchewan Health Research Foundation (SHRF).

Chapter 6

A mathematical model and computational framework for three-dimensional chondrocyte cell growth in a porous tissue scaffold placed inside a bi-directional flow perfusion bioreactor

Md. Shakhawath Hossain, D.J. Bergstrom, X.B. Chen

(Published in:: Biotechnol. Bioeng., 2015, DOI: 10.1002/bit.25678)

Abstract

The in vitro chondrocyte cell culture for cartilage tissue regeneration in a perfusion bioreactor is a complex process. Mathematical modelling and computational simulation can provide important insights into the culture process, which would be helpful for selecting culture conditions to improve the quality of the developed tissue constructs. However, simulation of the cell culture process is a challenging task due to the complicated interaction between the cells and local fluid flow and nutrient transport inside the complex porous scaffolds. In this study, a mathematical model and computational framework has been developed to simulate the three-dimensional (3D) cell growth in a porous scaffold placed inside a bi-directional flow perfusion bioreactor. The model was developed by taking into account the two-way coupling between the cell growth and local flow field and associated glucose concentration, and then used to perform a resolved-scale simulation based on the lattice Boltzmann method. The simulation predicts the local shear stress, glucose concentration, and 3D cell growth inside the porous scaffold for a period of thirty days of cell culture. The predicted cell growth rate was in good overall agreement with the experimental results available in the literature. This study demonstrates that the bi-directional flow perfusion culture system can enhance the homogeneity of the cell growth inside the scaffold. The model and computational framework developed is capable of providing significant insight into the culture process, thus providing a powerful tool for the design and optimization of the cell culture process.

6.1 Introduction:

Mathematical modelling and computational simulation of the dynamic *in vitro* tissue growth process can play a significant role in investigating the fluid flow and nutrient transport within a complex porous tissue scaffold that is placed inside a perfusion bioreactor (Singh *et al.*, 2009). To develop a realistic three-dimensional (3D) tissue growth model, accurate information regarding the biomechanical environment inside the scaffold and bioreactor is required. Due to the complexity of the porous tissue scaffold geometry, obtaining such biomechanical information inside the scaffold and bioreactor is difficult and even impossible when using state-of-the-art experimental techniques. Recently, several studies have been reported with regard to the development of an overall 3D tissue growth model for the cell culture process by means of computational fluid dynamics (CFD) (Porter *et al.*, 2005; Chung *et al.*, 2007; Voronov *et al.*, 2010; Sacco *et al.*, 2011; Hossain *et al.*, 2014). However, the aforementioned studies do not consider the interaction between the cell growth and the local fluid flow and nutrients supplied to the scaffold during the culture process. For example, the growth of tissue will change the effective geometry and hence modify the flow pattern. Hence the models presented in the aforementioned studies may not be applicable over an extended period of cell culture, particularly when the volume of the cells and newly generated tissue becomes significant so as to affect the local fluid flow. Typically the cell culture in the bioreactor can vary between 21 to 150 days (Adachi *et al.*, 2006; Li *et al.* 2014). In such cases, the growth of cells and tissues must be included in the model development.

Galban and Locke (1997) and Nava *et al.* (2013) adopted a moving boundary condition at the fluid-biomass interface to incorporate the cell and tissue growth into the model. The mesh movement was implemented using a Lagrangian-Eulerian technique. Galban and Locke (1997) represented the cell growth rate for the initial culture period by ignoring the time evolution of cell growth. Nava *et al.* (2013) compared the results between the 2D and 3D models and argued that the three-dimensionality of the scaffold geometry should be considered for the cell and tissue growth modelling. However, in their study only a small portion of the scaffold geometry was considered and the simulation was performed for only 5 culture days. Chung *et al.* (2007) and Sacco *et al.* (2011) adopted a volume-averaged computational approach and represented the averaged nutrient distribution, shear stress and cell volume fraction (CVF) for the porous tissue

scaffold cultured inside a perfusion bioreactor. The studies of Chung *et al.* (2007) and Sacco *et al.* (2011) concluded that the perfusion bioreactor is more effective compared to other non-perfusion bioreactors or static culture processes. In a perfusion bioreactor, the fluid flows through the porous scaffold and provides enhanced nutrient supply to the scaffold. The perfusion flow also induces shear stresses on the cells, which, within the appropriate range, can improve the cell growth (Chung *et al.* 2007). To incorporate the influence of the cell and tissue growth during the culture process, Chung *et al.* (2007) and Sacco *et al.* (2011) considered the porosity and permeability as time dependent by using a volume-averaged approach in their model development. However, the volume-averaged approach can only provide the average biomechanical properties and cell growth distribution within the porous scaffold. In an actual perfusion cell culture process, the supply of nutrients and the values of the shear stress are not homogeneous throughout the porous scaffold structure. The inhomogeneity of the nutrient and shear stress distribution inside the scaffold structure will cause uneven cell growth and tissue development on the cell-scaffold structure. Hence, to develop a comprehensive cartilage tissue growth model in a perfusion bioreactor, the local interaction among the biomechanical properties is important and should be considered in the development of a tissue growth model.

Recently, a bi-directional flow perfusion bioreactor has been developed, resulting in improved tissue growth over the static culture process (Gardel *et al.* 2013, Mayer *et al.* 2014). This highlights the need to understand the effect and advantage of the bi-directional perfusion approach on the cell and tissue growth. To this end, the resolved-scale cell growth simulation can play an important role by providing detailed local information on the biomechanical environment and the cell growth inside the scaffold structure. This will also facilitate the selection of the appropriate culture conditions or process parameters, including the inlet fluid velocity and nutrient concentration (Milan *et al.*, 2009; Hossain *et al.*, 2012). To perform a resolved-scale simulation for a porous scaffold geometry requires solving a coupled set of equations simultaneously over a large number of nodes. Another major challenge is to model the dynamic behavior of the scaffold surface due to the cell growth which requires the field variables to be recalculated at each time step. Both of these issues make the simulation both complex and time consuming.

To perform complex flow simulations, the lattice Boltzmann method (LBM) has become an attractive numerical methodology (Yu *et al.*, 2003). The simple stream and collide computational procedure and the local nature of the calculation can reduce the computational time compared to other methods (Yu *et al.*, 2003). The LBM is also suitable for simulating the flow through complex porous structures since the implementation of the boundary condition in this method is simple for a Cartesian coordinate system. LBM has been successfully implemented in the area of tissue engineering to model cartilage cell growth in previous studies (Galbusera *et al.*, 2007; Hussein *et al.*, 2008; Hossain *et al.* 2015). The dynamic surface growth phenomenon has also been included in LBM methods to simulate crystal growth by adopting a control-volume (CV) approach (Kang *et al.* 2004). Using a similar approach, Schulenburg *et al.* (2009) performed a 3D biofilm growth simulation, where the growth of the biofilm changed the geometry which subsequently influenced the fluid flow and nutrient transport. Based on the aforementioned studies, it can be argued that similar dynamic surface growth modelling is required and also feasible for the simulation of cell and tissue growth inside the porous scaffold during the culture process.

In this study, a mathematical model and computational framework has been developed using the multiple relaxation time (MRT) LBM to perform the resolved-scale chondrocyte growth simulation inside a 3D porous tissue scaffold cultured in a bi-directional flow perfusion bioreactor. A thin layer of chondrocyte cells is assumed to be attached at the surface of the scaffold strands. The overall chondrocyte growth model includes the interaction between the chondrocyte growth and the local flow field and glucose concentration by adopting the control-volume based dynamic surface growth phenomenon. The simulation investigates the cell growth process for a total of 30 culture days. The bi-directional flow system allowed the fluid to flow continuously in the positive streamwise direction for the first fifteen culture days. Then the flow direction was changed on the sixteenth culture day to allow the fluid to flow in the negative streamwise direction for the remaining fifteen culture days.

6.2 Mathematical Models and Numerical Method

6.2.1 Description of the bioreactor set-up

Fig. 6.1 shows the geometry of a simplified porous tissue scaffold placed inside a bioreactor. In the following model development, it is assumed that the change in the geometry of the scaffold is entirely caused by the cell growth and the influence of degradation of the scaffold during the culture process is ignored. In Fig. 6.1, the co-ordinate frame is centered at the mid-point of the bioreactor inlet plane and R denotes the radius of the scaffold strands. The overall length, width and height of the scaffold are $37R$, $6R$ and $4R$, respectively. The center-to-center distance between scaffold strands along the x and y direction is $6R$ and along the z-direction is $4R$. For ease in describing the results in the following discussion, the scaffold geometry is divided into three zones as indicated in Fig. 6.1 and denoted as the front, middle and rear zones, respectively. Each zone can be viewed as a single pore. The initial solid volume fraction, ε_s, which represents the ratio between the total volume of the scaffold strands and the volume of the scaffold domain is 0.28.

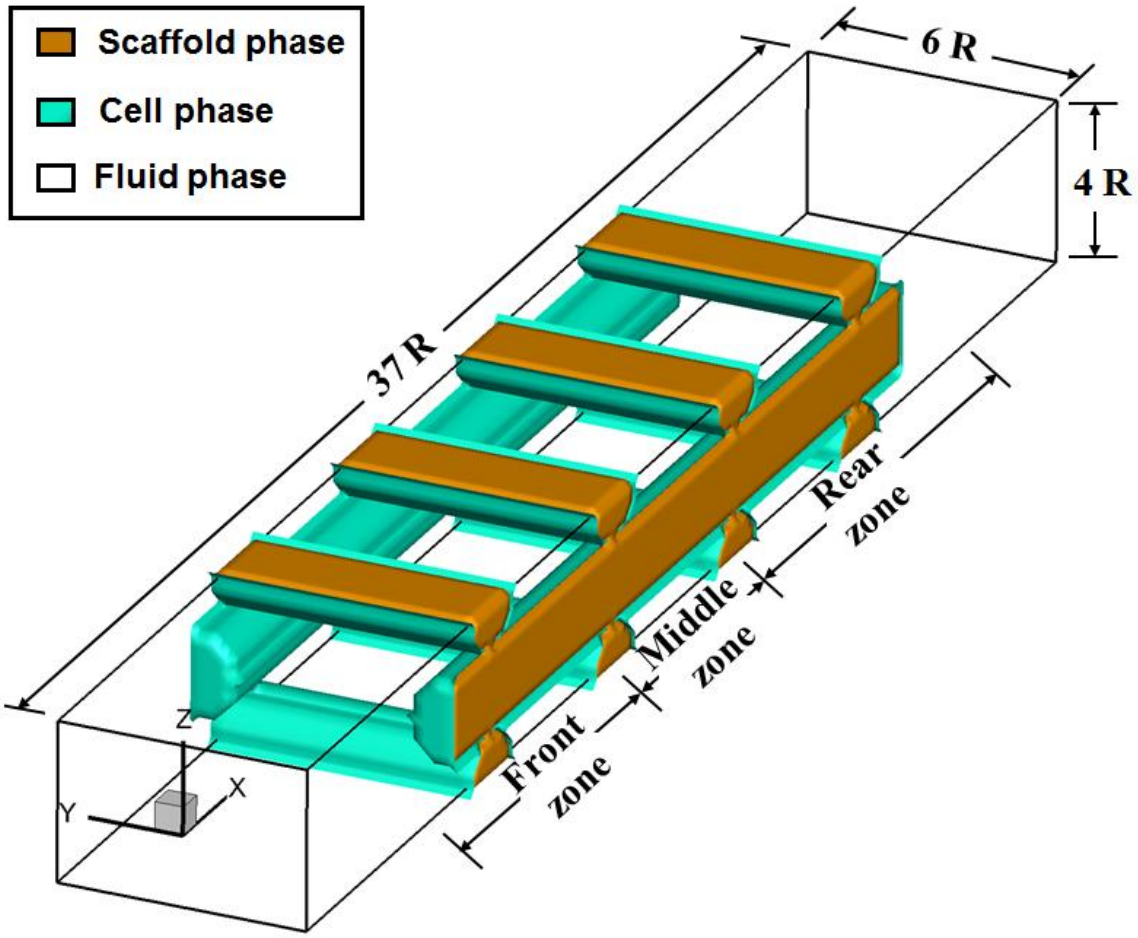

Figure 6.1: Schematic of the tissue scaffold with a strand radius R = 0.24 mm, placed inside a perfusion bioreactor

6.2.2 Mathematical models

6.2.2.1 Flow equations

The fluid flow through the porous tissue scaffold inside a perfusion bioreactor can be described by the continuity and momentum equations,

$$\frac{\partial u_i}{\partial x_i} = 0 \tag{6.1}$$

$$\rho \frac{\partial u_i}{\partial t} + \rho u_j \frac{\partial u_i}{\partial x_j} = -\frac{\partial p}{\partial x_i} + \frac{\partial}{\partial x_j}\left(\mu \frac{\partial u_i}{\partial x_j}\right) \tag{6.2}$$

where, ρ and μ represent the density and dynamic viscosity, respectively. The velocity field u_i, and pressure field p can be obtained by solving equation (6.1) and (6.2) with appropriate boundary and initial conditions.

For a Newtonian fluid, the viscous stress tensor, τ_{ij}, can be obtained from the velocity fields as follows,

$$\tau_{ij} = \mu\left(\frac{\partial u_i}{\partial x_j} + \frac{\partial u_j}{\partial x_i}\right) \tag{6.3}$$

The shear stress value, τ_w, at the surface of the scaffold strand and the cell phase was calculated by,

$$\tau_w = \sqrt{({\tau_{12}}^2 + {\tau_{13}}^2 + {\tau_{23}}^2)} \tag{6.4}$$

6.2.2.2 Nutrient transport equations

The single phase mass transfer inside the bioreactor and porous scaffold is governed by the convection-diffusion equation,

$$\frac{\partial C_g}{\partial t} + u_i \frac{\partial C_g}{\partial x_i} - \frac{\partial}{\partial x_i}\left(D_g \frac{\partial C_g}{\partial x_i}\right) = 0 \tag{6.5}$$

where C_g and D_g are the concentration and diffusion coefficient of glucose, respectively.

The consumption rate of glucose, R_g, at the cell-fluid interface is described by the Michaelis-Menten (M-M) kinetics,

$$R_g(C_g) = \frac{R_{mg}C_g}{K_{mg}+C_g} \tag{6.6}$$

where R_{mg} and K_{mg} represent the maximum consumption rate and half-saturation constant of glucose, respectively, and the consumption rate is assumed to be a function of the local glucose concentration C_g. The present study does not consider the diffusion of glucose through the cell phase.

6.2.2.3 Cell growth model

The cell growth can be modelled by the Monod growth kinetics as modified by Contois (Galban *et al.* 1999), i.e.

$$r_g(C_g) = \frac{k_g C_g}{k_s+C_g} \tag{6.7}$$

where r_g and k_g are the cell growth rate and the maximum specific growth rate respectively, and k_s is the saturation coefficient of glucose. In a perfusion bioreactor, the chondrocyte cell growth mainly occurs by consuming nutrients from the media. However, the positive influence of the mechanical stimuli, i.e. shear stress, can also influence the cell growth. Nava *et al.* (2013) modified the Monod-Contois (M-C) growth model to include the influence of the shear stress into the model. In this study, a modified M-C growth model has been adopted following Nava *et al.*'s approach i.e.,

$$r_g(C_g, \tau) = \frac{k_g C_g}{k_s+C_g} \cdot g(\tau) \tag{6.8}$$

where, $g(\tau)$ is considered as a modulation function which incorporated the influence of the shear stress acting on the surface of the cell layer as described by the following relation (Nava *et al.* 2013),

$$g(\tau) = \begin{cases} 0.6 + 4\tau & \tau \in [0, 0.1)\ \text{Pa} \\ 1 & \tau \in [0.1, 0.6]\text{Pa} \\ 2.5(1-\tau) & \tau \in (0.6, 1]\text{Pa} \\ 0 & \tau > 1\ \text{Pa} \end{cases} \quad (6.9)$$

The equation indicates a positive influence on the cell growth as the value varies from 0 Pa to 0.1 Pa, and a harmful influence as the values varies from 0.6 Pa to 1.0 Pa. For values of $\tau > 1.0$, the value of $g(\tau)$ is considered to be 0.

6.2.3 Numerical method

6.2.3.1 Fluid flow and mass transfer simulation

In this study the fluid flow and mass transfer simulation has been performed using the D3Q19 and D3Q7 MRT LBM, models respectively. The details of the MRT LBM methods used in the present paper can be found in our previous studies (Hossain *et al.* 2014; 2015). The number of nodes used for the numerical simulation was 222×37×25 in the *x*-, *y*- and *z*- directions respectively. The radius of the scaffold strands was R = 0.24 mm and the circular strand geometry were approximated by a stair-case type boundary. For the fluid flow simulation the spatial increment was δx = 0.04 mm and the time step was δt = 0.12 ms. The kinematic viscosity ν = 6 ×10^{-7} m^2/s was specified by a relaxation parameter value of s_ν= 1.6. The flow inside the bioreactor was driven by the pressure difference specified between the inlet and outlet planes. A bounce-back no-slip boundary condition was applied at the interface between the cell and fluid phases. The cell phase is assumed to be impermeable in the present simulation. A periodic boundary condition is applied at the side, upper and lower walls. In this study, the Reynolds number was calculated using the equation, $Re_d = \frac{Ud}{\nu}$, where d is the distance between the strands in the vertical z-direction and U is the bulk velocity at the inlet of the bioreactor. The Reynolds number for the simulation was $Re = 3.0$ with an inlet bulk velocity of U = 0.0037 m/s, which represents a typical inlet velocity in a perfusion culture process (Sacco *et al.*, 2011).

For the mass transfer simulation, a uniform glucose concentration, $C_g = 4.5 \times 10^{-3}$ g/cm^3 was specified at the inlet plane of the bioreactor. The glucose is transported through the scaffold and bioreactor by both diffusion and convection. The velocity field calculated from the flow equations was used to determine the convective glucose transport. At the cell-fluid interface, M-

M reaction kinetics was specified. A larger time step of δt = 5 ms was used for the mass transfer simulation. However, the value of δx was same as for the flow simulation. The boundary condition applied at the upper and lower walls, side walls and at the outlet of the bio-reactor was a zero concentration gradient normal to the boundary surface. A relaxation parameter of, s_D = 1.963 was used to specify the glucose diffusivity, D_g = 1×10^{-9} m^2/s. A summary of the model parameter values is given in Table 6.1.

Table 6.1: Numerical values of the model parameters used in the simulations

Definition	Value	Reference
Inlet glucose concentration, C_g	4.5×10^{-3} g/cm^3	This work
Glucose diffusivity, D_g	1.0×10^{-5} cm^2/s	Lin *et al.* (2013)
Cell growth rate constant, k_g	5.8×10^{-6} g/cm^3/s	Sacco *et al.* (2011)
Saturation coefficient for glucose, k_s	2.3×10^{-3} g/cm^3	Chung *et al.* (2010)
Glucose maximal consumption rate, R_{mg}	2×10^{-5} kg/(m^{3}s)	Chung *et al.* (2010)
Glucose half saturation constant, K_{mg}	6.3×10^{-3} kg/m^3	Chung *et al.* (2010)
Reference cell density, ρ_c	1 g/cm^3	Sacco *et al.* (2011)

6.2.3.2 Cell growth simulation

A compact uniform chondrocyte cell layer was assumed to be attached on the surface of the scaffold strands. The initial thickness of the cell layer was 0.001 mm. The growth of the chondrocyte cells was incorporated into the simulation by using the CV approach of Kang *et al.* (2004). The nodes at the cell-fluid interface are each associated with a CV with an initial mass m_0. The mass of the CV will gradually increase due to the cell growth. The cell growth rate was determined using equation (6.8) at each time step. From the cell growth rate, the increase in

the mass of the CVs over each time step was calculated using the following equation (Hossain *et al.* 2015):

$$m = m_0 + r_g \rho_c (\delta x^3) \delta t_c \quad (6.10)$$

In equation (6.10), m is the mass of the CV, ρ_c is the reference cell density and δt_c is the time step for the cell growth simulation. Whenever the mass, m, becomes higher than the threshold value, m_{max}, the cell phase grows by adding a new cell or solid node. The initial mass of the CVs at the cell-fluid interface was m_0 = 9.6×10^{-12} g. The threshold value was defined as m_{max} = 6.4×10^{-8} g. To reduce the computational effort, separate time steps have used in this study for chondrocyte cell growth, glucose transport and fluid flow simulation following the procedure described in Picioreanu *et al.* (2000) and Hossain *et al.* (2015). Since the cell growth is the slowest process, the largest time step is used for the cell growth simulation. In this study, the cell growth simulation used a time step of δt_c = 8.64s.

6.3 Discussion of results

In this section to investigate the advantages of the bi-directional perfusion flow bioreactor the simulation results will initially be discussed for the first 15 days of culture period during which the fluid was allowed to flow continuously in the positive streamwise direction. Fig 6.2a) and 6.2b) show the 3D cell growth distribution after 10 and 15 culture days, respectively. The value of the cell volume fraction (CVF), which represents the ratio between the volume of the cell phase and the volume of the scaffold domain, was ε_c = 0.01 and 0.0192 after 10 and 15 culture days, respectively. For comparison, in Sacco *et al.*'s (2011) experimental study of cartilage growth over a 15 day culture period, the increase in biomass volume fraction was $\varepsilon_b = 0.0225$ for an inlet velocity of 0.0039 m/s and a solid volume fraction of ε_s = 0.23. Recall that in the present study the initial solid volume fraction was ε_s = 0.28. Quantitatively the results in the present study compare well with Sacco *et al.*'s experimental results: the difference is approximately 15%. The discrepancies in the results are likely due to the variation in the scaffold and bioreactor geometry, inlet velocity, and model parameters. Fig. 6.2a) and 6.2b) clearly indicate an increase in CVF for all three zones of the scaffold domain; for a static culture process significant cell growth is typically found only on the periphery of the scaffold (Cartmell *et al.*

2003). However, the increase in the CVF in the front zone is significantly higher than that in the middle and rear zones, and the overall cell growth distribution inside the scaffold is strongly inhomogeneous. The time evolution of the CVF for the total scaffold and the three specific zones is presented in Fig. 6.3. The figure indicates that the maximum amount of cell growth occurs in the front zone, and the rate of growth in the CVF is much higher for the front zone compared to the middle and rear zones. In the first five culture days the increase in the CVF is very low for all three zones. From five culture days onward the CVF increases linearly in the front zone. After fifteen culture days, the CVF for the front, middle and rear zones are found to be 79, 13 and 8 percent of the total CVF, respectively. The total CVF increase is mostly contributed by the front zone during the first fifteen days of culture period.

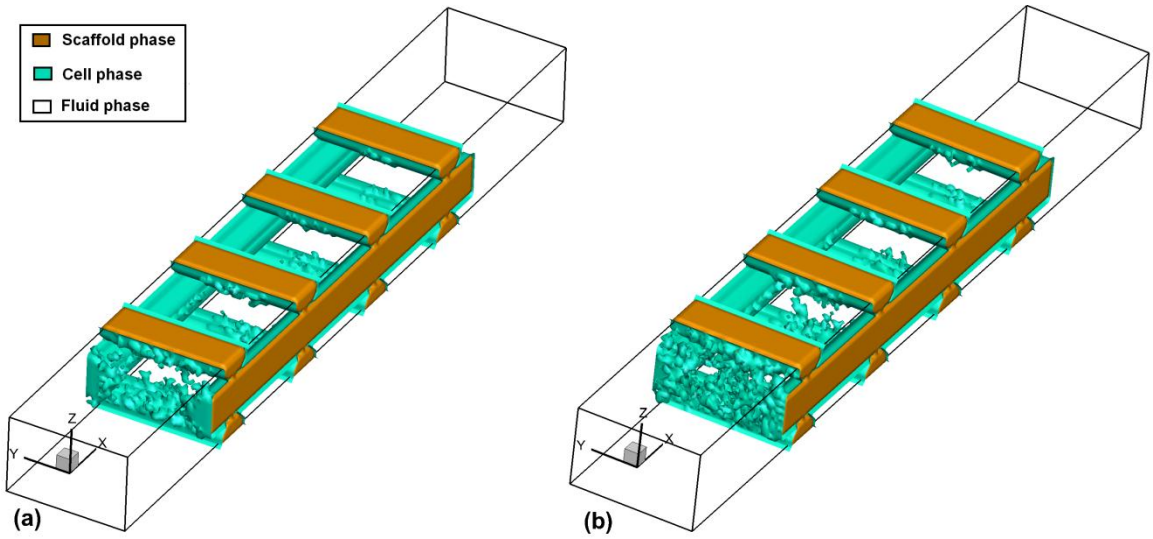

Figure 6.2: Three-dimensional cell growth distribution after cell culture of (a) 10 days and (b) 15 days

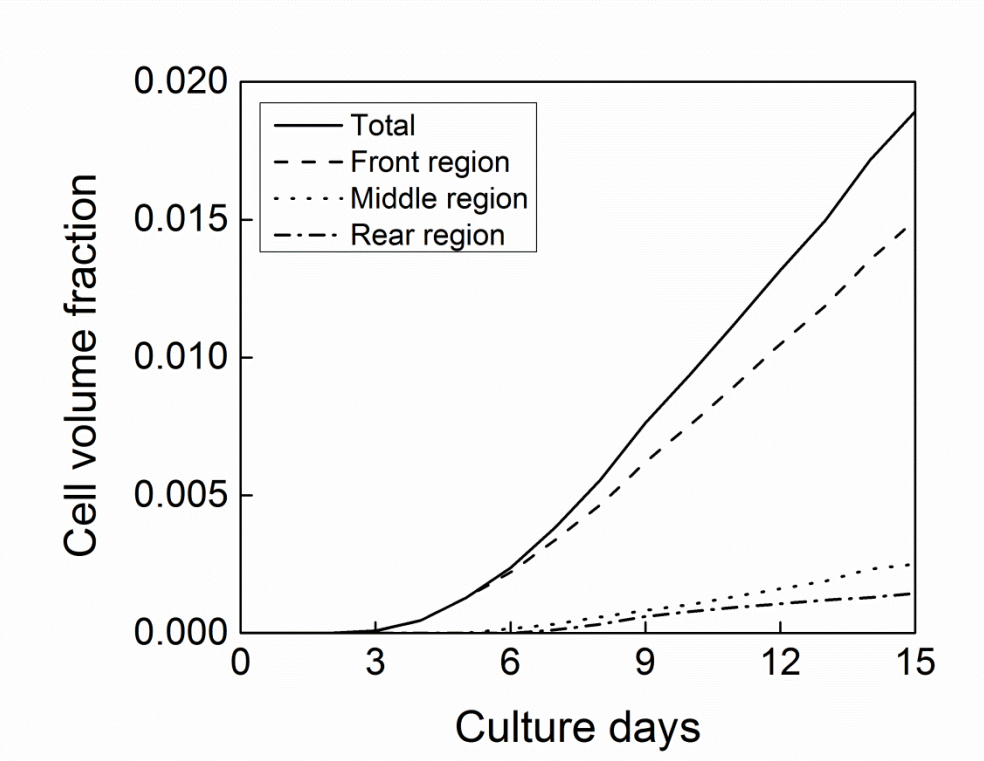

Figure 6.3: Transient growth of the cell volume fraction during the first 15 days of the cell culture process

The spatial inhomogeneity of the cell growth distribution inside the porous scaffold during the first 15 days of one-directional perfusion culture period can be explained by investigating the interaction between the local fluid flow, glucose transport and cell growth. In this context, the glucose concentration contours overlaid on the velocity vector fields for the *x*-*z* plane at $y/R = 0$ are shown in Fig. 6.4 for three different culture periods: a) 5, b) 10 and c) 15 days, respectively. The glucose concentration is normalized with the inlet glucose concentration and the white regions in Fig. 6.4 represent the cell-scaffold strand or solid phase. The high glucose concentration supplied at the bioreactor inlet has been transported into the scaffold by both convection and diffusion. However, due to the consumption of glucose by the cells attached to the strand surface; the glucose concentration is reduced near the cell-scaffold region. Recall that the cells attached to the strand surface consume glucose following the M-M reaction kinetics. For the present flow condition, the convective and diffusive transport of glucose fails to provide a uniformly high glucose concentration throughout the scaffold. In Fig. 6.4a), the higher

glucose concentration which enters the front region of the scaffold from the bioreactor inlet gradually decreases in the x direction. Note that Fig. 6.4a) represents five simulated culture days and the cell growth is only evident at the strand surfaces located at $x/R = 9$. For longer culture periods, the cell-phase continues to increase and higher amounts of glucose are consumed by the growing cell-phase. Hence, the glucose concentration values inside the scaffold after 10 simulated culture days presented in Fig. 6.4b) are lower than those shown in Fig. 6.4a). Fig. 6.4c) shows the glucose concentration distribution after fifteen culture days. For this culture period, the enlargement of the cell-seeded scaffold strands at the front zone is large enough to decrease the permeability and significantly reduce the supply of nutrients inside the scaffolds. The value of the maximum glucose concentration becomes less than 0.3 in the middle and the rear zones. From the velocity vector fields in Fig. 6.4, it is evident that the fluid accelerates while passing through the narrow gap between the transverse strands. A comparison among the vector fields for the different culture periods reveals that the pressure gradient specified between the inlet and outlet planes cannot maintain the same flow rate inside the bioreactor due to the enlargement of the cell-phase. The reduced fluid velocity inside the bioreactor subsequently reduces the convective nutrient transport throughout the porous scaffold.

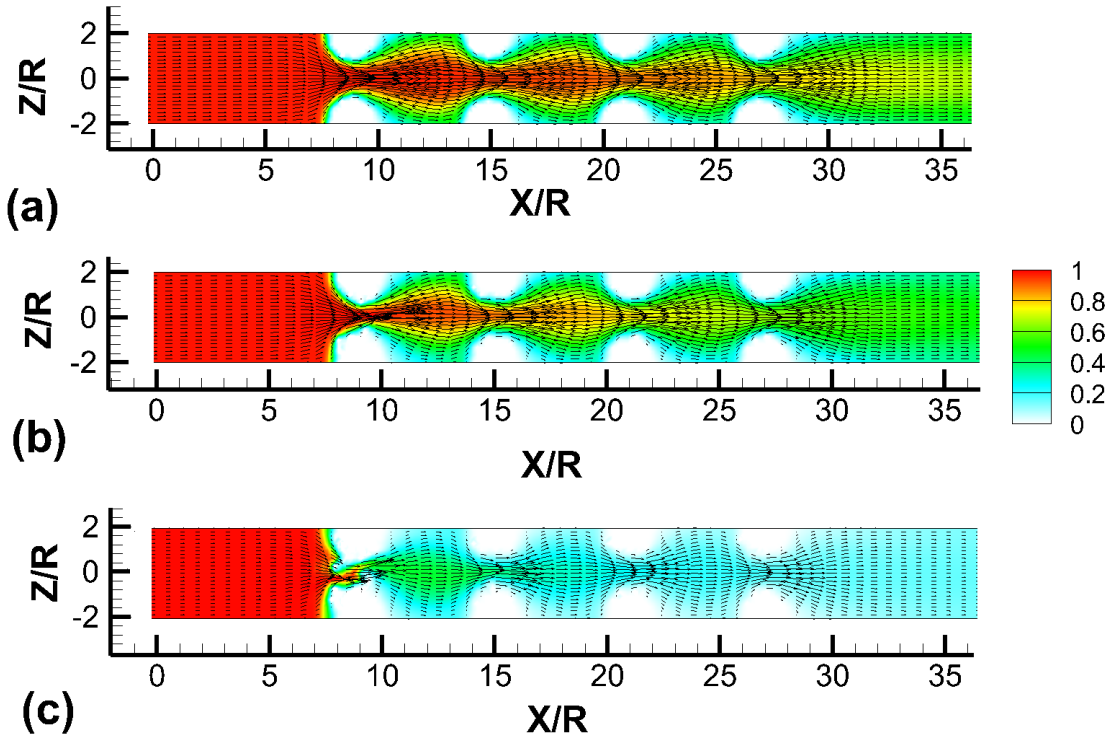

Figure 6.4: Normalized glucose concentration and velocity vector fields in the *x*-*z* plane at *y*/*R* = 0 after a cell culture period of (a) 5, (b) 10, and (c) 15 days

Fig. 6.5 shows the normalized glucose distribution and velocity vector field on the xy plane at *z*/*R* = 0 for three different culture periods: a) 5, b) 10 and c) 15 days, respectively. On the xy plane, the glucose transport is generally similar to that observed on the *x*-*z* plane. Early in the culture period, i.e. after 5 simulated culture days, the higher initial glucose concentration $C_g = 0.9$ to 1.0 can penetrate up to *x*/*R* = 27 from the bioreactor inlet. The larger velocity at *x*/*R* = 10, 16, 22 and 28 indicate the acceleration of the fluid due the reduction in flow area caused by the scaffold strands located transverse to the incoming flow. After 10 culture days, an increase in the cell volume can be seen in the front zone which in turn reduces the glucose supply. After fifteen culture days, the cell growth within the front zone reduces the permeability enough to significantly restrict the supply of glucose to the middle and rear zones of the scaffold, where the concentration value is limited to $C_g \leq 0.30$. At this stage of the culture process, on the *x*-*y* plane the cell-phase growing on the transverse strands is also evident at *x*/*R* = 9. The results presented

in Figs. 6.4 and 6.5 indicate that continuation of the culture process by supplying fluid flow in the positive x direction may increase the CVF in the front zone sufficient to completely block the supply of glucose to the downstream sections of the scaffold.

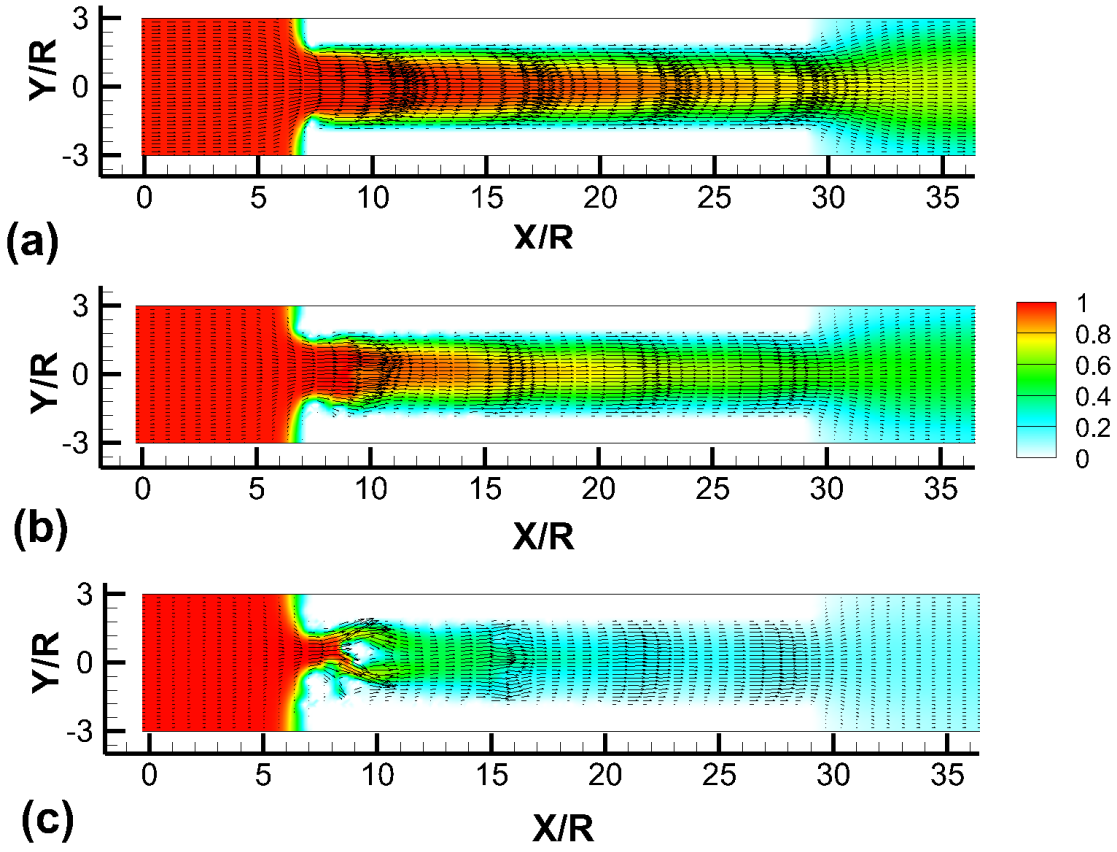

Figure 6.5: Normalized glucose concentration and velocity vector fields on the *x-y* plane at *z/R* = 0 after a cell culture period of (a) 5, (b) 10, and (c) 15 days

Recall that for the models used in this study, the cell growth also depends on the value of the shear stress induced on the cells by the fluid flow. Hence, it is of interest to investigate the magnitude of the shear stress levels developed inside the scaffold. Note that, for the growth model presented in Eq. (6.9) the cell growth rate is reduced when the shear stress values are higher than 0.6 Pa. Fig. 6.6 shows the shear stress contours on the *x-z* plane at *y/R* = 0 for three different culture periods: a) 5, b) 10 and c) 15 days, respectively. In Fig. 6.6a), the maximum

shear stress values are seen to occur at the shoulder of the strands. The value of the maximum shear stress increases during the culture process since the enlargement of the cell-scaffold strand due to the cell growth decreases the narrow transverse distance between the strands. Recall from Fig. 6.4 that the fluid tends to accelerate while flowing through the narrow passage between the strands. The acceleration of the fluid in these regions is the main cause of the enhanced shear stress values observed at the shoulder of the transverse cell-scaffold strands. From Fig. 6.6, it is evident that the maximum shear stress value increases from 0.4 Pa to 0.7 Pa from 5 to 10 culture days. The maximum shear stress value after fifteen culture days is also 0.7 Pa. The increase in maximum shear stress value is approximately 43% when the culture period increases from 5 to 10 days. Fig. 6.7 shows the shear stress contours on the *x-y* plane at $z/R = 0$ for three different culture periods. Again, the contour distributions and magnitude of the maximum shear stress values are different for the different culture periods. On the xy plane the maximum shear stress value increases from 0.4 Pa to 0.7 Pa when the culture time increases from 5 to 15 days. The local shear stress distribution presented in Fig. 6.6 and 6.7 indicate that, for the present flow condition, the shear stress values are mostly within the cell-viability range and only some small regions experience the detrimental effects of high shear stress values, i.e. those greater than 0.6 Pa. As such, in this study the shear stress primarily has a positive influence on the cell growth. It should be noted that in the regions of higher shear stress the possibility of shear-induced cell movement or detachment is high and this could influence the overall cell growth distribution. The potential detachment of cells in the regions of higher shear stress might reduce the blockage developed by the cell growth and thereby improve the glucose transport into the downstream sections of the scaffold. However, the cell growth model used in this study does not consider the shear-induced cell movement or detachment.

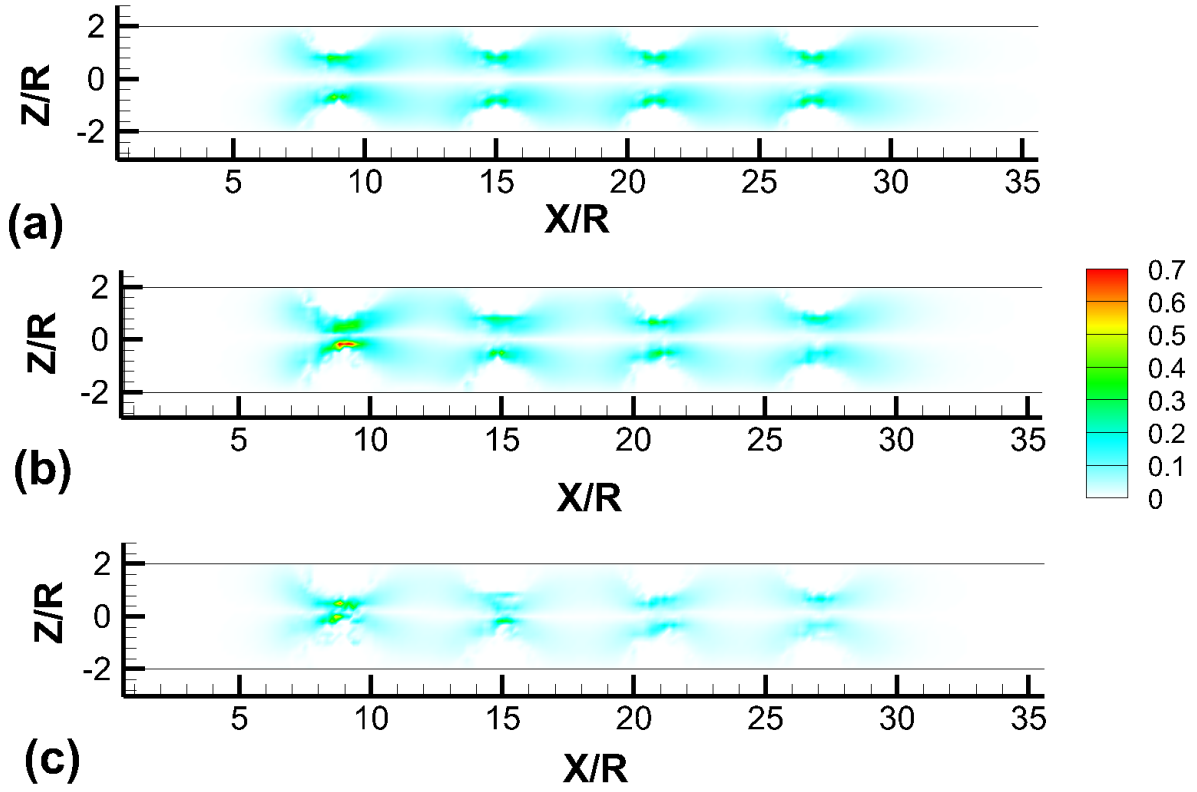

Figure 6.6: Shear stress (Pa) contours on the *x*-*z* plane at *y*/*R* = 0 after a cell culture period of (a) 5, (b) 10, and (c) 15 days

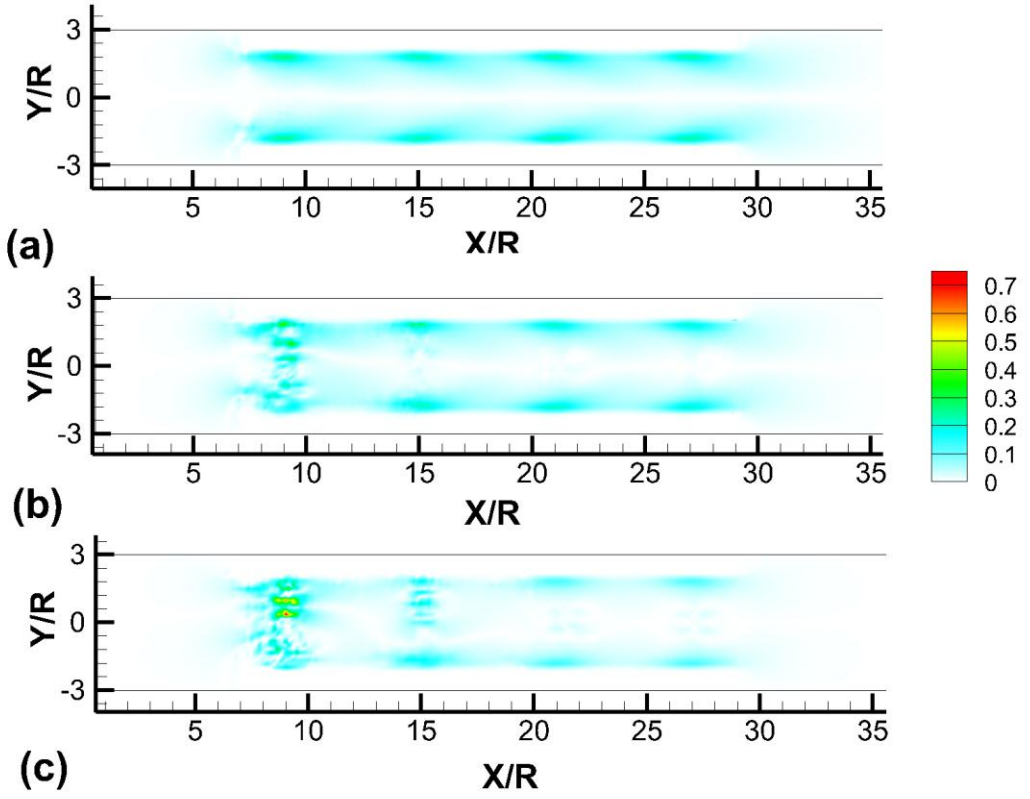

Figure 6.7: Shear stress (Pa) contours on the *x-y* plane at *z/R* = 0 after a cell culture period of (a) 5, (b) 10, and (c) 15 days

At the beginning of the sixteenth culture day, the direction of the fluid flow was altered by reversing the pressure values specified at the inlet and outlet planes. The higher glucose concentration was now being transported into the scaffold from the rear side of the bioreactor by the fluid moving in the negative x (or streamwise) direction. The transport phenomenon observed during the 16 to 30 days of culture period were similar to that observed during the first fifteen days except that the preferential direction was reversed. In this case, higher amounts of glucose were supplied to the rear zone and the glucose supply became lower in the middle and front zones. The effect of the change in the direction of the fluid flow and associated glucose supply is reflected in Fig. 6.8a) and 6.8b), which shows the 3D cell growth inside the porous scaffold after 25 and 30 culture days respectively. Note that in Fig 6.8, the cell growth distribution is viewed

from the rear end of the bioreactor. Fig. 6.8 indicates a significant increase in CVF in the rear and -- to a much more limited degree -- the middle zone after 25 and 30 culture days.

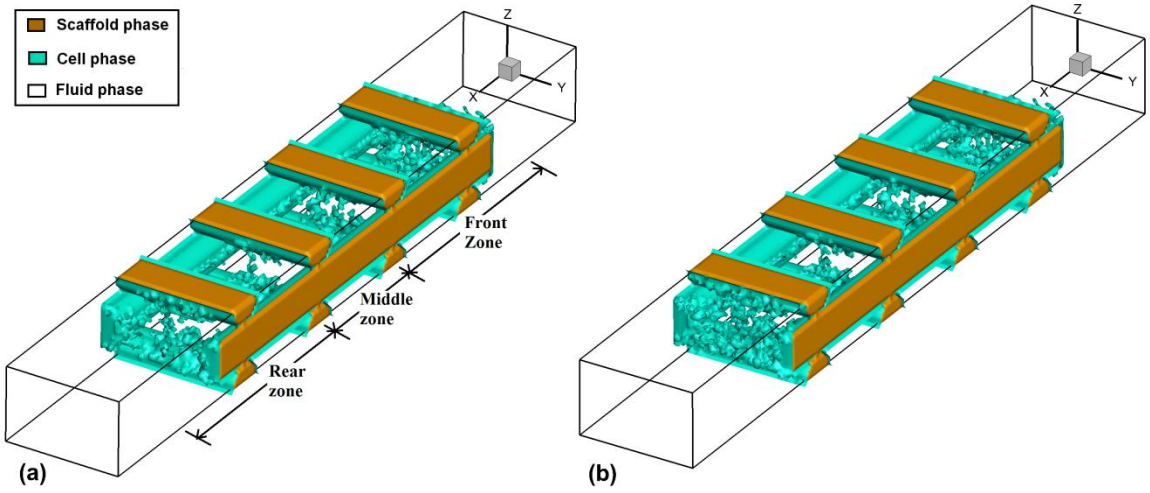

Figure 6.8: Three-dimensional cell growth distribution after the cell culture of (a) 25 days and (b) 30 days viewed from the rear end of the bioreactor

The transient development of the CVF for the entire scaffold and individual zones during the 16 to 30 days of culture period is presented in Fig. 6.9. During the last fifteen days of the total culture period the overall CVF increases from 0.0192 to 0.0328. At the end of the 30 day culture period the CVF for the front, middle and rear zones were 48, 12 and 40 percent of the total CVF respectively. The results clearly indicate that the bi-directional perfusion approach adopted in this study can significantly improve the homogeneity of the cell growth distribution inside the porous scaffold but only for the front and rear zones. At the end of 30 culture days, the CVF is still significantly lower in the middle zone compared to the front and rear zones.

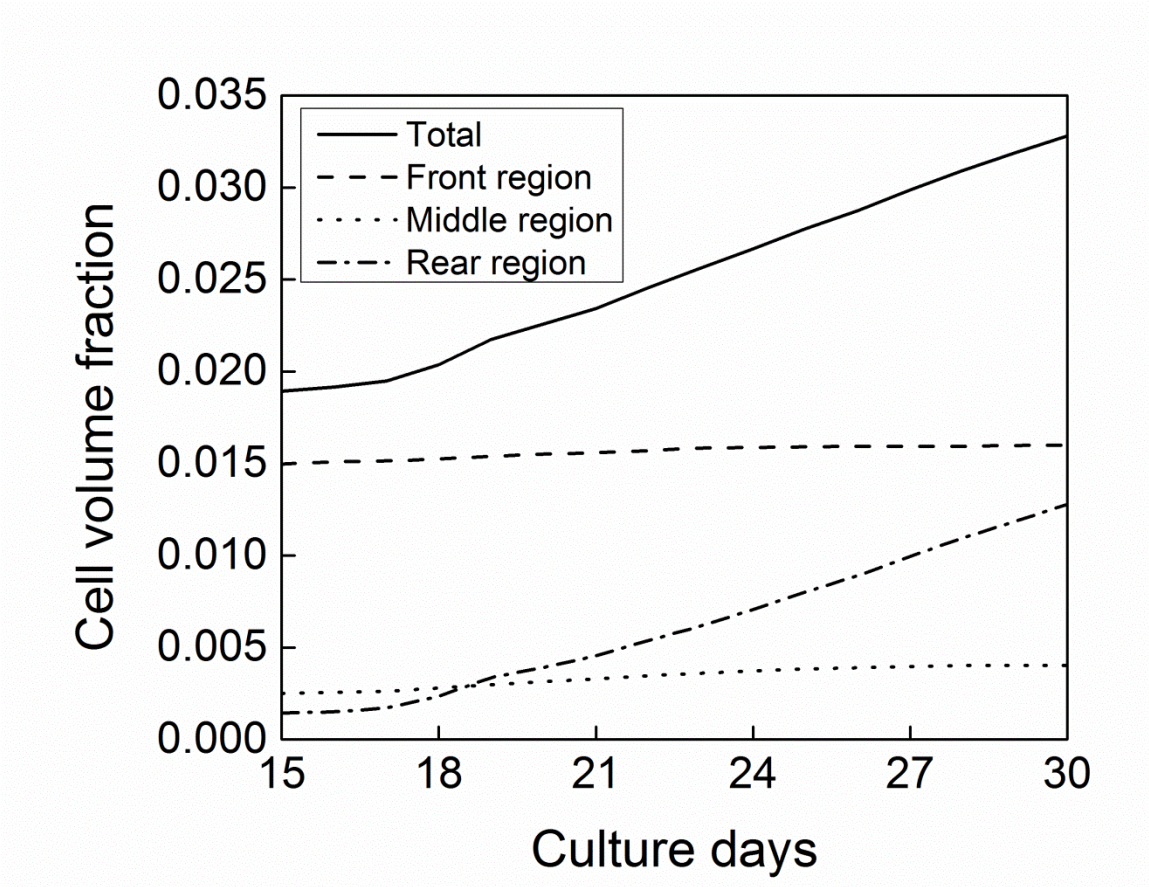

Figure 6.9: Transient growth of the cell volume fraction during the last fifteen days of the cell culture process

6.4 Conclusion:

Simulation of the cell culture process is a challenging endeavor, mostly due to the complicated interaction between the cells and local fluid flow and associated nutrient transport inside the complex porous scaffolds. This study presents the development of a mathematical model and computational framework for the resolved-scale simulation of the cell culture process. Specifically, it has been performed for a porous tissue scaffold (with $\varepsilon_s = 0.28$) that is cultured inside a bi-directional flow perfusion bioreactor to obtain the cell growth distribution during a period of 30 culture days. Initially the fluid flow was maintained in the positive x direction, and then after 15 culture days, the flow direction was reversed. The model solves the coupled fluid

flow, glucose transport and cell growth model equations, and considers a two-way coupling between the cell growth and local flow field and glucose concentration to mimic the realistic culture process. After 30 culture days, the overall CVF was ε_c = 0.0328. In this study, the scaffold considered by the simulation was divided into three zones: for the first 15 days of the culture period the cell growth occurred mainly in the front zone due to the enhanced supply of glucose. At the end of the first 15 culture days, the CVF increase in the front zone significantly reduced the local permeability of the porous scaffold. This limited the supply of glucose to downstream sections of the scaffold, which in turn significantly reduced the cell growth in the middle and rear zones. An enhanced level of cell growth was achieved in the rear zone by reversing the fluid flow direction during the last fifteen days of the culture period, which distributed a much higher concentration of glucose to this part of the scaffold. Using the approach above, after thirty days of culturing, the CVF was found to be 48, 12 and 40 percent of the total CVF in the front, middle and rear zones, respectively. The relatively low value of the CVF in the middle zone indicates that transporting a sufficient level of glucose into this region to support enhanced cell growth remains a challenge even for a bi-directional perfusion reactor.

In summary, the simulation results reported in this study suggest that the bi-directional perfusion flow bioreactor is a promising approach for the *in vitro* cell culture process. Furthermore, the mathematical model and computational framework developed in this study represents a viable tool for evaluating optimal design variables for the scaffold architecture, input culture parameters and bi-directional flow configuration of the bioreactor, e.g. the duration of the perfusion from each direction. In the future, the authors intend to include shear-induced detachment, death and transport of cells into the overall cell growth model, and also perform simulations for different flow configurations.

Acknowledgements

The authors acknowledge the support to the present research from the Natural Sciences and Engineering Research Council (NSERC) of Canada and Saskatchewan Health Research Foundation (SHRF).

Chapter 7

Concluding remarks

7.1 Contributions

In this thesis, a mathematical model and computational framework has been developed to study the 3D cell growth inside a porous scaffold placed in a perfusion bioreactor and to investigate the fluid flow and nutrient transport during the culture process. The major contributions of this thesis are as follows:

I. Development of a computational code by implementing the 3D MRT LBM models required to solve the coupled fluid flow, mass transfer and cell growth simulation in a porous tissue scaffold.

II. Implementation of a cell growth equation which considers the local nutrient supply as well as the shear stress level induced on the cells in the cell growth simulation.

III. Implementation of the dynamic two-way coupling between the cell growth and local flow field and nutrient concentration using a multi-time scale simulation approach. During the initial culture period the porous scaffold structure was relatively simple with a regular strand geometry. However, for longer culture periods the geometry of the strand surface changed due to the cell growth and influenced the local fluid flow and nutrient transport through the porous scaffold. The computational code developed in this research is capable of handling the dynamic scaffold strand surface growth phenomena.

The simulation results presented in this thesis also provide quantification of the cell growth rate, nutrient transport and biomechanical properties, i.e. fluid velocity and shear stress level, acting on the cells. The simulation results also predict the 3D cell growth distribution in a porous scaffold placed inside a bi-directional flow perfusion bioreactor. A summary of the major conclusions for each chapter which collectively address the overall thesis objectives is provided in the following section.

7.2 Conclusions

In Chapter 3 a coupled mass, momentum and convection-diffusion-reaction equation has been solved, and a resolved-scale simulation of fluid flow and mass transfer has been performed to predict the cell growth rate at the surfaces of two circular tissue strands placed in tandem within a channel representative of a perfusion bioreactor. The results in Chapter 3 demonstrate that for a circular strand the maximum shear stress occurs slightly upstream of the strand shoulder. The maximum and minimum nutrient (oxygen and glucose) concentration values occur at the front and rear stagnation points of the circular strands, respectively. The distance between the strands was also varied to study the influence of the front strand on the cell growth rate on the surface of the rear strand. The supply of nutrients and cell growth rate is much higher at the front strand compared to the rear strand. Increasing the distance between the strands from 3R to 4R (with R being the strand radius) increases the nutrient supply and results in an approximately 10% increase in the cell growth rate on the surface of the rear strand. Note that the cell growth rate was calculated using a growth equation which considers multiple nutrients as well as the shear stress level induced on the cells. The results presented in this chapter suggest that an optimal distance between the strands exists for designing scaffolds. The optimization should consider both the shear stress level acting on the cells and the nutrient transport to the cells.

In Chapter 4, a resolved-scale simulation of the fluid flow, nutrient (glucose) and waste (lactate) transport through a simplified tissue scaffold consisting of a repeatable unit or pore inside a perfusion bioreactor was performed. For a low inlet velocity and low inlet glucose concentration, the supply of glucose can become limited even for a single pore; the convective transport is not high enough to overcome the nutrient consumption by the thin layer of cells attached on the strand surface. The lactate transport results show a higher accumulation of lactate in the regions with lower velocity. However, in the perfusion bioreactor the decrease in the pH value due to the production of lactate did not cause the overall level to fall below the critical pH value required for a viable cell culture condition. The results presented in this chapter demonstrate the need for increasing the glucose supply within the pore. The improved glucose supply can be achieved by increasing the inlet glucose concentration and inlet velocity. However, increasing the inlet velocity will also increase the shear stress levels acting on the cells, and higher levels of shear stress may be detrimental for cell growth. Increasing the inlet

glucose concentration may also increase the amount of lactate production, which subsequently could cause the pH value of the medium to fall below the critical value. As such an optimization would be required to determine the appropriate inlet conditions to ensure both an adequate supply of nutrients and favourable shear stress level for promoting cell growth inside the scaffold. The present model and framework represent a viable tool for obtaining the optimal parameters.

In Chapter 5, a computational model was developed to simulate the scaffold-free chondrocyte culture process over a flat plate placed inside a perfusion bioreactor for 150 days by including the two-way coupling between the cell growth and the local flow field and glucose concentration to represent a realistic cell growth process. The simulation results indicate that for longer culture periods, the influence of the growing cell phase on the local fluid velocity, shear stress and glucose concentration distribution becomes significant. The growing cell phase is observed to restrict the glucose transport inside the bioreactor and the shear stress values are found to result in an increase in the overall cell growth. The results from such realistic computational studies of cell growth are especially important since to perform experiments for extremely long culture periods is often not feasible.

The final goal for this thesis was to implement a computational model which is capable of considering the two-way coupling between the cell growth and local fluid flow and nutrient transport for the 3D cell growth in a relatively complex porous scaffold. In Chapter 6, the 3D cell growth was performed for 30 culture days by placing the cell-seeded scaffold with a solid volume fraction of $\varepsilon_s = 0.28$ inside a bi-directional flow perfusion bioreactor. Initially the fluid flowed in the positive streamwise direction and after 15 culture days the flow direction was reversed. In this chapter, the scaffold considered for the simulation was divided into three zones referred to as the front, middle and rear zones. During the first fifteen days of the culture process the cell growth occurred mainly in the front zone due to the enhanced supply of glucose. The cell growth in the front zone reduced the permeability of the porous scaffold and limited the supply of glucose to the middle and rear zones of the scaffold, which in turn significantly reduced the cell growth in those two zones. Reversing the direction of the fluid flow and glucose supply for the final 15 days of the culture period improved the cell growth in the rear zones. At the end of 30 culture days the CVF was found to represent 48, 12 and 40 percent of the total CVF in the front, middle and rear zones respectively. Note that the CVF in the middle zone is still much less

than that is the front and rear zones. However, the bi-directional approach eliminated the limitation of glucose supply and hence improved the cell growth in the rear zone of the scaffold. The simulation results presented in this chapter suggest that the bi-directional perfusion flow bioreactor is promising for the *in vitro* cell culture. The developed mathematical model and computational framework will be a viable tool to realistically simulate the 3D cell growth and to evaluate the optimal design variables for the scaffold structure and bioreactor configuration.

Overall the results of this thesis provide important insights into the culture process and demonstrate the capability of mathematical modelling and computational methods to realistically simulate the cell growth even for relatively long culture periods. The capability of the model to consider the two-way coupling between the local cell growth and fluid flow and glucose concentration is a significant improvement over previous studies in this field.

7.3 Recommendations for future research

The *in vitro* cell culture in a bioreactor is a complex process. Although, the model and framework developed in this thesis show significant promise for performing realistic cell growth simulation over longer culture periods, there are still some important issues to be addressed and included into the model.

In the present thesis, the cells are considered as rigid and impermeable to fluid flow and nutrient transport. For the fluid flow a no-slip boundary condition was applied at the cell surface. A reaction boundary condition is applied at the surface of the cell phase to perform the mass transfer simulation. However, cells are not completely solid as assumed in the model and a certain amount of nutrients will be transported by diffusion through the cell-phase during the culture process. Investigation of the diffusion transport through the cell-phase and consumption of the nutrients by the cells located away from the surface of the cell-phase is important for longer culture periods. In the future this issue should be included into the model.

In the present model, the cell-phase is considered as a compact and solid structure but realistically during the tissue formation ECM production also occurs along with the cell growth. The production and degradation of the ECM and the interaction of the cell-ECM phase with the local biomechanical environment should be included into the model to simulate the actual tissue growth process. The degradability of the scaffold materials and shear-induced cell movement

and deformation should also be included into the model and framework to mimic the actual cell and tissue culture process.

In the present thesis, a specific set of input culture parameters i.e. inlet velocity and nutrient concentration, distance between the scaffold strands, duration of the flow from each direction in the bidirectional flow bioreactor etc. was used to obtain the simulation results. In the future, different values of the input culture parameters can be used to obtain the most suitable or optimal culture condition.

In this thesis, one of the key objectives was to use a cell growth equation where the cell growth will be influenced by the local nutrients supply and shear stress induced on the cells. Another objective of the study was to understand the influence of the waste generation on the cell growth. However, a single cell growth equation which addresses the aforementioned issues is not available in the literature. Therefore, different cell growth equations were adopted from the literature and modified to calculate the cell growth rate. In chapter 3, although the cell growth equation was a function of multiple nutrients supply and shear stress induced on the cells, the equation did not consider the influence of the waste generation. The modified cell growth equation used in chapter 4 considered the nutrient supply, waste generation and the influence of shear stress values on the cell growth. However, the equation did not included harmful effect of shear stress on the cell growth. In chapter 5 and 6, the harmful effect of the shear stress was included, however the influence of waste generation was not considered. In the future, it is essential to develop a complete cell growth equation to address all the aforementioned issues.

Finally, the cell growth equation and the overall cell growth model needs to be thoroughly validated by comparison to biological experiments performed for 15 to 30 culture days. Such experimental studies will improve the knowledge regarding the realistic culture process as well as provide benchmark results for the numerical studies. The numerical studies should be performed with same scaffold and bioreactor geometry and input culture parameters to compare the results obtained by experiments and subsequently validate the developed model and framework.

Appendix A

A1. D3Q19 MRT LBM model for fluid flow

In this study a D3Q19 MRT LBM model was used to simulate the fluid flow. This model uses a cubic lattice with 19 discrete lattice points to define the 3D space as shown in Fig. A1.

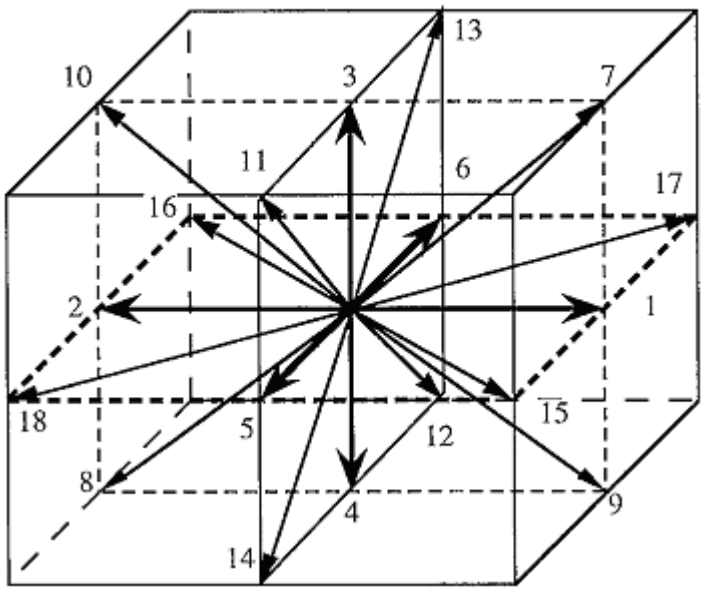

Figure A1: Discrete velocity vectors for D3Q19 lattices (Mei *et al.* 2000)

The discretized MRT LBM equation can be written as (d'Humières *et al.* 2002; Voronov *et al.* 2010):

$$|f(x_i + e_\alpha \delta t, t + \delta t)\rangle - |f(x_i, t)\rangle = -M^{-1} S \left[|m(x_i, t)\rangle - |m^{eq}(x_i, t)\rangle\right] \pm |F\rangle \quad \text{(A1)}$$

In the equation above, $|\cdot\rangle$ is used to represent the column vectors and $|f\rangle$ are the distribution functions (DF) at each lattice point. The left hand side of Eq. A1 represents the streaming process and the right hand side represents the collision process. In the streaming process, the particle population streams to their adjacent location from x_i to $x_i + e_\alpha \delta t$ with a velocity e_α along each characteristic direction; in the collision process, particles interact with each other at each node and as a result, change their velocity directions accordingly.

$|m\rangle$ is the moment vector and for the D3Q19 model the corresponding 19 moments are arranged in the following order (d'Humières *et al.* 2002; Premnath *et al.* 2012):

$$|m\rangle = \left(\rho, e, \varepsilon, j_x, q_x, j_y, q_y, j_z, q_z, 3P_{xx}, 3\pi_{xx}, P_{ww}, \pi_{ww,} P_{xy}, P_{yz}, P_{xz}, m_x, m_y, m_z\right)^T \quad \text{(A2)}$$

Here the ρ is the mass density; e and $\varepsilon = e^2$ represent the kinetic energy (independent of density) and the squared energy, respectively; j_x, j_y, j_z are the components of the momentum, i.e. $j_x = \rho u_x$, $j_y = \rho u_y$, $j_z = \rho u_z$; q_x, q_y, q_z are the components of the energy flux, $3P_{xx}, P_{xy}, P_{yz}, P_{xz}$ are the components of the symmetric traceless viscous shear tensor; $P_{ww} = P_{yy} - P_{zz}$, where P_{yy} and P_{zz} are the normal components of the viscous stress tensor; π_{xx} and π_{ww} are two moments which have the same symmetry as the diagonal part of the traceless viscous tensor p_{ij}; m_x, m_y and m_z are three moments which are part of a third rank tensor with the symmetry of $j_k P_{mn}$ d'Humières *et al.* (2002) and Premnath *et al.* (2012).

The moment vector can be mapped as,

$$|m\rangle = M\,|f\rangle \quad \text{(A3)}$$

where M is the transformation matrix and is given by (d'Humières *et al.* 2002; Premnath *et al.* 2012),

$$
\begin{vmatrix}
1 & 1 & 1 & 1 & 1 & 1 & 1 & 1 & 1 & 1 & 1 & 1 & 1 & 1 & 1 & 1 & 1 & 1 & 1 \\
-30 & -11 & -11 & -11 & -11 & -11 & -11 & 8 & 8 & 8 & 8 & 8 & 8 & 8 & 8 & 8 & 8 & 8 & 8 \\
12 & -4 & -4 & -4 & -4 & -4 & -4 & 1 & 1 & 1 & 1 & 1 & 1 & 1 & 1 & 1 & 1 & 1 & 1 \\
0 & 1 & -1 & 0 & 0 & 0 & 0 & 1 & -1 & 1 & -1 & 1 & -1 & 1 & -1 & 0 & 0 & 0 & 0 \\
0 & -4 & 4 & 0 & 0 & 0 & 0 & 1 & -1 & 1 & -1 & 1 & -1 & 1 & -1 & 0 & 0 & 0 & 0 \\
0 & 0 & 0 & 1 & -1 & 0 & 0 & 1 & 1 & -1 & -1 & 0 & 0 & 0 & 0 & 1 & -1 & 1 & -1 \\
0 & 0 & 0 & -4 & 4 & 0 & 0 & 1 & 1 & -1 & -1 & 0 & 0 & 0 & 0 & 1 & -1 & 1 & -1 \\
0 & 0 & 0 & 0 & 0 & 1 & -1 & 0 & 0 & 0 & 0 & 1 & 1 & -1 & -1 & 1 & 1 & -1 & -1 \\
0 & 0 & 0 & 0 & 0 & -4 & 4 & 0 & 0 & 0 & 0 & 1 & 1 & -1 & -1 & 1 & 1 & -1 & -1 \\
0 & 2 & 2 & -1 & -1 & -1 & -1 & 1 & 1 & 1 & 1 & 1 & 1 & 1 & 1 & -2 & -2 & -2 & -2 \\
0 & -4 & -4 & 2 & 2 & 2 & 2 & 1 & 1 & 1 & 1 & 1 & 1 & 1 & 1 & -2 & -2 & -2 & -2 \\
0 & 0 & 0 & 1 & 1 & -1 & -1 & 1 & 1 & 1 & 1 & -1 & -1 & -1 & -1 & 0 & 0 & 0 & 0 \\
0 & 0 & 0 & -2 & -2 & 2 & 2 & 1 & 1 & 1 & 1 & -1 & -1 & -1 & -1 & 0 & 0 & 0 & 0 \\
0 & 0 & 0 & 0 & 0 & 0 & 0 & 1 & -1 & -1 & 1 & 0 & 0 & 0 & 0 & 0 & 0 & 0 & 0 \\
0 & 0 & 0 & 0 & 0 & 0 & 0 & 0 & 0 & 0 & 0 & 0 & 0 & 0 & 0 & 1 & -1 & -1 & 1 \\
0 & 0 & 0 & 0 & 0 & 0 & 0 & 0 & 0 & 0 & 0 & 1 & -1 & -1 & 1 & 0 & 0 & 0 & 0 \\
0 & 0 & 0 & 0 & 0 & 0 & 0 & 1 & -1 & 1 & -1 & -1 & 1 & -1 & 1 & 0 & 0 & 0 & 0 \\
0 & 0 & 0 & 0 & 0 & 0 & 0 & -1 & -1 & 1 & 1 & 0 & 0 & 0 & 0 & 1 & -1 & 1 & -1 \\
0 & 0 & 0 & 0 & 0 & 0 & 0 & 0 & 0 & 0 & 0 & 1 & 1 & -1 & -1 & -1 & -1 & 1 & 1
\end{vmatrix}
$$

$|m^{eq}\rangle$ is the equilibrium moment vector with the following components (d'Humières *et al.* 2002; Premnath *et al.* 2012),

$$\rho^{(eq)} = \rho,\ j_x^{(eq)} = j_x,\ j_y^{(eq)} = j_y,\ j_z^{(eq)} = j_z \tag{A4}$$

$$e^{(eq)} = -11\rho + \frac{19}{\rho_0}\left(j_x^{\,2} + j_y^{\,2} + j_z^{\,2}\right) \tag{A5}$$

$$\varepsilon^{(eq)} = w_\varepsilon\,\rho + \frac{w_{\varepsilon j}}{\rho_0}\left(j_x^{\,2} + j_y^{\,2} + j_z^{\,2}\right) \tag{A6}$$

$$q_x^{(eq)} = -\frac{2}{3}j_x,\ q_y^{(eq)} = -\frac{2}{3}j_y,\ q_z^{(eq)} = -\frac{2}{3}j_z \tag{A7}$$

$$p_{xx}^{(eq)} = \frac{1}{3\rho_0}\left[2\,j_x^{\,2} - \left(j_y^{\,2} + j_z^{\,2}\right)\right], \qquad p_{ww}^{(eq)} = \frac{1}{\rho_0}\left[j_y^{\,2} - j_z^{\,2}\right] \tag{A8}$$

$$p_{xy}^{(eq)} = \frac{1}{\rho_0} j_x j_y, \quad p_{yz}^{(eq)} = \frac{1}{\rho_0} j_y j_z, \quad p_{xz}^{(eq)} = \frac{1}{\rho_0} j_x j_z \tag{A9}$$

$$\pi_{xx}^{(eq)} = w_{xx} p_{xx}^{(eq)}, \ \pi_{ww}^{(eq)} = w_{xx} p_{ww}^{(eq)} \tag{A10}$$

$$m_x^{(eq)} = m_y^{(eq)} = m_z^{(eq)} = 0 \tag{A11}$$

In the equations above w_ϵ, $w_{\epsilon j}$ and w_{xx} are the free parameters for this D3Q19 model (d'Humières *et al.* 2002).

The collision matrix S in moment space is a diagonal matrix which contains the values of the relaxation parameters (d'Humières *et al.* 2002)

$$S = diag\,(0, s_1, s_2, 0, s_4, 0, s_4, 0, s_4, s_\nu, s_{10}, s_\nu, s_{10}, s_\nu, s_\nu, s_\nu, s_{16}, s_{16}, s_{16}) \tag{A12}$$

The kinematic viscosity ν is evaluated from the following relation (d'Humières *et al.* 2002),

$$\nu = \frac{1}{3}\left(\frac{1}{s_\nu} - \frac{1}{2}\right)\frac{\delta x^2}{\delta t} \tag{A13}$$

The values of the relaxation parameters and free parameters can be obtained through linear analysis of the lattice Boltzmann equation evolution operator (Lallemand and Luo 2000; d'Humières *et al.* 2002). In this study the following values are adopted: $w_\epsilon = 0$, $w_{\epsilon j} = -475/63$, $w_{xx} = 0$, $s_1 = 1.19$, $s_2 = s_{10} = 1.4$, $s_4 = 1.2$, $s_{16} = 1.98$, and $s_\nu = 1.6$. With the above parameters the model has following constraints: the maximum speed is 0.19 m/s (Mach number 0.33) and the lattice viscosity $\nu > 2.54 \times 10^{-3}$ m^2/s (d'Humières *et al.* 2002).

A2. D3Q7 MRT LBM model for mass transfer

In this study, a D3Q7 MRT LBM model was used to simulate the mass transfer. The model is analogous to the so-called athermal MRT LBM scheme and is used to solve the convection-diffusion equation (CDE). In this model, a cubic lattice with only 7 discrete lattice directions is used to define the 3-D space as shown in Fig. A2.

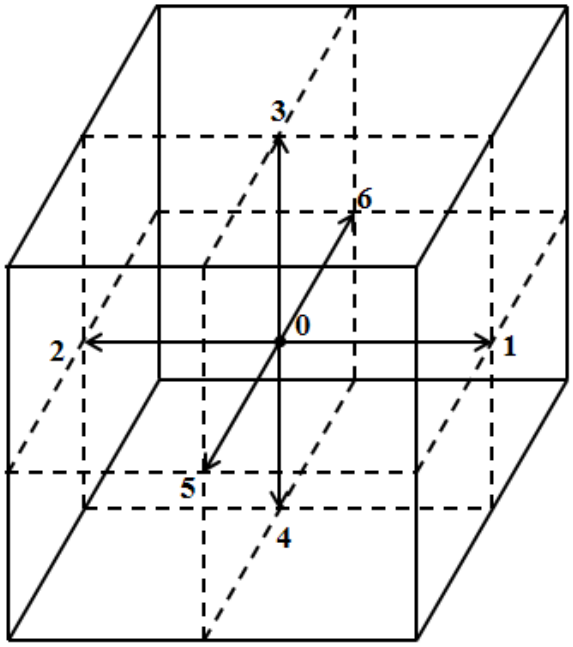

Figure A2: Discrete velocity vectors for D3Q7 lattices

The discretized MRT LBM equation can be written as (Yoshida and Nagaoka 2010),

$$|g(x_i + e_\alpha \delta t, t + \delta t)\rangle - |g(x_i, t)\rangle = -M^{-1} S \left[|m(x_i, t)\rangle - |m^{eq}(x_i, t)\rangle\right] \quad \text{(A14)}$$

The macroscopic variable, i.e. concentration can be obtained by solving the discrete version of equation A14 and using the following relationship:

$$C = \sum_{\alpha=0}^{6} g_\alpha \quad \text{(A15)}$$

The moment vector can be mapped as (Yoshida and Nagaoka 2010),

$$|m\rangle = M\,|g\rangle \tag{A16}$$

The equilibrium moments are defined as:

$$m^{eq} = \left(m_0^{eq}, m_1^{eq}, m_2^{eq}, m_3^{eq}, m_4^{eq}, m_5^{eq}, m_6^{eq}\right)^T = (0, uC, vC, wC, aC, 0,0)^T \tag{A17}$$

where, $a = 3/4$

The transformation matrix M and the relaxation matrix S are specified by Yoshida and Nagaoka (2010) as follows:

$$\boldsymbol{M} = \begin{bmatrix} 1 & 1 & 1 & 1 & 1 & 1 & 1 \\ 0 & 1 & -1 & 0 & 0 & 0 & 0 \\ 0 & 0 & 0 & 1 & -1 & 0 & 0 \\ 0 & 0 & 0 & 0 & 0 & 1 & -1 \\ 6 & -1 & -1 & -1 & -1 & -1 & -1 \\ 0 & 2 & 2 & -1 & -1 & -1 & -1 \\ 0 & 0 & 0 & 1 & 1 & -1 & -1 \end{bmatrix}.$$

$$\boldsymbol{S}^{-1} = \begin{bmatrix} \tau_0 & 0 & 0 & 0 & 0 & 0 & 0 \\ 0 & \tau_{xx} & \tau_{xy} & \tau_{xz} & 0 & 0 & 0 \\ 0 & \tau_{xy} & \tau_{yy} & \tau_{yz} & 0 & 0 & 0 \\ 0 & \tau_{xz} & \tau_{yz} & \tau_{zz} & 0 & 0 & 0 \\ 0 & 0 & 0 & 0 & \tau_4 & 0 & 0 \\ 0 & 0 & 0 & 0 & 0 & \tau_5 & 0 \\ 0 & 0 & 0 & 0 & 0 & 0 & \tau_6 \end{bmatrix}$$

For an isotropic diffusion process, i.e. when the flux of the diffusing molecules through some particular plane is proportional to the concentration gradient orthogonal to the plane (Saltzman 2004), the off-diagonal components of relaxation matrix S i.e. τ_{xy}, τ_{xz} and τ_{yz} are zero. The diffusion coefficients are related to the relaxation parameters and for the isotropic case are given by the following relation (Yoshida and Nagaoka 2010),

$$D = \frac{1}{4}\left(\frac{1}{s_D} - \frac{1}{2}\right)\frac{\delta x^2}{\delta t} \tag{A18}$$

In Eq. A16, s_D is the relaxation parameter which is given by $s_D = 1/\tau_D$, where τ_D is the relaxation time scale. Note that, $\tau_{xx} = \tau_{yy} = \tau_{zz} = \tau_D$ and for numerical stability of the model the value of τ_D should be greater than 0.5 (Li *et al.* 2013).

A3. Control volume based cell growth simulation

In the control volume based cell growth simulation each lattice node is located inside a control volume (CV). The circles in Fig. A3 represent the lattice nodes and the CVs are indicated by dashed boxes.

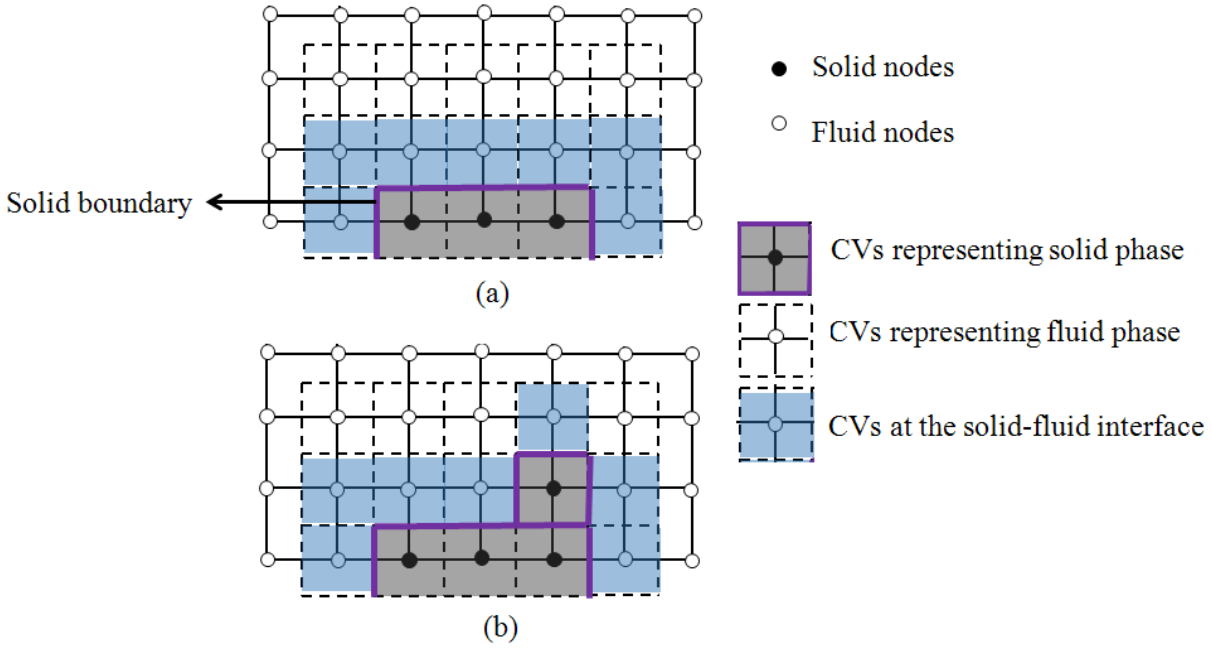

Figure A3: Schematic illustration of lattice nodes and control volume

To perform the CV-based cell growth simulation the algorithm described in Section 5.3 was implemented. According to the algorithm, the first step was to identify the CVs at the solid-fluid interface. Fig. A3a) shows the CVs at the solid-fluid interface which surround the CVs represent the solid phase. Note that the solid boundary is located halfway between the lattice nodes. This is due to the implementation of the half-way bounce back boundary condition which is second order accurate (Yu *et al.* 2003). The next step is to update the mass of the CVs at the solid-fluid interface based on the cell growth in each time step. If the mass of a CV at the solid-

fluid interface exceeds the threshold value, the lattice node inside the CV becomes a solid node and a new CV is selected from the surrounding fluid CVs based on a uniform probability to represent a new solid-fluid interface CV as shown in Fig. A3b).

Appendix B

Verification and validation

B1. Assessment of numerical error in the D3Q19 MRT LBM model: Poiseuille flow simulation

Poiseuille channel flow (White 2009) was selected as a test case to verify the implementation of the LBM and assess the equivalent "order" of the numerical scheme D3Q19 MRT LBM which was used to perform the simulation. The flow inside the channel was driven in the streamwise (*x*) direction by the pressure difference specified between the inlet and outlet planes. A no-slip boundary condition (BC) was applied at the channel upper and lower walls, and a periodic BC was applied at the channel side walls. Three different grids were considered as detailed in Table B1. The ratio of the channel height (H) and length (L) was H/L = 1/4 for all three cases.

	Number of nodes in the *x* direction, N_x	Number of nodes in the *z* direction, N_z
Case I	100	25
Case II	132	33
Case III	160	40

Table B1: Number of nodes used for different cases

Note that, a three-dimensional (3D) domain was used for the simulation and the number of nodes used the y-direction was N_y = 3.

The error between the numerical solution and exact solution was calculated using the following equation:

$$\varepsilon = \sqrt{\frac{(u_{numerical} - u_{exact})^2}{N_z}} \quad \text{(B1)}$$

where N_z is the number of nodes in the *z*-direction. The velocity profile at *x* = L/2 in the *z*-direction was considered for evaluating Eq. B1 for all three cases. The exact solution is given by a parabolic velocity profile with a maximum value of

$$u_{max} = \left(-\frac{dp}{dx}\right)\frac{H^2}{16\mu} \tag{B2}$$

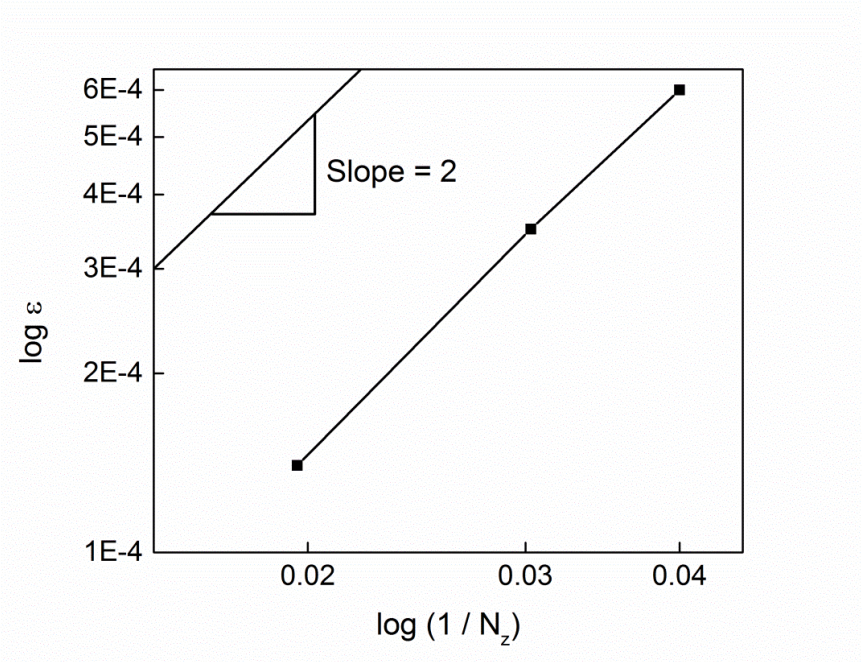

Figure B1: Error in velocity as a function of grid spacing

Fig. B1 shows a log-log plot of the error ε versus the grid interval $(1/N_z)$. The line has a slope equal to 2.03 which implies that the scheme is second order accurate. The maximum relative error which occurred at the first internal node for three different cases is shown in Table B2.

	Maximum relative error $\left(\frac{\lvert u_{exact} - u_{numerical}\rvert}{u_{exact}}\right)$
Case I	0.0179
Case II	0.012
Case III	0.0084

Table BII: Maximum relative error for different cases

B2. Model validation: flow over a circular cylinder

In perfusion bio-reactors, the fluid is directed to flow through a porous scaffold and the movement of the fluid inside the bio-reactor is relatively slow, typically within the creeping flow region. The average velocity inside a scaffold placed in a perfusion bio-reactor is approximately 3.5×10^{-4} m/s (Yan *et al.* 2011), and typically the Reynolds number (Re_d) based on the diameter of the scaffold strands ranges from 0.01 to 0.1 (Yan *et al.* 2011; Singh and Hutmacher 2009). Since the scaffolds are typically made of arrays of circular strands, the implementation of the D3Q19 MRT LBM model was validated by performing a flow simulation over a circular cylinder mounted in a three-dimensional (3D) channel within the laminar flow region. Although the flow around a circular cylinder has been studied for different Reynolds number regimes, an analytical solution for the 3D flow over a circular cylinder within the laminar or creeping flow regime has not been documented in the literature to the best of author's knowledge. Ribeiro *et al*. (2012) conducted an experimental and numerical study of 3D flow past a confined cylinder for aspect ratios of AR = 16, 8 and 2, respectively, with a blockage ratio of BR = 0.5 and Reynolds numbers ranging from 10 to 64. Hence, the present simulation was performed for Reynolds number in the range of Re_d = 12 to 64 and the simulation results were compared with the experimental and computational results of Ribeiro *et al.* (2012).

A schematic of the channel can be seen in Fig. B2. The channel was 300 mm long, 128 mm wide and 32 mm deep. The diameter of the cylinder was 16 mm, and the cylinder spanned the entire channel width. The aspect ratio of the cylinder was AR = L/d = 8 and the blockage ratio were 0.5. The cylinder was located 120 mm downstream of the channel inlet and positioned at the mid-plane. The coordinate frame was aligned with the center of the cylinder. The number of nodes used for the simulation was 400×192×48 in the *x*, *y* and *z* directions, respectively. The flow inside the channel was driven by the pressure difference specified between the inlet and outlet planes. A bounceback no-slip boundary condition was applied on the channel side walls, while an IB-type boundary condition was used for the curved wall of the cylinder.

The computational set-up in our simulation is similar to that used by Ribeiro *et al.* (2012) with exactly the same aspect ratio and blockage ratio, although their channel was much longer. However, the present channel length was sufficient to ensure fully developed channel flow upstream of the cylinder. In this flow, the velocity field near the walls was influenced by the

viscous shear on those surfaces. For the summary analysis presented below, the velocity profiles are examined in the *y*-center plane of the channel.

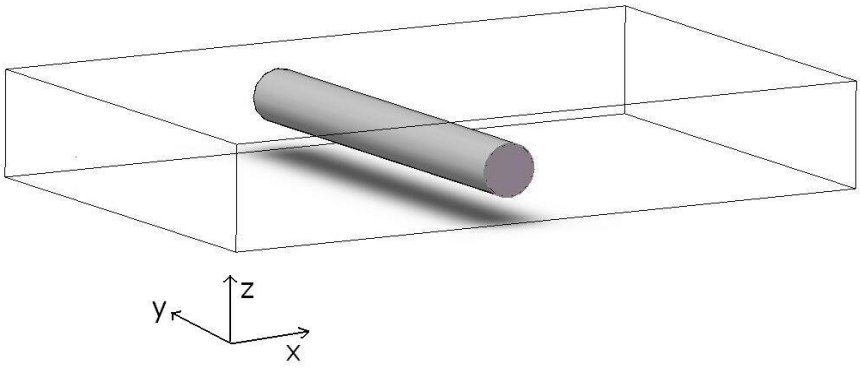

Figure B2: Schematic of the cylinder and channel.

Fig.'s B3a) and B3b) show the streamwise velocity profile 4*R* upstream and 4*R* downstream of the cylinder, respectively, for a Reynolds number of Re_d = 50. Based on symmetry, only one-half of the profile is shown. In Fig. B3 a), the present results are in close agreement with the measurements of Ribeiro *et al*. (2012) for Re_d = 50. In Fig. B3b) there is some small deviation from the measurements at the centreline and in the outer region.

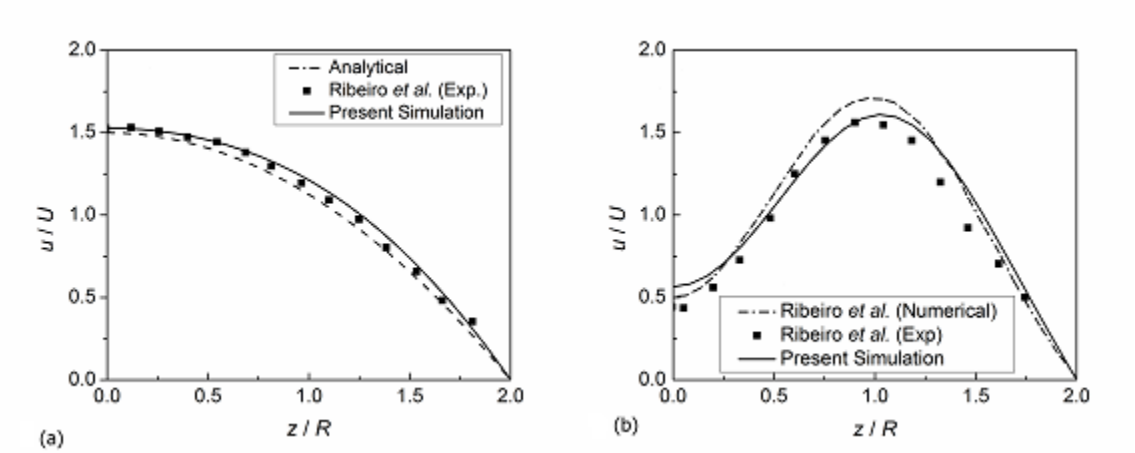

Figure B3: Transverse profile of the streamwise velocity for *Re* = 50 at: (a) *x*/*R* = -4, (b) *x*/*R* = 4.

The present study considered Reynolds numbers ranging from Re_d = 12 to 64. Beginning at Re_d = 14, a pair of closed vortices is formed immediately behind the cylinder, which agrees well with other numerical and experimental studies (Mandujano *et al.* 2005; Ribeiro *et al*. 2012).

Fig. B4 plots the streamlines for Re_d = 45 and two symmetric vortices are clearly evident. The length of these vortices, l_v, which is sometimes referred to as the recirculation length, increases almost linearly with Re in the laminar regime. The variation of l_v with Re_d is shown in Fig. B5, and compares well with both Ribeiro *et al.*'s (2012) experimental and numerical results.

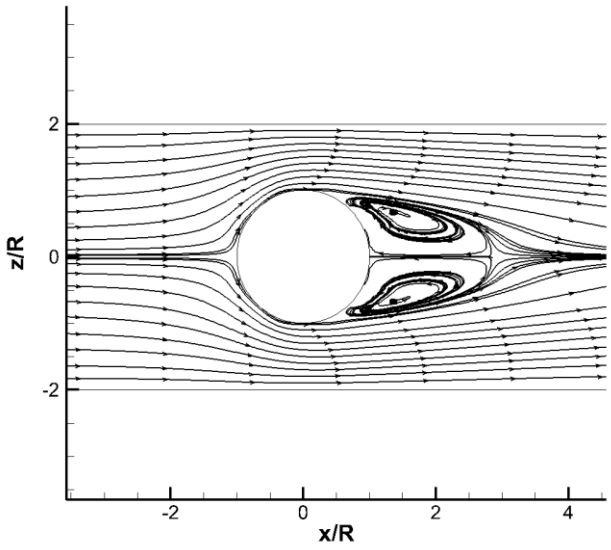

Figure B4: Streamlines on the x-z plane for Re_d =45 (Hossain *et al.* 2015).

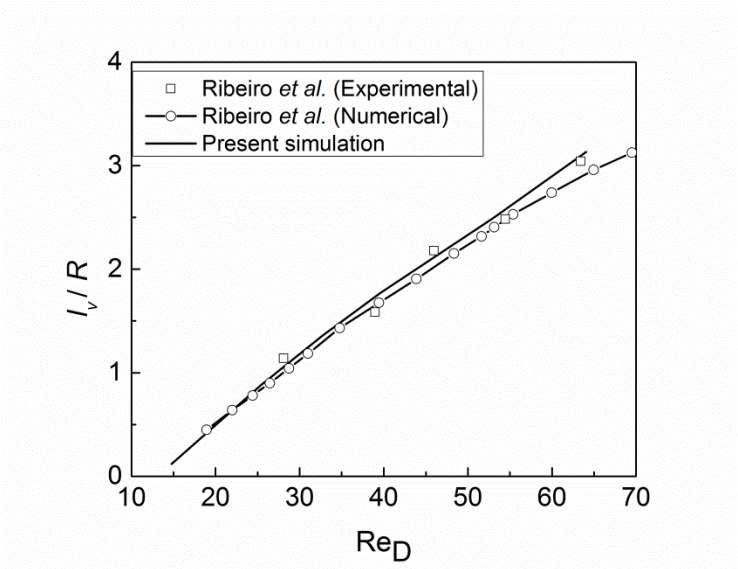

Figure B5: Variation of the recirculation length with Reynolds number.

Finally, Fig. B6 plots the streamwise velocity profile along the center-line of the channel. The velocity profiles are in good agreement with the experimental and computational results of Ribeiro *et al.* (2012), although both simulations predict a somewhat more rapid recovery in velocity immediately downstream of the cylinder.

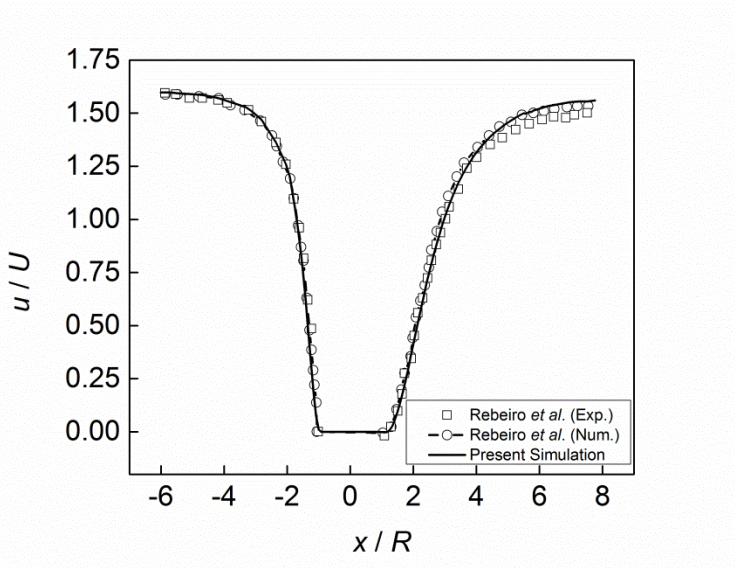

Figure B6: Streamwise velocity along the centerline for a Reynolds number of $Re_d = 14$.

The comparison of the present simulation with Ribeiro *et al.*'s work demonstrates the ability of the D3Q19 MRT LBM model to provide realistic solution for representative flow in the low Reynolds number regime.

B3. Comment on computational time

To perform the 3D cell growth simulation the computational code used the MRT LBM models. The number of nodes used in the final study for the numerical simulation was 222×37×25 in the *x*, *y* and *z* directions, respectively such that the total number of nodes was 205350.

The simulation of a single culture day required about 10000 iterations which used 45 minutes of wall-clock time on a desktop computer with 31.8 GB RAM and Intel(R) Core(TM) i7-3770 CPU @ 3.40GHz processor. The simulation of fifteen culture days used only 22.5 hours of wall-clock time and therefore, the present computational framework seems effective in terms of the time required to perform the simulation for longer culture periods. Typically the duration of the culture period can vary between fifteen to ninety culture days.

Appendix C

Permissions to republish chapters and figures

1. Permission to republish chapter 1

Dear Prof. Hossain,

It is our pleasure to grant you permission to publish **any part or all of** the ASME paper "Investigation of the In Vitro Culture Process for Skeletal-Tissue-Engineered Constructs Using Computational Fluid Dynamics and Experimental Methods," by Shakhawath Hossain; X. B. Chen; D. J. Bergstrom, J Biomech Eng. 2012; 134(12), as cited in your letter in the thesis entitled MATHEMATICAL MODELLING AND COMPUTATIONAL SIMULATION OF IN VITRO TISSUE CULTURE PROCESS to be published by University of Saskatchewan.
Permission is granted for the specific use as stated herein and does not permit further use of the materials without proper authorization. Proper attribution must be made to the author(s) of the materials. **Please note**: if any or all of the figures and/or Tables are of another source, permission should be granted from that outside source or include the reference of the original source. ASME does not grant permission for outside source material that may be referenced in the ASME works.
As is customary, we request that you ensure proper acknowledgment of the exact sources of this material, the authors, and ASME as original publisher. Acknowledgment must be retained on all pages printed and distributed.
Many thanks for your interest in ASME publications.
Sincerely,

Beth Darchi
Publishing Administrator
ASME
2 Park Avenue, 6th Floor
New York, NY 10016-5990
Tel 1.212.591.7700
darchib@asme.org

2. Permission to republish Fig. 2.3

ELSEVIER LICENSE
TERMS AND CONDITIONS
Mar 18, 2015

This is a License Agreement between Md Shahawath Hossain ("You") and Elsevier ("Elsevier") provided by Copyright Clearance Center ("CCC"). The license consists of your order details, the terms and conditions provided by Elsevier, and the payment terms and conditions.

All payments must be made in full to CCC. For payment instructions, please see information listed at the bottom of this form.

Supplier	Elsevier Limited The Boulevard,Langford Lane Kidlington,Oxford,OX5 1GB,UK
Registered Company Number	1982084
Customer name	Md Shahawath Hossain
Customer address	414 A, 108th Street Saskatoon, SK S7H 1P9
License number	3592130661757
License date	Mar 18, 2015
Licensed content publisher	Elsevier
Licensed content publication	Journal of Biomechanics
Licensed content title	3-D computational modeling of media flow through scaffolds in a perfusion bioreactor
Licensed content author	Blaise Porter,Roger Zauel,Harlan Stockman,Robert Guldberg,David Fyhrie
Licensed content date	March 2005
Licensed content volume number	38
Licensed content issue number	3
Number of pages	7
Start Page	543
End Page	549
Type of Use	reuse in a thesis/dissertation
Portion	figures/tables/illustrations
Number of figures/tables/illustrations	1
Format	both print and electronic
Are you the author of this Elsevier article?	No

Will you be translating?	No
Original figure numbers	7
Title of your thesis/dissertation	MATHEMATICAL MODELLING AND COMPUTATIONAL SIMULATION OF IN VITRO TISSUE CULTURE PROCESSES
Expected completion date	Apr 2015
Estimated size (number of pages)	190
Elsevier VAT number	GB 494 6272 12
Permissions price	0.00 USD
VAT/Local Sales Tax	0.00 USD / 0.00 GBP
Total	0.00 USD
Terms and Conditions	

3. Permission to republish Fig. 2.4

JOHN WILEY AND SONS LICENSE
TERMS AND CONDITIONS
Mar 18, 2015

This Agreement between Md Shahawath Hossain ("You") and John Wiley and Sons ("John Wiley and Sons") consists of your license details and the terms and conditions provided by John Wiley and Sons and Copyright Clearance Center.

License Number	3592140147131
License date	Mar 18, 2015
Licensed Content Publisher	John Wiley and Sons
Licensed Content Publication	Biotechnology & Bioengineering
Licensed Content Title	Enhancement of cell growth in tissue-engineering constructs under direct perfusion: Modeling and simulation
Licensed Content Author	C.A. Chung,C.W. Chen,C.P. Chen,C.S. Tseng
Licensed Content Date	Feb 15, 2007
Pages	14
Type of use	Dissertation/Thesis
Requestor type	University/Academic
Format	Print and electronic
Portion	Figure/table
Number of figures/tables	1
Original Wiley	10. (a)

figure/table number(s)	
Will you be translating?	No
Title of your thesis / dissertation	MATHEMATICAL MODELLING AND COMPUTATIONAL SIMULATION OF IN VITRO TISSUE CULTURE PROCESSES
Expected completion date	Apr 2015
Expected size (number of pages)	190
Requestor Location	Md Shahawath Hossain 414 A, 108th Street Saskatoon, SK S7H 1P9 Canada Attn: Md Shahawath Hossain
Billing Type	Invoice
Billing Address	Md Shahawath Hossain 414 A, 108th Street Saskatoon, SK S7H 1P9 Canada Attn: Md Shahawath Hossain
Total	0.00 USD

4. Permission to republish Fig. 2.5

JOHN WILEY AND SONS LICENSE
TERMS AND CONDITIONS
Mar 18, 2015

This Agreement between Md Shahawath Hossain ("You") and John Wiley and Sons ("John Wiley and Sons") consists of your license details and the terms and conditions provided by John Wiley and Sons and Copyright Clearance Center.

License Number	3592140356974
License date	Mar 18, 2015

Licensed Content Publisher	John Wiley and Sons
Licensed Content Publication	Biotechnology & Bioengineering
Licensed Content Title	A fluid dynamics approach to bioreactor design for cell and tissue culture
Licensed Content Author	Jonathan Dusting,John Sheridan,Kerry Hourigan
Licensed Content Date	May 8, 2006
Pages	13
Type of use	Dissertation/Thesis
Requestor type	University/Academic
Format	Print and electronic
Portion	Figure/table
Number of figures/tables	1
Original Wiley figure/table number(s)	3
Will you be translating?	No
Title of your thesis / dissertation	MATHEMATICAL MODELLING AND COMPUTATIONAL SIMULATION OF IN VITRO TISSUE CULTURE PROCESSES
Expected completion date	Apr 2015
Expected size (number of pages)	190
Requestor Location	Md Shahawath Hossain 414 A, 108th Street Saskatoon, SK S7H 1P9 Canada Attn: Md Shahawath Hossain
Billing Type	Invoice
Billing Address	Md Shahawath Hossain 414 A, 108th Street Saskatoon, SK S7H 1P9 Canada Attn: Md Shahawath Hossain
Total	0.00 USD
Terms and Conditions	

5. Permission to republish Chapter 3

SPRINGER LICENSE
TERMS AND CONDITIONS
Mar 17, 2015

This is a License Agreement between Md Shahawath Hossain ("You") and Springer ("Springer") provided by Copyright Clearance Center ("CCC"). The license consists of your order details, the terms and conditions provided by Springer, and the payment terms and conditions.

All payments must be made in full to CCC. For payment instructions, please see information listed at the bottom of this form.

License Number	3591541072385
License date	Mar 17, 2015
Licensed content publisher	Springer
Licensed content publication	Biomechanics and Modeling in Mechanobiology
Licensed content title	Prediction of cell growth rate over scaffold strands inside a perfusion bioreactor
Licensed content author	Md. Shakhawath Hossain
Licensed content date	Jan 1, 2014
Volume number	14
Issue number	2
Type of Use	Thesis/Dissertation
Portion	Full text
Number of copies	100
Author of this Springer article	Yes and you are a contributor of the new work
Order reference number	None
Title of your thesis / dissertation	MATHEMATICAL MODELLING AND COMPUTATIONAL SIMULATION OF IN VITRO TISSUE CULTURE PROCESS
Expected completion date	Apr 2015

Estimated size(pages)	190
Total	0.00 USD

Questions? customercare@copyright.com or +1-855-239-3415 (toll free in the US) or +1-978-646-2777.

6. Permission to republish Chapter 5

SPRINGER LICENSE
TERMS AND CONDITIONS

Aug 06, 2015

This is a License Agreement between Md Shahawath Hossain ("You") and Springer ("Springer") provided by Copyright Clearance Center ("CCC"). The license consists of your order details, the terms and conditions provided by Springer, and the payment terms and conditions.

All payments must be made in full to CCC. For payment instructions, please see information listed at the bottom of this form.

License Number	3683190534577
License date	Aug 06, 2015
Licensed content publisher	Springer
Licensed content publication	Biomechanics and Modeling in Mechanobiology
Licensed content title	Computational modelling of the scaffold-free chondrocyte regeneration: a two-way coupling between the cell growth and local fluid flow and nutrient concentration
Licensed content author	Md. Shakhawath Hossain
Licensed content date	Jan 1, 2015
Type of Use	Thesis/Dissertation
Portion	Full text
Number of copies	1

Author of this Springer article	Yes and you are a contributor of the new work
Order reference number	None
Title of your thesis / dissertation	MATHEMATICAL MODELLING AND COMPUTATIONAL SIMULATION OF IN VITRO TISSUE CULTURE PROCESSES
Expected completion date	Aug 2015
Estimated size(pages)	200
Total	0.00 USD
Terms and Conditions	

7. Permission to republish Chapter 6

JOHN WILEY AND SONS LICENSE
TERMS AND CONDITIONS

Aug 06, 2015

This Agreement between Md Shahawath Hossain ("You") and John Wiley and Sons ("John Wiley and Sons") consists of your license details and the terms and conditions provided by John Wiley and Sons and Copyright Clearance Center.

License Number	3683190968215
License date	Aug 06, 2015
Licensed Content Publisher	John Wiley and Sons
Licensed Content Publication	Biotechnology & Bioengineering
Licensed Content Title	A mathematical model and computational framework for three-dimensional chondrocyte cell growth in a porous tissue scaffold placed inside a bi-directional flow perfusion bioreactor
Licensed Content Author	Md. Shakhawath Hossain,D.J. Bergstrom,X.B. Chen
Licensed Content Date	Jul 14, 2015
Pages	1
Type of use	Dissertation/Thesis
Requestor type	Author of this Wiley article

Format	Print and electronic
Portion	Full article
Will you be translating?	No
Title of your thesis / dissertation	MATHEMATICAL MODELLING AND COMPUTATIONAL SIMULATION OF IN VITRO TISSUE CULTURE PROCESSES
Expected completion date	Aug 2015
Expected size (number of pages)	200
Requestor Location	Md Shahawath Hossain 414 A, 108th Street Saskatoon, SK S7H 1P9 Canada Attn: Md Shahawath Hossain
Billing Type	Invoice
Billing Address	Md Shahawath Hossain 414 A, 108th Street Saskatoon, SK S7H 1P9 Canada Attn: Md Shahawath Hossain
Total	0.00 USD

8. Permission to republish Figure A1

ELSEVIER LICENSE
TERMS AND CONDITIONS
Jul 30, 2015

This is a License Agreement between Md Shahawath Hossain ("You") and Elsevier ("Elsevier") provided by Copyright Clearance Center ("CCC"). The license consists of your order details, the terms and conditions provided by Elsevier, and the payment terms and conditions.

All payments must be made in full to CCC. For payment instructions, please see information listed at the bottom of this form.

Supplier	Elsevier Limited The Boulevard,Langford Lane Kidlington,Oxford,OX5 1GB,UK
Registered Company Number	1982084
Customer name	Md Shahawath Hossain
Customer address	414 A, 108th Street Saskatoon, SK S7H 1P9
License number	3678990172106
License date	Jul 30, 2015
Licensed content publisher	Elsevier
Licensed content publication	Journal of Computational Physics
Licensed content title	Lattice Boltzmann Method for 3-D Flows with Curved Boundary
Licensed content author	Renwei Mei,Wei Shyy,Dazhi Yu,Li-Shi Luo
Licensed content date	1 July 2000
Licensed content volume number	161
Licensed content issue number	2
Number of pages	20
Start Page	680
End Page	699
Type of Use	reuse in a thesis/dissertation
Portion	figures/tables/illustrations
Number of figures/tables/illustrations	1
Format	both print and electronic
Are you the author of this Elsevier article?	No
Will you be translating?	No
Original figure numbers	Figure A1
Title of your thesis/dissertation	MATHEMATICAL MODELLING AND COMPUTATIONAL SIMULATION OF IN VITRO TISSUE CULTURE PROCESSES
Expected completion date	Aug 2015

Estimated size (number of pages)	200
Elsevier VAT number	GB 494 6272 12
Permissions price	0.00 USD
VAT/Local Sales Tax	0.00 USD / 0.00 GBP
Total	0.00 USD
Terms and Conditions	

References

Adachi T, Osako Y, Tanaka M, Hojo M, Hollister SJ (2006) Framework for optimal design of porous scaffold microstructure by computational simulation of bone regeneration. Biomaterials 27: 3964–3972.

Adrian RJ (1997) Dynamic ranges of velocity and spatial resolution of particle image velocimetry. Meas. Sci. Technol. 8: 1393-1398.

Adrian RJ (2005) Twenty years of particle image velocimetry. Exp. Fluids 39: 159-169.

Bancroft GN, Sikavitsas VI, Mikos AG (2003) Design of a flow perfusion bioreactor system for bone tissue engineering application. Tissue Eng. 9(3): 549-554.

Bawolin NK, Li MG, Chen XB, Zhang WJ (2010) Modelling material-degradation induced elastic property of tissue engineering scaffolds. ASME J. Biomech. Eng. 132: 111001 (1-7).

Betchen LJ, Straatman AG (2010) An investigation of the effects of a linear porosity distribution on non-equilibrium heat transfer in high-conductivity graphite foam. Num. Heat Trans. A 58: 605-624.

Bibby SRS, Fairbank JCT, Urban MR, Urban JPG (2002) Cell viability in scoliotic discs in relation to disc deformity and nutrient levels. Spine 27(20): 2220-2228.

Bilgen B, Barabino GA (2007) Location of scaffolds in bioreactors modulates the hydrodynamic environment experienced by engineered tissues. Biotechnol. Bioeng. 98(1): 282-294.

Blitterswijk CV (2008) Tissue Engineering. Elsevier Inc., London, UK.

Boccaccio A, Ballini A, Pappalettere C, Tullo D, Cantore S, Desiate A (2011) Finite element method (FEM), Mechanobiology and Biomimetic scaffolds in Bone tissue engineering. Int. J. Biol. Sci. **7**(1): 112-132.

Bottaro DP, Liebmann-Vinson A, Heidaran MA (2002) Molecular signaling in bioengineered tissue microenvironment. Ann. N.Y. Acad. Sci. 961: 143-153.

Boubriak OA, Urban JPG, Cui Z (2006) Monitoring of metabolite gradients in tissue-engineered constructs. J. R. Soc. Interface 3; 637-648.

Bouzidi M, Firdaouss M, Lallemand P (2001) Momentum transfer of a lattice Boltzmann fluid with boundaries. Phys. Fluids., 13: 3452–3459.

Bown MR, MacInnes JM, Allen RWK, Zimmerman WBJ (2006) Three-dimensional velocity measurements using stereoscopic micro-PIV and PTV. Meas. Sci. Technol. 17: 2175-2185.

Brinkman HC (1949) On the permeability of media consisting of closely packed porous particles. Appl. Sci. Res., A1: 81-86.

Bruneau C-H, Mortazavi I (2008) Numerical modeling and passive flow control using porous media. Comput. Fluids 37: 488-498.

Cartmell SH, Porter BD, Garcia AJ, Guldberg RE (2003) Effects of medium perfusion rate on cell-seeded three-dimensional bone constructs *in vitro*. Tissue Eng. 9(6): 1197-1203.

Chen Y, Zhou S, Li Q (2011) Microstructure design of biodegradable scaffold and its effect on tissue regeneration. Biomaterials 32: 5003-5014.

Cheng G, Youssef BB, Markenscoff P, Zygourakis K (2006) Cell population dynamics modulate the rates of tissue growth processes. Biophys. J. 90(3): pp.713-724.

Chung CA, Chen CW, Chen CP, Tseng CS (2007) Enhancement of cell growth in tissue-engineering constructs under perfusion modeling and simulation. Biotech. Bioeng. 97(6): 1603-1616.

Chung CA, Ho S-Y (2010) Analysis of collagen and glucose modulated cell growth within tissue engineered scaffolds. Annals of Biomed. Eng. 38: 1655-1663.

Cioffi M, Boschetti F, Raimondi MT, Dubini G (2006) Modelling evaluation of the fluid-dynamic microenvironment in tissue-engineered constructs: a micro-CT based model. Biotechnol. Bioeng. 93(3): 500-510.

Claes L, Heigele C (1999) Magnitudes of local stress and strain along bony surfaces predicts the course and type of fracture healing. J. Biomech. 32: 255–266.

d'Humières D, Ginzburg I, Krafczyk M, Lallemand P, Luo L-S (2002) Multiple-relaxation-time lattice Boltzmann models in three dimensions. Phil. Trans. R. Soc. Lond. A. 360: 437-456.

Dani A, Cockx A, Guiraud P (2006) Direct numerical simulation of mass transfer from spherical bubbles: the effect of interface contamination al low Reynolds number. Int. J. Chem. Reactor Eng., 4:1-21.

Darcy H (1856) Les fontaines publiques de la ville de diljon. Dalmont, Paris.

Davisson T, Robert MS, Sah L, Ratcliffe A (2002) Perfusion increases cell content and matrix synthesis in chondrocyte three-dimensional cultures. Tissue Eng. 8(5): 807-816.

De Boodt S, Truscello S, Zcan S, Leroy T, Van Oosterwyck H, Berckmans D, Schrooten J (2010) Bi-modular flow characterization in tissue engineering scaffolds using computational fluid dynamics and particle imaging velocimetry. Tissue Eng. C 16(6): 1553-1564.

Djilali N (2007) Computational modeling of polymer electrode membrane (PEM) fuel cells: challenges and opportunity. Energy 32: 269-280.

Dusting J, Sheridan J, Hourigan K (2006) A fluid dynamics approach to bioreactor design for cell and tissue culture. Biotechnol. Bioeng. 94(6): 1196-1208.

Ferziger JH, Peric M (2002) Computational Methods for Fluid Dynamics. Springer.

Flekkoy EG (1993) Lattice Bhatnagar-Gross-Krook models for miscible fluids. Phys. Rev. E, 47(6): 4247-4257.

Fouras A, Dusting J, Lewis R, Hourigan K (2007) Three-dimensional synchrotron x-ray particle image velocimetry. J. Appl. Phys. 102(6): 064916(1-6).

Fraser KH, Taskin ME, Griffith BP, Wu ZJ (2011) The use of computational fluid dynamics in the development of ventricular assists devices. Med. Eng. Phys. 33: 263-280.

Freed LE, Marquis JC, Langer R, Vunjak-Novakovic G (2004) Kinetics of chondrocyte growth in cell-polymer implants. Biotechnol. Bioeng. 43(7): 597-604.

Galban CJ, Locke BR (1997) Analysis of cell growth in a polymer scaffold using a moving boundary approach. Biotechnol Bioeng 56:422– 432.

Galban CJ, Locke BR (1999) Analysis of cell growth kinetics and substrate diffusion in a polymer scaffold. Biotech. Bioeng. 65(2): 121-132.

Galbusera F, Cioffi M, Raimondi MT, Pietrabissa R (2007) Computational modeling of combined cell population dynamics and oxygen transport in engineered tissue subject to interstitial perfusion. Comput. Meth. Biomech. Biomed. Eng. 10(4): 279-287.

Gardel LS, Correia-Gomes C, Serra LA, Gomes ME, Reis RL (2013) A novel bidirectional continuous perfusion bioreactor for the culture of large-sized bone tissue-engineered constructs. J. Biomed. Mater. Res. B Appl Biomater. 101(8): 1377-1386.

Gilbert E, Mosher M, Gottipati A, Elder S (2014) A Novel Through-Thickness Perfusion Bioreactor for the Generation of Scaffold-Free Tissue Engineered Cartilage. Processes 2: 658-674.

Golfier F, Wood BD, Orgogozo L, Quintard M, Bues M (2009) Biofilms in porous media: development of macroscopic transport equations via volume averaging with closure for local mass equilibrium conditions. Adv. Water Res. 32: 463-485.

Gutierrez RA, Crumpler ET (2007) Potential effect of geometry on wall shears stress distribution across scaffold surfaces. Annals Biomed. Eng. 36(1): 77-85.

Hidalgo-Bastida LA, Thirunavukkarasu S, Griffiths S, Cartmell SH, Naire S (2012) Modeling and design of optimal flow perfusion bioreactors for tissue engineering applications. Biotechnol. Bioeng. 109 (4): 1095-1099.

Hollister SJ (2005) Porous scaffold design for tissue engineering. Nature Mat. 4: 518-524.

Horner HA, Urban JPG (2001) Effect of nutrient supply on the viability of cells from the nucleus pulposus of the intervertebral disc. Spine 26(23): 2543-2549.

Hossain MS, Bergstrom DJ, Chen XB (2014) Prediction of cell growth over a circular strand of a scaffold using the lattice Boltzmann method. Proceedings of the ASME FEDSM 2014, August 3-7, 2014, Chicago, IL, USA.

Hossain MS, Bergstrom DJ, Chen XB (2015) Biomech. Model. Mechanobiol. Computational modelling of the scaffold-free chondrocyte regeneration: a two-way coupling between the cell growth and local fluid flow and nutrient concentration. DOI: 10.1007/s10237-015-0666-0.

Hossain MS, Chen XB, Bergstrom DJ (2015) Fluid flow and mass transfer over circular strands using the lattice Boltzmann method. Heat Mass Transfer. DOI: 10.1007/s00231-015-1514-6.

Hossain MS, Bergstrom DJ, Chen XB (2015) Modelling and simulation of the chondrocyte cell growth, glucose consumption and lactate production within a porous tissue scaffold inside a perfusion bioreactor. Biotecnol. Rep. 5: 55-62.

Hossain MS, Chen XB, Bergstrom DJ (2012) Investigation of the *in vitro* culture process for skeletal-tissue-engineered constructs using computational fluid dynamics and experimental methods. ASME J. Biomech. Eng. 134: 121003(1-12).

Hossain, MS, Bergstrom, DJ, Chen, XB (2014) Prediction of cell growth rate over scaffold strands inside the perfusion bioreactor. Biomech. Model Mechanobiol. DOI: 10.1007/s10237-014-0606-4.

Hunziker EB (2001) Articular cartilage repair: basic science and clinical progress. A review of the current status and prospects. Osteoarthr Cartil 10: 432-463.

Hussein MA, Esterl S, Portner R, Wiegandt K, Becker T (2008) On the lattice Boltzmann method simulation of a two-phase flow bioreactor for artificially grown cartilage cells. J. Biomech. 41: 3455-3461.

Isakssona H, Comas O, Donkelaar C, Mediavilla J, Wilsonb W, Huiskesb R, Itoa K (2006) Bone regeneration during distraction osteogenesis: Mechano-regulation by shear strain and fluid velocity. J. Biomech. 35: 2002-2011.

Jackson AR, Huang C-Y, Gu WY (2011) Effect of endplate calcification and mechanical deformation on the distribution of glucose in intervertebral disc: a 3-d finite element study. Comput. Methods Biomech. Biomed. Engin. 14(2): 195-204.

Jia Y, Bagnaninchib PO, Yang Y, Haj AE, Hinds MT, Kirkpatrick SJ, Wang RK (2009) Doppler optical coherence tomography imaging of local fluid flow and shear stress within micro porous scaffolds. J. Biomed. Optics 14(3): 034014.

Kang Q, Zhang D, Lichtner PC, Tsimpanogiannis IN (2004) Lattice Boltzmann model for crystal growth from supersaturated solution. Geophys. Res. Let. 31: L21604.

Khayyeri H, Checa S, Tagil M, Prendergast PJ (2009) Corroboration of Mechanobiological Simulations of Tissue Differentiation in an In Vivo Bone Chamber Using a Lattice-Modeling Approach. J. Orthop. Res. 27(12): 1659-1666.

Kim GB, Je JH, Lee SJ (2007) Synchrotron X-ray PIV technique for measurement of blood flow velocity. Synchrotron Radiation Instrumentation: Ninth International Conference, American Institute of Physics, 879: 1891-1894.

Korossis S, Bolland F, Kearney J, Fisher J, Ingham E (2005) Bioreactors in tissue engineering. Topics Tissue Eng. 2: 1–23.

Lacroix D, Prendergast PJ, Li G, Marsh D (2002) Biomechanical model to simulate tissue differentiation and bone regeneration: application to fracture healing. Med. Biol. Eng. Comp. 40: 14-21.

Laganà M, Raimondi MT (2012) A miniaturized, optically accessible bioreactor for systematic 3D tissue engineering research. Biomed. Microdevices 14(1): 225-234.

Lallemand P, Luo L-S (2000) Theory of the lattice Boltzmann method: dispersion, dissipation, isotropy, Galilean invariance, and stability. Phys. Rev. E. 61(6): 6546-6542.

Langer R, Vacanti JP (1993) Tissue engineering. Science 260: 920-926.

Lanza RP, Langer R, Vacanti J (2000) Principles of Tissue Engineering. Academic Press, San Diego, California.

Lemon G, King JR (2007) Multiphase modeling of cell behavior on artificial scaffolds: effects of nutrient depletion and spatially non-uniform porosity. Math. Med. Biol. 24(1): 57-83.

Lendenmann U, Egli T (1997) Kinetic models for the growth of Escherichia coli with mixtures of sugars under carbon-limited conditions. Biotech. Bioeng. 59(1): 99-107.

Li D, Tang T, Lu J, Dai K (2009) Effects of flow shear stress and mass transport on the construction of a large-scale tissue-engineered bone in a perfusion bioreactor. Tissue Eng. A 15: 2773–83.

Li L, Mei R, Klausner JF (2013) Boundary conditions for thermal lattice Boltzmann equation method. J. Comp. Phys. 237: 366-395.

Li S, Glynne-Jones P, Andriotis OG, Ching KY, Jonnalagadda US, Oreffo ROC, Hill M, Tare RS (2014) Application of an acoustofluidic perfusion bioreactor for cartilage tissue engineering. Lab Chip 14: 4475- 4485.

Lima R, Wada S, Tanaka S, Takeda M, Ishikawa T, Tsubota K, Imai Y, Yamaguchi T (2008) *In vitro* blood flow in a rectangular PDMS microchannel: experimental observations using a confocal; micro-PIV system. Biomed. Microdevices 10(2): 153-167.

Lin T-H, Jhang H-Y, Chu F-C, Chung CA (2013) Computational modelling of nutrient utilization in engineered cartilage. Biotechnol. Prog. 29: 452-462.

Liu D, Chua C-K, Leong K-F (2013) A mathematical model for fluid shear-sensitive 3D tissue construct development. Biomech. Model Mechanobiol. 12: 19-31.

Mandujano F, Peralta-Fabi, R (2005) On the viscous steady flow around a circular cylinder. Rev. Mex. de Física. 51(1): 87-99.

Marlovits S, Tichy B, Truppe M, Gruber D, Vécsei V (2003) Chondrogenesis of aged human articular cartilage in a scaffold-free bioreactor. Tissue Eng. 9(6): 1215-1216.

Mayer N, Silvia L, Talo G, Lovati AB, Riboldi SA, Moretti M, Mallein-Gerin F (2014) The use of a bi-directional perfusion bioreactor for cartilage engineering promotes the reconstruction of hyaline cartilage. Osteoarthr. Cartilage. 22: S487.

McCoy RJ, Jungreuthmayer C, O'Brien FJ (2012) Influence of flow rate and scaffold pore size on cell behavior during mechanical simulation in flow perfusion bioreactor. Biotechnol. Bioeng. 109 (6): 1583-1594.

Mei R, Shyy W, Yu D, Luo L-S (2000) Lattice Boltzmann method for 3-D flows with curved boundaries. J. Comp. Phys.161: 680-699.

Meinhart CD, Wereley ST, Gray MHB (2000) Volume illumination for two dimensional particle image velocimetry. Meas. Sci. Technol. 11: 809-814.

Meyer U, Meyer T, Handschel J, Wiesmann HP (2009) Fundamentals of Tissue Engineering and Regenerative Medicine. Springer-Verlag Berlin Heidelberg, Germany.

Mielnik MM, Saetran LR (2004) Micro particle image velocimetry - an overview. Turbulence 10: 83-90.

Milan J, Planell JS, Lacroix D (2010) Simulation of bone tissue formation within a porous scaffold under dynamic compression. Biomech. Model. Mechanobiol. 9: 583-596.

Milan JL, Planell JA, Lacroix D (2009) Computational modelling of the mechanical environment of osteogenesis within a polylactic acid-calcium phosphate glass scaffold. Biomaterials 30: 4219-4226.

Murphy CM, O'Brien FJ, Litlle DG, Schindeler A. (2013) Cell-scaffold interactions in the bone tissue engineering triad. Euro. Cells and Mat. 26: 120-132.

Nagai T, Furukawa KS, Sato M, Ushida T, Mochida J (2008) Characteristics of a Scaffold-Free Articular Chondrocyte Plate Grown in Rotational Culture. Tissue Eng.: Part A, 14(7): 1183-1193.

Nava MM, Raimondi MT, Pietrabissa R (2013) A multiphysics 3D model of tissue growth interstitial perfusion in a tissue-engineering bioreactor. Biomech Model Mechanobiol. 12: 1169-1179.

Northrup MA, Kulp TJ Angel SM (1991b) Application of fluorescent particle imaging to measuring flow in complex media. Analytica. Chimica. Acta. 255: 275-282.

Northrup MA, Kulp TJ, Angel SM (1991a) Fluorescent particle image velocimetry: application to flow measurement in refractive index-matched porous media. Applied Optics 30(1): 3034-3040.

Patankar SV (1980) Numerical heat transfer and fluid flow. McGraw-Hill, NY, USA.

Pauwels F (1960) A new theory on the influence of mechanical stimuli on the differentiation of supporting tissue. The tenth contribution to the functional anatomy and causal morphology of the supporting structure. Z. Anat Entwickl Gesch 121: 478–515.

Peurrung LM, Rashidi M, Kulp TJ (1995) Measurement of porous medium velocity fields and their volumetric averaging characteristics using particle tracking velocimetry. Chem. Eng. Sci. 50(14): 2243-2253.

Picioreanu C, van Loosdrecht MCM, Heijnen JJ (2000) Effect of diffusive and convective substrate transport on biofilm structure formation: a two-dimensional modeling study. Biotechnol Bioeng. 69: 504–515.

Pintelon TRR, Creber SA, Schulenburg DAG, Johns ML (2010) Validation of 3D simulations of reverse osmosis membrane biofouling. Biotech. Bioeng. 106 (4): 677-689.

Pintelon TRR, Picioreanu C, Loosdrecht MCM, Johns ML (2011) The effect of biofilm permeability on bio-clogging of porous media. Biotechnol. Bioeng. 109 (4): 1031-1042.

Plunkett N, O'Brian FJ (2011) Bioreactors in tissue engineering. Technology and Health Care 19: 55–69.

Porter B, Zauel R, Stockman H, Guldberg R, Fyhrie D (2005) 3-D computational modeling of media flow through scaffolds in a perfusion bioreactor. J of Biomech. 38: 543-549.

Pörtner R, Nagel-Heyer S, Goepfert C, Adamietz P, Meenen NM (2005) Bioreactor design for tissue engineering. J. Biosci. Bioeng. 100(3): 235-245.

Premnath KN, Pattison MJ,Banerjee S (2009) Generalized latticeBoltzmann equation with forcing term for computation of wall-bounded turbulent flows. Physical Rev E 79(2):026703.

Prendergast PJ, Lacroix D (2002) A mechano-regulation model for tissue differentiation during fracture healing: analysis of gap size and loading. J. Biomech. 35: 1163-1171.

Provin C, Takano K, Sakai Y, Fujii T, Shirakashi R (2008) A method for the design of 3D scaffolds for high-density cell attachment and determination of optimum perfusion culture conditions. J. Biomech. 41: 1436-1449.

Raffel M, Willert C, Kompenhans J (1998) Particle Image Velocimetry - A Practical Guide. Springer. New York, USA.

Raimondi MT, Boschetti F, Falcone L, Migliavacca F, Remuzzi A, Dubini G (2004) The effect of media perfusion on three-dimensional cultures of human chondrocytes: Integration of experimental and computational approaches. Biorheology 41: 401-410.

Raimondi MT, Causin P, Mara A, Nava M, Laganà M, Sacco R (2011) Breakthroughs in Computational Modeling of Cartilage Regeneration in Perfused Bioreactors. IEEE Trans. Biomed. Eng. 58(12): 3496-3499.

Raimondi MY, Moretti M, Cioffi M, Giordano C, Boschetti F, Laganà K, Pietrabissa R (2006) The effect of hydrodynamic shear on 3D engineered chondrocyte systems subject to direct perfusion. Biorheology 43: 215-222.

Ribeiro VM, Coelho PM, Pinho FT, Alves MA (2012) Three-dimensional effects in laminar flow past a confined cylinder. Chem. Eng. Sci. 84: 155-169.

Rodrigues CAV, Fernandes TG, Diogo MM, da Silva CL, Cabral JMS (2011) Stem cell cultivation in bioreactors. Biotechnol. Adv. 29: 815-829.

Sacco R, Causin P, Zunino P, Raimondi MT (2011) A multiphysics/multiscale 2D numerical simulation of scaffold-based cartilage regeneration under interstitial perfusion in a bioreactor. Biomech. Model. Mechanobiol. 10(4): 577-589.

Saltzman WM (2004) Tissue Engineering: Principles for the design of replacement organs and tissues. Oxford University Press, Oxford, New York, USA

Santiago JG, Wereley ST, Meinhart CD, Beebe DJ, Adrian RJ (1998) A particle image velocimetry system for microfluidics. Exp. Fluids 25(4): 316-319.

Sayed AAM, Hussein MA, Becker T (2010) An innovative lattice Boltzmann model for simulating Michaelis-Menten-based diffusion-advection kinetics and its application within a cartilage cell bioreactor. Biomech. Model Mechanobiol 9: 141-151.

Schulenburg DAG, Pintelon TRR, Picioreanu C, Loosdrecht MCM, Johns ML (2008) Three-dimensional simulations of biofilm growth in porous media. AIChE J., 55: 494-504

Sengers BG, Heywood HK, Lee DA, Oomens CWJ, Bader DL (2005) Nutrient utilization by bovine articular chondrocytes: a combined experimental and theoretical approach. ASME J. Biomech. Eng. 127 (5): 758-766.

Sergi D, Grossi L, Leidi T, Ortona A (2014) Surface growth effects on reactive capillary-driven flow: lattice Boltzmann investigation. Engineering Applications of Computational Fluid Mechanics, 8 (4): 549 - 561.

Shakeel M (2011) Continuum modeling of cell growth and nutrient transport in a perfusion bioreactor. Ph.D. thesis, School of Mathematics and IT Department, University of Nottingham.

Shimizu H, Bode PM, Bode HR (1995) Patterns of oriented cell division during the steady-state morphogenesis of the body column in hydra. Developmental Dynamics, 204: 349-357.

Singh H, Ang ES, Lim TT, Hutmacher DW (2006) Flow modeling in a novel non-perfusion conical bioreactor. Biotechnol. Bioeng. 97(5): 1291-1299.

Singh H, Hutmacher DW (2009) Bioreactor studies and computational fluid dynamics. Adv Biochem Engin/Biotechnol. 112: 231–249.

Singh H, Teoh SH, Low HT, Hutmacher DW (2005) Flow modeling within a scaffold under the influence of uni-axial and bi-axial bioreactor reaction. J. Biotechnol. 119: 181-196.

Sozer E, Shyy W (2007) Modeling of fluid dynamics and heat transfer through porous media for rocket propulsion. 43rd AIAA/ASME/SAE/ASEE Joint Propulsion Conference & Exhibit, Cincinnati, OH.

Spencer TJ, Hidalgo-Bastida LA, Cartmell SH, Halliday I, Care CM (2013) In silico multi-scale model of transport and dynamic seeding in a bone tissue engineering perfusion bioreactor. Biotech. Bioeng. 110: 1221-1230.

Sucosky P, Osorio DF, Brown JB, Neitzel GP (2004) Fluid Mechanics of a Spinner-Flask Bioreactor. Biotechnol. Bioeng. 85(1): 34-46.

Sullivan SP, Sani FM, Johns ML, Gladden LF (2005) Simulation of packed bed reactors using lattice Boltzmann method. Chem. Eng. Sci., 60: 3405-3418.

Tagil M, Aspenberg P (1999) Cartilage induction by controlled mechanical stimulation in vivo," J Orthop. Res. 17: 200–204.

von der Schulenburg DAG, Pintelon TRR, Picioreanu C, van Loosdrecht MCM, Johns ML. 2009. Three-Dimensional simulations of biofilm growth in porous media. Biotech. Bioeng. 55(2): 494-504.

Voronov R, van Gordon S, Sikavitsas VI, Papavassiliou DV. 2010. Computational modelling of flow-induced shear stresses within 3D salt-leached porous scaffolds imaged via micro-CT. J. Biomech. 43: 1279-1286.

Vunjak-Novakovic G, Freed LE, Biron RJ, Langer R (2004) Effects of mixing on tissue engineered cartilage. AIChE J. 42(3): 850-860.

Whitaker S (1986) Flow in porous media I: a theoretical derivation of Darcy's law. Transport Porous Med. 1(1): 3-25.

White FM (2009) Fluid Mechanics. 7th Ed. McGraw Hill. New York, NY, USA.

Wu M-H, Urban JPG, Cu, ZF, Cui Z, Xu X (2007) Effect of extracellular pH on matrix synthesis by chondrocytes in 3D agarose gel. Biotechnol. Prog. 23: 430-434.

Xie YZ, Hardouin P, Zhu ZN, Tang TT, Dai KR, Lu JX (2006) Three-dimensional flow perfusion culture system for stem cell proliferation inside the critical-size betatricalcium phosphate scaffold. Tissue Eng. 12: 3535–43.

Yan X, Bergstrom DJ, Chen XB (2011) Modelling of the flow within scaffolds in perfusion bio-reactors. Am. J. Biomed. Eng. 1: 72-77.

Yan X, Chen XB, Bergstrom DJ (2011) Modeling of the flow within scaffolds in perfusion bio-reactors. American J. Biomed. Eng. 1(2): 72-77.

Yeatts AB, Fisher JP (2011) Bone tissue engineering bioreactors: Dynamic culture and influence of shear stress. Bone 48: 171-181.

Yoshida H, Nagaoka M (2010) Multiple-relaxation-time lattice Boltzmann model for the convection and anisotropic diffusion equation. J. Comp. Phys. 229: 7774-7795.

Yu D, Mei R, Luo L-S, Shyy W. 2003. Viscous flow computations with the method of lattice Boltzmann equation. Prog. Aero. Sci. 39: 329-367.

Yu H, Luo LS, Girimaji SS (2006) LES of turbulent square jet flow using an MRT lattice Boltzmann method. Compt. and fluids, 35: 957-965.

Zacharof M-P, Lovitt RW (2013) Modelling and simulation of cell growth dynamics, substrate consumption and lactic acid production kinetics of *Lactococcus lactis*. Biotechnol. Bioprocess Eng. 18: 52-64.

Zhang J, Johnson PC, Poepl AS (2007) An immersed boundary lattice Boltzmann approach to simulate deformable liquid capsules and its application to microscopic blood flows. Phys. Biol. 4: 285-295.

Zhang T, Shi B, Guo Z, Chai Z, Lu J (2012) General bounce-back scheme for concentration boundary condition in the lattice Boltzmann method. Phys. Rev. E 85: 016701(1-14).

Zhou S (2005) Nutritional gradients in native and tissue-engineered cartilage. Ph.D. thesis, Oxford University.

Zhou S, Cui Z, Urban JPG (2008) Nutrient gradients in engineered cartilage: metabolic kinetics measurement and mass transfer modelling. Biotech. Bioeng., 101 (2): 408–421.

Zinn M, Witholt B, Egli T (2004) Dual nutrient limited growth: models, experimental observations and applications. J. Biotech. 113: 263-279.